Millimeter-Wave Applications of Semiconductor Dielectric Waveguides with Plasma Layers (Surface or Buried) Generated from Semiconductor Lasers

Final Report

Jerome K. Butler, Ph.D.
Electrical Engineering

September 1992

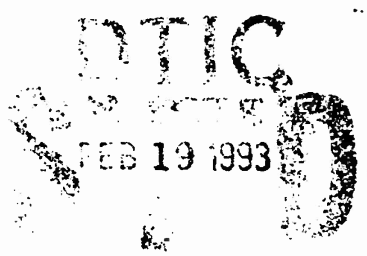

U. S. Army Research Office

DAAL03-89-K-0029

Southern Methodist University
Dallas, TX 75275

DISCLAIMER NOTICE

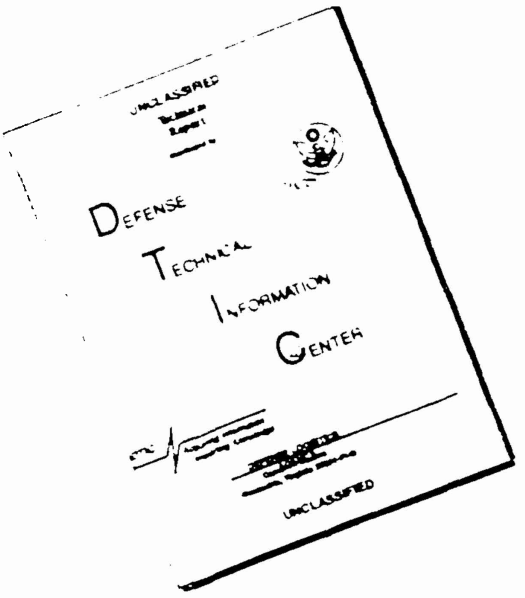

THIS DOCUMENT IS BEST QUALITY AVAILABLE. THE COPY FURNISHED TO DTIC CONTAINED A SIGNIFICANT NUMBER OF PAGES WHICH DO NOT REPRODUCE LEGIBLY.

The view, opinions, and/or findings contained in this report are those of the author and should not be construed as an official Department of the Army position, policy, or decision, unless so designated by other documentation.

SECURITY CLASSIFICATION OF THIS PAGE

REPORT DOCUMENTATION PAGE

1a. REPORT SECURITY CLASSIFICATION Unclassified	1b. RESTRICTIVE MARKINGS
2a. SECURITY CLASSIFICATION AUTHORITY	3. DISTRIBUTION/AVAILABILITY OF REPORT Approved for public release: distribution unlimited
2b. DECLASSIFICATION/DOWNGRADING SCHEDULE	
4 PERFORMING ORGANIZATION REPORT NUMBER(S)	5. MONITORING ORGANIZATION REPORT NUMBER(S) ARO 25339.5-EL
6a. NAME OF PERFORMING ORGANIZATION Box 302 Southern Methodist University 6b. OFFICE SYMBOL (If applicable)	7a. NAME OF MONITORING ORGANIZATION US Army Research Office
6c. ADDRESS (City, State, and ZIP Code) Dallas, Texas 75275-0335	7b. ADDRESS (City, State, and ZIP Code) P.O. Box 12211 Research Triangle Park, NC 27709-2211
8a. NAME OF FUNDING/SPONSORING ORGANIZATION Army Research Office 8b. OFFICE SYMBOL (If applicable)	9. PROCUREMENT INSTRUMENT IDENTIFICATION NUMBER DAAL03-89-K-0029
8c. ADDRESS (City, State, and ZIP Code) Research Triangle Park, NC 27709-2211	10. SOURCE OF FUNDING NUMBERS PROGRAM ELEMENT NO. / PROJECT NO. / TASK NO. / WORK UNIT ACCESSION NO.

11. TITLE (Include Security Classification)
Millimeter-Wave Applications of Semiconductor Dielectric Waveguides with Plasma Layers (Surface or Buried) Generated from Semiconductor Lasers

12. PERSONAL AUTHOR(S)
Jerome K. Butler

13a. TYPE OF REPORT	13b. TIME COVERED	14. DATE OF REPORT (Year, Month, Day)	15. PAGE COUNT
Final	FROM Dec 88 TO Sep 92	92 Sept. 30	70

16. SUPPLEMENTARY NOTATION The view, opinions and/or findings contained in this report are those of the author and should not be construed as an official Department of the Army position, policy, or decision, unless so designated by other documentation.

17 COSATI CODES			18. SUBJECT TERMS (Continue on reverse if necessary and identify by block number)
FIELD	GROUP	SUB-GROUP	

19 ABSTRACT (Continue on reverse if necessary and identify by block number)

Abstract
This research program was aimed at the theoretical and experimental investigations of semiconductor devices and waveguides with applications in millimeter wave systems. The major components considered included waveguide phase shifters, attenuators, and periodic structures designed to operate at the Second Bragg frequency. Most of the effort was directed at theoretical and experimental understanding of the second-order Bragg structures since these components produce the most efficient radiating antennas. With a goal of locking several independent oscillators through gratings in the dielectric waveguide, the grating plays one of the most important roles in the system integration. Accordingly, we developed two comprehensive computer models of dielectric gratings and made experimental measurements on more than fifty waveguide structures.

20. DISTRIBUTION/AVAILABILITY OF ABSTRACT ☐ UNCLASSIFIED/UNLIMITED ☐ SAME AS RPT. ☐ DTIC USERS	21. ABSTRACT SECURITY CLASSIFICATION Unclassified
22a. NAME OF RESPONSIBLE INDIVIDUAL	22b. TELEPHONE (Include Area Code) / 22c. OFFICE SYMBOL

DD FORM 1473, 84 MAR 83 APR edition may be used until exhausted. All other editions are obsolete.

SECURITY CLASSIFICATION OF THIS PAGE

UNCLASSIFIED

TABLE OF CONTENTS

SUMMARY

This project was concerned with the development of millimeter wave dielectric waveguides and waveguide structures periodic dielectric variations. A chief technical objective of this effort was toward the development of a novel highly integrated solid-state high-power millimeter wave source which can be focussed to yield a coherent narrow beam, capable of producing an effective scanning radiation pattern. When the waveguide material is partly fabricated by an optoelectronic or photoactive material such gallium arsenide, semiconductor surface emitting lasers may be used to induce a controllable periodic charge carrier plasma within the surface of the waveguide.

Dielectric waveguides at millimeter wave frequencies are desirable because these guiding structures have relatively small dimensions and systems can be easily integrated on single wafer chips. The components have applications for: (1) grating surface emitting antennas, (2) millimeter wave filters, (3) millimeter wave phase shifters and others. Extensive development of theoretical and computer models of dielectric waveguides have been accomplished. Experiments using both semiconductor (silicon) and insulator (alumina) waveguide materials have been performed.

A key factor pertaining to periodic waveguides used as an antenna is the overall length of the structure (aperture dimension). If the structure is long (too many grating periods), most of the total input power may be extracted over a length much smaller than the actual grating section. In addition, radiation at broadside (Second Bragg condition), is minimized for very long gratings. For effective designs, careful tradeoffs between grating length and grating strength need to be considered. In the experimental work some of the early waveguides had relatively short grating sections, however, later we started making much longer grating regions. (The resulting antenna dimensions were about two inches.) The new waveguide structures were excellent in quality and exhibited classical w-b dispersion characteristics around the second Bragg condition.

The ultimate goal of this project was to progress toward development of a high-power scanning millimeter-wave antenna. High powers will be accomplished by locking a large number of individual millimeter wave oscillators. (An alternative design is to have a single master oscillator that feeds into a periodic configuration of pairs of an amplifier and a grating.) Because of these potential designs we have experimentally studied grating sections with input from both directions. An experimental configuration used split the oscillator power for launching at both ends of the grated waveguide structure. With the new arrangement, power was launched into the dielectric waveguide from both the right and left directions. (This configuration corresponds to a situation where the grating region would separate two oscillators to be locked into one coherent system. The grating acts both as a feedback mechanism as well as the antenna.) Depending on the relative phase of the two inputs, the far-field radiation pattern can be maximized or minimized. The two-side incidence case shows that in the out of phase condition, the radiation power is minimum at the second Bragg frequency.

In addition to the improvement of the design program of the periodic waveguides, we performed simulation experiments of waveguide structures that have excited plasma layers. These new periodic structures have a fixed grating waveguide coupled with a separate confined plasma layer in the opposed waveguide surface. Typically the new structures would be fabricated on wafers composed of either (1) silicon on sapphire (the grating formed in the sapphire layer and the plasma layer excited in the silicon layer), or (2) gallium arsenide on aluminum gallium arsenide (the grating formed in the aluminum gallium arsenide layer and the plasma layer excited in the gallium arsenide layer). In our experiments, we started with an Al_2O_3 waveguide with a grating formed on one surface. The waveguide was designed to radiate broadside. Next, a layer of metal foil was attached to the waveguide on the side opposite the grating layer. (The metal foil was to simulate an excited plasma layer with high electron/hole concentrations.) The radiation pattern measured with the foil attached produced a beam at about 30^{o} to the broadside direction. This implies that a corresponding silicon on sapphire structure would electronically scan about 30^{o}.

PROGRESS REPORT

TWENTY COPIES REQUIRED

1. ARO PROPOSAL NUMBER: 25339-EL

2. PERIOD COVERED BY REPORT: 1 January 1989 - 30 June 1989

3. TITLE OF PROPOSAL: Millimeter-Wave Appl of Semiconductor Dielectric Waveguides with Plasma Layers (Surface or Buried)gen fr semicond laser

4. CONTRACT OR GRANT NUMBER: DAAL03-89-K-0029

5. NAME OF INSTITUTION: Southern Methodist University

6. AUTHORS OF REPORT: Jerome K. Butler

7. LIST OF MANUSCRIPTS SUBMITTED OR PUBLISHED UNDER ARO SPONSORSHIP DURING THIS REPORTING PERIOD, INCLUDING JOURNAL REFERENCES:

G. Hadjicostas, J. K. Butler, G. A. Evans and N. W. Carlson, "A Numerical Investigation of Wave Interactions in Dielectric Waveguides with Periodic Surface Corrugations," IEEE J. Quantum Electronics (Submitted for Publication)

8. SCIENTIFIC PERSONNEL SUPPORTED BY THIS PROJECT AND DEGREES AWARDED DURING THIS REPORTING PERIOD:

J. K. Butler
G. Hadjicostas
R. Ayekavadi

Jerome K. Butler
Department of Electrical Engineering
Southern Methodist University
Dallas, TX 75222

BRIEF OUTLINE OF RESEARCH FINDINGS

The work over the first six months on this program has been concentrated on the development of the theory of gratings on dielectric waveguides. There are several theoretical approaches that can be used for the analysis of gratings; the most common approach is to apply a perturbation method such as the coupled-mode theory. However, these approximate methods are inaccurate for gratings fabricated with films of thin metals or plasma induced gratings. Therefore, our grating studies employ the Boundary Element Method which can be applied to most waveguide structures of interest.

In the next phase of the program we will make measurements of dielectric strucutures in the vicinity of 94 GHz. Consequently, we have prepared simple dielectric waveguides using alumina (Al_2O_3)which has an approximate relative dielectric constant of 10. Four waveguides with slightly different grating periods have been fabricated with a typical guide shown in the figure below. (The cross-section of the waveguide and a standard scale were photographed using an optical microscope.) The gratings were cut in the alumina using a diamond saw. The overall length of the waveguide is approximately 30 periods. Simple waveguide calculations indicate the millimeter wavelength along the guided structure is approximately 1 mm at 94 GHz so that the grating period of 1 mm produces causes resonance at the 2nd Bragg condition.

Fig. 1 A dielectric waveguide of Al_2O_3. The grating was fabricated using a diamond saw.

PROGRESS REPORT

TWENTY COPIES REQUIRED

1. ARO PROPOSAL NUMBER: 25339-EL

2. PERIOD COVERED BY REPORT: 1 July 1989 - 31 December 1989

3. TITLE OF PROPOSAL: Millimeter-Wave Appl of Semiconductor Dielectric Waveguides with Plasma Layers (Surface or Buried)gen fr semicond laser

4. CONTRACT OR GRANT NUMBER: DAAL03-89-K-0029

5. NAME OF INSTITUTION: Southern Methodist University

6. AUTHORS OF REPORT: Jerome K. Butler

7. LIST OF MANUSCRIPTS SUBMITTED OR PUBLISHED UNDER ARO SPONSORSHIP DURING THIS REPORTING PERIOD, INCLUDING JOURNAL REFERENCES:
G. Hadjicostas, J.K. Butler, G.A. Evans, N.W. Carlson and R. Amentea, "A Numerical Investigation of Wave Interactions in Dielectric Waveguides with Periodic Surface Corrugations," IEEE J. Quantum Electronics (accepted for publication).

8. SCIENTIFIC PERSONNEL SUPPORTED BY THIS PROJECT AND DEGREES AWARDED DURING THIS REPORTING PERIOD:

J.K. Butler, Gururaj Ayekavadi, Chao Suan Yeh

Jerome K. Butler
Department of Electrical Engineering
Southern Methodist University
Dallas, TX 75222

BRIEF OUTLINE OF RESEARCH FINDINGS

The work over the last six months has been divided between theoretical and experimental studies of periodic waveguides. We are developing theory to estimate the transmission and reflection characteristics (Scattering parameters) of a dielectric waveguide with periodic teeth cut in the dielectric. Our laboratory has cut approximately 15 dielectric guides fabricated with Al_2O_3 as discussed in the previous progress report.

Experimental measurements in the 90-100 GHz range is proceeding at an excellent pace. Experimental and theoretical results are in also excellent agreement. There are a large number of publications that indicate that 2nd order Bragg reflectors do not radiate at the second Bragg frequency. However, we have shown theoretically and experimental radiation (Broadside) from finite length grating structures.

In the next period we will continue our measurements of the radiation fields from the grating surface emitters (GSE) fabricated with Al_2O_3. In addition we will start fabrication of silicon on sapphire dielectric structures. The Si on sapphire dielectric waveguides can be controlled by optical signals.

PROGRESS REPORT

TWENTY COPIES REQUIRED

1. ARO PROPOSAL NUMBER: 25339-EL

2. PERIOD COVERED BY REPORT: 1 January 1990 - 30 June 1990

3. TITLE OF PROPOSAL: Millimeter-Wave Appl of Semiconductor Dielectric Waveguides with Plasma Layers (Surface or Buried)gen fr semicond laser

4. CONTRACT OR GRANT NUMBER: DAAL03-89-K-0029

5. NAME OF INSTITUTION: Southern Methodist University

6. AUTHORS OF REPORT: Jerome K. Butler

7. LIST OF MANUSCRIPTS SUBMITTED OR PUBLISHED UNDER ARO SPONSORSHIP DURING THIS REPORTING PERIOD, INCLUDING JOURNAL REFERENCES:

G. Hadjicostas, J. K. Butler, G. A. Evans, N. W. Carlson, and R. Amantea, "A Numerical Investigation of Wave Interactions in Dielectric Waveguides with Periodic Surface Corrugations," IEEE J. Quantum Electron. (In press.)

R. Ayekavadi, C. S. Yeh, J. K. Butler and G. A. Evans, "Experimental Verification of Grating Theory for Surface Emitting Structures," SPIE Abstract (Submitted).

8. SCIENTIFIC PERSONNEL SUPPORTED BY THIS PROJECT AND DEGREES AWARDED DURING THIS REPORTING PERIOD:

J. K. Butler
R. Ayekavadi
C. S. Yeh

Jerome K. Butler
Department of Electrical Engineering
Southern Methodist University
Dallas, TX ~~75222~~ 75275

BRIEF OUTLINE OF RESEARCH FINDINGS

The work of the last six months has been in both theoretical and experimental studies.

Our experimental work has been concerned with the fabrication of dielectric waveguides in Al_2O_3. Since we are performing experimental measurements at about 100 GHz, most of the waveguide structures have been fabricated with Al_2O_3 plates that are 40 mils thick. (The waveguide cross sections are 40 mils x 2 mm. These structures support the dominant TE or TM modes depending upon the polarization of the exciting wave that is fed to the dielectric structure.) To date we have made about 20 different waveguide structures that have 2nd order Bragg resonances in the range of 85 to 105 GHz. Since these structures are tedious to make, it usually takes about 3 days of laboratory work. The basic aim in the fabrication of the different structures is to understand the necessary grating geometries that will produce weak or strong gratings. A strong grating will outcouple a major portion of the electromagnetic power that enters the grating after about 20-30 periods while a weak grating outcouples the light after more than 100 periods. In general, the grating period is dependent upon several parameters including the height of the teeth in the waveguide. However, we have found that most of the structures have grating periods of about 1.1 mm at 100 GHz, so that a grating with 24 periods is about 2.6 cm in length. We have also found that for structures with teeth height greater than about 15 mils that most of the power entering the grating section is outcoupled after about 24 periods. Consequently, the radiating apertures are about 2 cm wide. On some structures we have fabricated two regions with different grating periods; one grating is strong and the other is weak. We have made these structures in order to study the effects of reflection and transmission of strong grating sections. The strong grating is designed at a particular frequency to radiate broadside (2nd Bragg Condition). The weak grating is designed for the 2nd Bragg at a different frequency.

On all the dielectric waveguides with designed gratings we measured the the radiation pattern at several different frequencies (about the 2nd Bragg frequency). On some structures we excite the grating with equal amounts of power at both ends of the waveguide. By adjusting the phase of the wave at either end of the waveguide, the radiation field can be maximized or nulled at the 2nd Bragg frequency. This study is important when we eventually start to couple several oscillators *via* the grating region. One long range goal is to couple many sources using the gratings for outcoupling as well as feedback to the various oscillators.

Theoretical work is proceeding. The boundary element approach to solving for the characteristics of periodic structures is being fully developed. This approach is best for structures of arbitrary-shaped teeth. It is by nature a non-perturbative approach.

Experimental Verification of Grating Theory for Surface Emitting Structures*

R. G. N. Ayekavadi, C. S. Yeh and J. K. Butler
214-692-3113 (o), 214-692-4099 (fax)
Department of Electrical Engineering
Southern Methodist University
Dallas, TX 75275

G. E. Evans
David Sarnoff Research Center
Princeton, NJ 08543-5300

Surface emitting structures are modelled using a rigorous Floquet-Bloch analysis of periodic structures. The theory evaluates phase constants, attenuation coefficients, reflection, transmission and outcoupling of power from a single grating section. In the fabrication of dielectric grating structures, the waveguide and grating dimensions were computed using approximate methods that employ the average dielectric constant of the corrugated region. The grating structures were designed so that only the n=-1 spatial harmonic radiates (2nd order Bragg grating). The far-field patterns of the experimental structures were compared with the theoretical results obtained using the rigorous Floquet-Bloch analysis. The reflection, transmission and outcoupling of power from a single grating section are also obtained from experiment and theory . Experimental verification of the model is achieved using millimeter waves of 100 GHz in dielectric waveguides fabricated from Al_2O_3.

*Supported in part by the U. S. Army Research Office.

PROGRESS REPORT

TWENTY COPIES REQUIRED

1. ARO PROPOSAL NUMBER: 25339-EL

2. PERIOD COVERED BY REPORT: 1 July 1990 - 31 December 1990

3. TITLE OF PROPOSAL: Millimeter-Wave Appl of Semiconductor Dielectric Waveguides with Plasma Layers (Surface or Buried)gen fr semicond laser

4. CONTRACT OR GRANT NUMBER: DAAL03-89-K-0029

5. NAME OF INSTITUTION: Southern Methodist University

6. AUTHORS OF REPORT: Jerome K. Butler

7. LIST OF MANUSCRIPTS SUBMITTED OR PUBLISHED UNDER ARO SPONSORSHIP DURING THIS REPORTING PERIOD, INCLUDING JOURNAL REFERENCES:

"Experimental Verification of Grating Theory for Surface-emitting Structures," R. Ayekavadi, C. S. Yeh, J. K. Butler, G. A. Evans, P. Stabile and A. Rosen, OE-LASE '91

SPIE Meeting 20-25 Jan. 1991, Los Angeles, CA

8. SCIENTIFIC PERSONNEL SUPPORTED BY THIS PROJECT AND DEGREES AWARDED DURING THIS REPORTING PERIOD:

R. Ayekavadi
C. S. Yeh
J. K. Butler

9. REPORT OF INVENTIONS (BY TITLE ONLY):

Jerome K. Butler
Department of Electrical Engineering
Southern Methodist University
Dallas, TX 75222

BRIEF OUTLINE OF RESEARCH FINDINGS

Briefly, the work over the last period has progressed along both theoretical and experimental development of dielectric surface emitting structures.

Experimental work over the past period has been concerned with the design and fabrication of periodic waveguides fabricated with Al_2O_3. The waveguides were designed for first order Bragg radiation in the frequency range from 90 to 100 GHz. A number of waveguides have been designed and constructed including some with multiple sections of corrugations on them. The radiation pattern from these waveguides were measured by electronic scanning of the frequency. The experimental pattern was compared with that obtained from a simulation based on the Huygen-Fresnel radiation theory (for the -1 order Floquet-Bloch wave). By frequency scanning the local millimeter wave sources, the far-field pattern scanned relative to the normal of the waveguide. For most of the waveguide structures, the far-field beam or major lobe scanned from 1.8 to 2.0 degrees per GHz. Thus, the beam could be frequency scanned about 20 degrees over a 10 GHz range or about 10 percent of the operating frequency.

Experimental studies were also carried on a two section grating structure, illustrated below. Each grating section was about 25 teeth long or about 30 mm. The separation between the grating ends was about 20 to 25 mm. Each of the grating was designed to radiate broadside at different frequencies. For example one was designed to radiate at about 98 GHz while the other at 102 GHz. The two section waveguide was then excited with a 100 GHz source. The power was split so that the double grating section was excited with equal amounts of power from both directions. The experimental and theoretical radiation patterns had very close agreement. When the field at the input of each grating had identical phase, the far-field pattern produced a single broadside lobe.

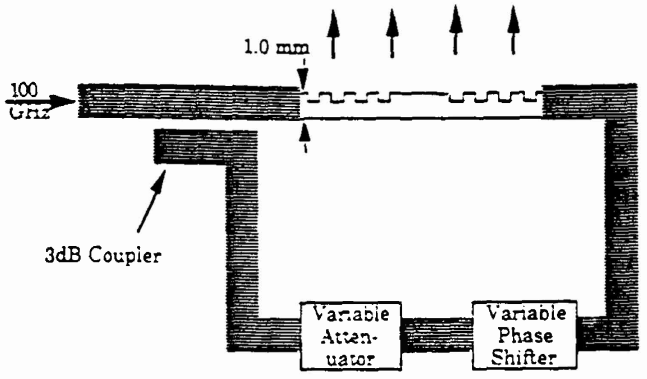

PROGRESS REPORT

TWENTY COPIES REQUIRED

1. ARO PROPOSAL NUMBER: 25339-EL

2. PERIOD COVERED BY REPORT: 1 January 1991 - 30 June 1991

3. TITLE OF PROPOSAL: Millimeter-Wave Appl of Semiconductor Dielectric Waveguides with Plasma Layers (Surface or Buried)gen fr semicond laser

4. CONTRACT OR GRANT NUMBER: DAAL03-89-K-0029

5. NAME OF INSTITUTION: Southern Methodist University

6. AUTHORS OF REPORT: Jerome K. Butler

7. LIST OF MANUSCRIPTS SUBMITTED OR PUBLISHED UNDER ARO SPONSORSHIP DURING THIS REPORTING PERIOD, INCLUDING JOURNAL REFERENCES:

R. Ayekavadi, C. S. Yeh, J. K. Butler, G. A. Evans, P. Stabile, and A. Rosen, "Experimental verification of grating theory for surface emitting structures," Laser Diode Technology and Applications III, vol. SPIE 1418, pp. 74-85, Jan. 23-25, 1991.

R. Ayekavadi, C. S. Yeh, and J. K. Butler, "Design and performance of corrugated waveguide structures based on slab waveguide principles," Emerging Optoelectronic Technologies Conference, Indian Institute of Science, Bangalore, India, Dec. 16-19, 1991. (Accepted)

8. SCIENTIFIC PERSONNEL SUPPORTED BY THIS PROJECT AND DEGREES AWARDED DURING THIS REPORTING PERIOD:

J. K. Butler
R. Ayekavadi
C. S. Yeh

9. REPORT OF INVENTIONS (BY TITLE ONLY):

Jerome K. Butler
Department of Electrical Engineering
Southern Methodist University
Dallas, TX 75222

BRIEF OUTLINE OF RESEARCH FINDINGS

Experimental work over the past period continued with design and fabrication of periodic waveguides fabricated with Al_2O_3. Some of the early waveguides made during the program had relatively short grating sections, however, lately we have started making much longer grating regions. Our new waveguide structures seem to be excellent in quality and tend to exhibit classical ω–β dispersion characteristics around the second Bragg condition. The modal attenuation coefficient α also has the classically sharp null condition at the second Bragg frequency. The experimental plots are shown below.

To perform necessary characterization of the structures, the far-field radiation patterns were also measured. In our previous report we discussed the experimental configuration that split the oscillator power that feeds the grated waveguide structure. With the new arrangement, power is launched into the dielectric waveguide from both the right and left directions. (This configuration corresponds to a situation where the grating region would separate two oscillators to be locked into one coherent system. The grating acts both as a feedback mechanism as well as the antenna.) Depending on the relative phase of the two inputs, the far-field radiation pattern can be maximized or minimized. The two-side incidence case shows that in the out of phase condition, the radiation power is minimum at the second Bragg frequency.

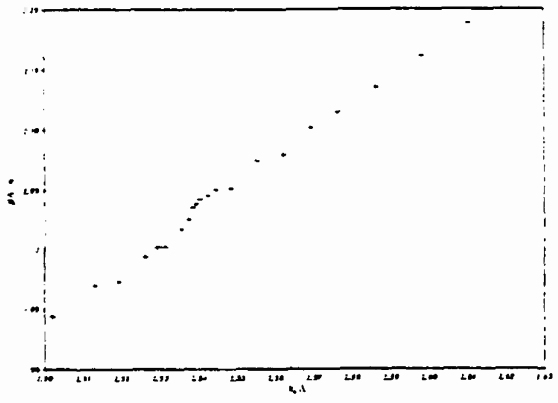

Figure 3: Dispersion relation of the waveguide at.

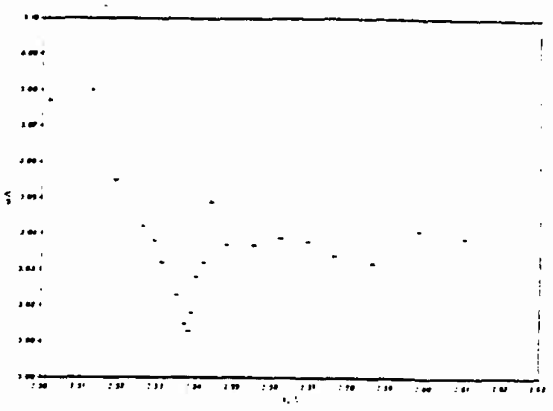

PROGRESS REPORT

TWENTY COPIES REQUIRED

1. ARO PROPOSAL NUMBER: 25339-EL

2. PERIOD COVERED BY REPORT: 1 July 1991 - 31 December 1991

3. TITLE OF PROPOSAL: Millimeter-Wave Appl of Semiconductor Dielectric Waveguides with Plasma Layers (Surface or Buried)gen fr semicond laser

4. CONTRACT OR GRANT NUMBER: DAAL03-89-K-0029

5. NAME OF INSTITUTION: Southern Methodist University

6. AUTHORS OF REPORT: Jerome K. Butler

7. LIST OF MANUSCRIPTS SUBMITTED OR PUBLISHED UNDER ARO SPONSORSHIP DURING THIS REPORTING PERIOD, INCLUDING JOURNAL REFERENCES:

J. K. Butler, W. E. Ferguson, G. A. Evans, P. Stabile and A. Rosen, "A boundary element technique applied to the analysis of waveguides with periodic surface corrugations," IEEE J. Quantum Electronics, Submitted for publications. (Review attached).

C. S. Yeh, N. Urimindi, J. K. Butler, G. A. Evans, P. J. Stabile, and A. Rosen, "Experimental and theoretical investigation of periodic corrugated dielectric waveguides," OE Lase '92, 19-25 January 1992, Los Angeles, CA. (Invited Paper to be presented.)

8. SCIENTIFIC PERSONNEL SUPPORTED BY THIS PROJECT AND DEGREES AWARDED DURING THIS REPORTING PERIOD:

J. K. Butler
R. Ayekavadi
C. S. Yeh
J. Liu
N. Urimindi

9. REPORT OF INVENTIONS (BY TITLE ONLY):

Jerome K. Butler
Department of Electrical Engineering
Southern Methodist University
Dallas, TX 75222

BRIEF OUTLINE OF RESEARCH FINDINGS

Experimental and theoretical progress over the past period has progressed at an excellent rate. We are extremely happy with the correlation of theoretical calculations with experimental measurements of the periodic waveguides fabricated on the Al_2O_3 material.

In addition to the improvement of the design program of the periodic waveguides, we have performed simulation experiments of waveguide structures that have excited plasma layers. These new periodic structures have a fixed grating waveguide coupled with a separate confined plasma layer in the opposed waveguide surface. Typically the new structures would be fabricated on wafers composed of either (1) silicon on sapphire (the grating formed in the sapphire layer and the plasma layer excited in the silicon layer), or (2) gallium arsenide on aluminum gallium arsenide (the grating formed in the aluminum gallium arsenide layer and the plasma layer excited in the gallium arsenide layer). In our experiments, we started with an Al_2O_3 waveguide with a grating formed on one surface. The waveguide was designed to radiate broadside. Next, a layer of metal foil was attached to the waveguide on the side opposite the grating layer. (The metal foil was to simulate an excited plasma layer with high electron/hole concentrations.) The radiation pattern measured with the foil attached produced a beam at about 30° to the broadside direction. This implies that a corresponding silicon on sapphire structure would electronically scan about 30°.

Review of submitted paper:

Dear Dr. Walpole

Here is the review of the manuscript by Butler et. al. which was passed to me by Paul Jessop.

Report on "A Boundary Element ...."

This paper is excellently written and represents an important contribution to the analysis of integrated gratings. The paper also has considerable pedagogical value and should therefore be published as is.

A Boundary Element Technique Applied to the Analysis of Waveguides with Periodic Surface Corrugations *

J. K. Butler and W. E. Ferguson
Southern Methodist University
Dallas, TX 75275
G. A. Evans, P. Stabile, and A. Rosen
David Sarnoff Research Center
Princeton, NJ 08543-5300

August 25, 1991

Abstract

Boundary integral formulation is used to characterize Floquet-Bloch modes of two-dimensional multilayered periodic waveguides. A new technique is described for matching fields inside the grating to those external to the grating region. Although a simple four layer structure is used to illustrate the method an extension to multilayer waveguide structures is straight forward. The mathematical formalism has been simplified, allowing for more efficient computations using fast Fourier transform algorithms.

*Supported in part by the Army Research Office and the Department of the Air Force.

THEORITICAL AND EXPERIMENTAL INVESTIGATION OF PERIODIC CORRUGATED DIELECTRIC WAVEGUIDES*

C. S. Yeh, N. Urimindi and J. K. Butler

Department of Electrical Engineering
Southern Methodist University, Dallas, TX 75275

P. Stabile and A. Rosen

David Sarnoff Research Center, Princeton, NJ 08543-5300

ABSTRACT

In this experimental study we investigate the guided mode-radiation mode coupling of periodic dielectric waveguides. The dispersion relation and the attenuation constant along the dielectric waveguide were measured around the second Bragg frequency. The far field radiation pattern was also measured. Floquet theorem was applied to solve wave equations. Zero order approximation was used in the design of waveguides. For surface emitting structures used in surface emitting lasers and couplers, the most important parameter is the dispersion relation and attenuation constant along the corrugated waveguide around the second Bragg frequency. The dispersion and attenuation measurement shows that the attenuation constant minimum occurs at the second Bragg frequency. This corresponds to the maximum Q point of the corrugated waveguide. Two side incidence shows that in the out of phase condition the radiation power is minimum at the second Bragg frequency and have two lobes.

* Supported in part by the Army Research Office.

PERSONNEL

Personnel listed below were supported on this project.

Professor Jerome K. Butler was the Principle Investigator on this project. He has developed both a theoretical and experimental program in millimeter-wave systems at Southern Methodist University. Most of the experimental work in our laboratory has been done in W-Band systems. In addition, many of the ideas and work of this program have been tied to the experimental surface emitter program at the David Sarnoff Research Center.

Dr. George Hadjicostas participated in the early work of this program. He developed some early experiments of plasma excitation in silicon waveguides. He was also key in the theoretical analysis of periodic waveguides using the Boundary Element Method.

Mr. Raj Ayekavadi was a graduate student who developed our techniques for fabricating periodic structures in Al_2O_3 waveguides. He also developed a theoretical multilayer slab model and the associated computer code, to fabricate periodic structures in the W-Band spectrum. Mr. Ayekavadi is presently writing his dissertation and should be completed this academic year.

Dr. Chao Suan Yeh has just completed his dissertation "Theoretical and Experimental Investigation of Slab Waveguides with Periodic Grating Layers." Dr. Yeh has been a very innovative experimentalist. He developed most of the experimental apparatus used for testing the periodic structures at the W-Band frequencies. He suggested and performed the experimental measurements for the plasma simulated waveguides and the dispersion curves that characterize the periodic structures.

Mr. N. Urimindi is relatively new to this project and is making periodic waveguide structures in both silicon and alumina waveguide materials. High resistive silicon is being used so that we can integrate the periodic structures with active sources.

Mr. Jin Liu was recently added to the project. He has been concerned with the development of new theoretical models. His major work is concerned with development of two dimensional models and the w-b diagrams and corresponding radiation characteristics of plasma induced structures.

PUBLICATIONS

The following publications were output from the work on this project.

G. Hadjicostas, J. K. Butler, G. A. Evans, N. W. Carlson and R. Amantea, *"A Numerical Investigation of Wave Interactions in Dielectric Waveguides with Periodic Surface Corrugations,"* IEEE J. Quantum Electron., vol. QE-26, pp. 893-902, May 1992. This publication was one of our initial theoretical studies. The principle contribution was an understanding of the boundary element method and its application to periodic structures. This technique is probably the most accurate method for analyzing periodic structures. Most of the early theoretical models were only approximate and could not handle periodic strucutures with alternating regions of low and very high conductivity (metal in the limiting case) materials.

R. Ayekavadi, C. S. Yeh, J. K. Butler, G. A. Evans, P. Stabile and A. Rosen, *"Experimental Verification of Grating Theory for Surface Emitting Structures,"* Proceedings SPIE, vol 1418, pp. 74-85, 1991. The publication is the first to compare the experimental and theoretical results of periodic structures fabricated with alumina material.

C. S. Yeh, N. Urimindi, J. K. Butler, P. Stabile, and A. Rosen, *"Theoretical and Experimental Investigation of Periodic Corrugated Dielectric Waveguides,"* Proceedings SPIE, vol 1634, pp. 50-60, 1992. The initial studies of radiation from a grating region with input from both ends was presented in this paper. A major concern of the surface emitting system which locks several sources together to form a single coherent oscillator is that the system will emit no radiation, i.e., the natural mode is totally internal. An alternative approach to a multiple source locked oscillator system is to have a master oscillator feeding a system of sources (amplifiers), grating antennas, sources, grating antennas, etc.

J. K. Butler, W. E. Ferguson, G. A. Evans, P. J. Stabile, and A. Rosen, *"A Boundary Element Technique Applied to the Analysis of Waveguides with Periodic Surface Corrugations,"* IEEE J. Quantum. Electron., vol QE-28, pp. 1701-1709, Jul. 1992. This publication presents a completely new analytical method for analyzing periodic waveguides. The power this new approach is that it can be applied to dielectri waveguides with more complicated dielectric profiles. In particular, millimeter wave sturctures with an inhomogeneous layer of plasma and a separate periodic layer.

R. Ayekavadi, C. S. Yeh, J. K. Butler, G. A. Evans, P. Stabile, and A. Rosen, *"Design and Performance of Corrugated Waveguides Based on Slab Waveguide Principles,"* Emerging Optoelectronic Technologies Conference, Indian Institute of Science, Bangalore, India, Dec. 16-19, 1991.

N. Urimeidi, C. S. Yeh, J. Liu and J. K. Butler, *"Surface Emitting Characteristics of Silicon Waveguides,"* To be presented at 17th International Conference on Infrared and Millimeter waves, Dec. 13-18, California Inst. of Tech., Pasadena. California.

C. S. Yeh, N. Urimindi, J. Liu and J. K. Butler, *"Expermental analysis of Metal Coated Dielectric Waveguides,"* To be presented at 17th International Conference on Infrared and Millimeter waves, Dec. 13-18, California Inst. of Tech., Pasadena. California.

A Numerical Investigation of Wave Interactions in Dielectric Waveguides with Periodic Surface Corrugations

G. HADJICOSTAS, JEROME K. BUTLER, FELLOW, IEEE, GARY A. EVANS, SENIOR MEMBER, IEEE, NILS W. CARLSON, MEMBER, IEEE, AND ROBERT AMANTEA, SENIOR MEMBER, IEEE

Abstract—The modal properties of planar multilayered waveguides with a rectangular surface corrugation are investigated. A rigorous full Floquet numerical analysis is performed for the fundamental TE mode of the infinite periodic structure. The algorithm is based on a boundary element solution of the integral wave equation in the grating region. A generalized transverse resonance-type matrix equation is sought that matches all continuity, periodicity, and boundary conditions. The resonant solutions of this characteristic equation represent all the surface and leaky waves supported by the structure. The exact dispersion characteristics, as well as the amplitudes of the space harmonics, are computed and discussed in connection to radiation losses and coupling mechanisms near resonant Bragg conditions. In particular, a specific double-heterostructure GaAs–AlGaAs waveguide geometry has been examined in detail. Under appropriate boundary conditions, an estimate of the power reflection coefficient is computed for a finite length distributed Bragg reflector.

I. Introduction

IN this paper, we present a rigorous numerical analysis of mode propagation in periodic optical waveguides with a rectangular surface corrugation. This class of open thin-film structures has attracted considerable interest because of their important applications in distributed Bragg reflector (DBR) and distributed feedback (DFB) lasers, beam steering devices, and as output and input couplers.

The analysis of wave propagation in transversely bounded open periodic waveguides becomes complicated by the possible presence of radiated waves. The problem has been analyzed in the past by numerous methods and under a wide variety of possible assumptions. The coupled wave formulation [1]–[9] and the modal approach [10]–[16] are among the most commonly used techniques. In their complete form, both techniques can produce exact results. They constitute merely alternate representations of the electromagnetic field inside the grating: one in terms of phase matched, oppositely traveling waves with slowly varying amplitudes, and the other in terms of waves with an infinite number of space harmonics (Floquet–Bloch waves) with amplitudes which are inherently adjusted as to satisfy the grating boundary conditions. It is the introduction of various simplifying assumptions that reduces the full and exact formulations to the approximate theories encountered in the literature.

Typical assumptions in the coupled wave formulation (confusingly referred to as coupled mode approach) include: 1) retaining only one scattered wave in addition to the fundamental (two-wave coupled wave theory), and 2) neglecting second derivatives of the field amplitudes (first order, two- or multiwave coupled wave theory). These assumptions frequently yield simple analytical results; however, they often require *a priori* knowledge of the coupling phenomena and the physical mechanisms involved.

On the other hand, the modal formulation (otherwise known as the Floquet–Bloch approach) is inherently accurate. Even though the wave amplitudes are obtained by a multiple-step computational process, the formulation does not require any *a priori* assumptions. Based on the results obtained from the rigorous analysis, simplifications can be subsequently introduced that may discard waves with negligible amplitudes (truncated two- or four-wave modal theory).

Recent investigations of second-order gratings using the coupled wave approach [17]–[18] describe the field in the grating as a sum of two oppositely propagating waves $A(z)$, $B(z)$ with slowly varying amplitudes and propagation constants K and $-K$ where $K = 2\pi/\Lambda$ and Λ is the grating period. The presence of radiation and other scattered waves simply affects the coupling between the amplitudes $A(z)$ and $B(z)$ through the introduction of added constants to the usual set of two-wave coupled wave equations. These constants have the form of overlap integrals and represent the reactions of the various scattered waves back to their generating or phase-matched oppositely traveling waves. It is assumed that only the two fundamental waves give rise to and have feedback from other scattered waves. In addition, higher derivatives and other terms are excluded from the coupled wave equations. The method [17], [18] is essentially a perturbation–iteration technique in which the initially assumed field distribution is modi-

Manuscript received October 5, 1989; revised October 10, 1989. This work was supported in part by the U.S. Army Research Office and the U.S. Department of the Air Force.

G. Hadjicostas and J. K. Butler are with the School of Engineering and Applied Science, Southern Methodist University, Dallas, TX 75275.

G. A. Evans, N. W. Carlson, and R. Amantea are with the David Sarnoff Research Center, Princeton, NJ 08543.

IEEE Log Number 9034735.

0018-9197/90/0500-0893$01.00 © 1990 IEEE

fied by the improved perturbation method suggested in [19]. The resulting set of equations is thus solved in a self-consistent manner that allows them to be used even with thick corrugated gratings.

Peng *et al.* [14] used the modal formulation to numerically solve the cases of holographic and rectangularly corrugated multilayered films. As opposed to the perturbation technique discussed above, here, the exact field representations are assumed in each region and are subsequently matched at the layer boundaries. In the uniform regions surrounding the grating region, the field is expressed as an infinite summation of harmonics $\psi_n(x)\exp(-\gamma_n z)$ which may be regarded as modes with a simple sinusoidal transverse variation, which propagate along z with a propagation constant γ_n ($\exp(j\omega t)$ assumed). Inside the grating region, the transverse variation of $\psi_n(x)$ becomes considerably more complicated because of the coupling between all of the space harmonics due to the periodic variation in the dielectric constant in this region. For every nth harmonic, the transverse propagation constants and wave amplitudes describing $\psi_n(x)$ have to be calculated beforehand by numerical solution of a truncated matrix eigenvalue problem.

The computational method described in this paper relies on the numerical solution of the integral wave equation inside the grating region. This formalism has distinct advantages over the more traditional ones, especially when the boundary conditions are imposed through a collocation (point-matching) technique. The unknown field quantities together with all the boundary conditions of the problem are explicitly incorporated in the defining equation. For the problem at hand, the boundary conditions on the longitudinal interfaces of the grating layer are functionally known because of the Floquet expansion of the fields in the uniform layers above and below it. On the other hand, the boundary conditions for the transverse interface between the periodic unit cells are naturally provided by Floquet's theorem and continuity requirements. Thus, the method can be applied in a rather straightforward way towards a rigorous solution of the periodic problem, without any *a priori* assumptions and to a user-specified accuracy. The boundary integral formulation is a natural choice for this problem because we seek the field solution only on the grating layer interfaces in order to set up a transverse resonance-type characteristic equation for the propagating mode.

In the following section, the determinantal equation for the propagating waves is set up. A brief discussion describing the transformation of Maxwell's equation from its usual differential form to an integral equation is presented. Some considerations regarding the selection of the appropriate Green's function and the handling of existing singularities are pointed out. A boundary element method [20]–[21] is subsequently applied to discretize the integral equation; the resulting homogeneous matrix equation together with appropriate continuity and periodicity conditions constitutes the secular (determinantal) equation for the problem. Essentially, the procedure is the one applied by Matsumoto *et al.* [15] for the solution of the metallic/plasma stripe leaky wave antenna.

In Section III, the results are described in terms of dispersion–attenuation (Brillouin) diagrams $k_0\Lambda - \beta\Lambda/\alpha\Lambda$. Furthermore, the magnitudes of the most important space harmonics are given. The spectral characteristics of the radiating (fast harmonic) constituent of the propagating wave are examined before and after the second Bragg resonant condition. In Section IV, based on the amplitude findings of the previous section, an estimate of the power reflection coefficient from a finite length second-order DBR geometry is calculated. A selected four-wave (two fundamental components and two associated space harmonics) coupled wave formalism has been applied, based on the fact that the amplitude of the (-1) radiating component decreases to negligible levels in the vicinity of the second Bragg.

II. Mathematical Formulation

Consider the double-heterostructure GaAs–AlGaAs waveguide geometry with a grating shown in Fig. 1. The substrate (AlGaAs) and superstrate (air) regions are assumed to be half spaces. The grating consists of the periodic juxtaposition of homogeneous rectangular Region A (dielectric constant κ_3) and Region B (dielectric constant κ_1). A time harmonic TE wave propagates in the axial z direction as $\exp(j\omega t - \gamma_0 z)$, with the field invariant with respect to y. The complex propagation constant $\gamma_0 = \alpha + j\beta$. Since the dielectric materials of such a structure are regionally homogeneous, the field in each region satisfies the scalar Helmholtz equation

$$\left(\frac{\partial^2}{\partial x^2} + \frac{\partial^2}{\partial z^2}\right)\Psi(x, z) + k_0^2\kappa\Psi(x, z) = 0 \qquad (1)$$

where for the TE case, $\Psi = E_y$; k_0 is the free-space propagation constant and κ is the relative dielectric constant of the region. In the uniform layers above and below the grating, the field expressions have to appear in the Floquet form in order to satisfy the boundary conditions on the grating surface. In the ith layer, the solution becomes

$$\Psi_i(x, z) = \sum_n \psi_{in}(x)\exp(-\gamma_n z) \qquad (2)$$

where

$$\gamma_n = \alpha + j\beta_n = \alpha + j(\beta + nK); \quad n = \cdots, -1, 0, 1, \cdots. \qquad (3)$$

(It should be noted that β_0 is identical to β.) The transverse wave functions outside the grating are given by

$$\psi_n(x) = \begin{cases} A_{1n}\exp\left[h_{1n}(w_2 - x)\right]; & x > w_2 \\ A_{3n}\cos(h_{3n}x) + B_{3n}\sin(h_{3n}x); & -w_3 < x < 0 \\ A_{4n}\cos(h_{4n}x) + B_{4n}\sin(h_{4n}x); & -w_3 - w_4 < x < -w_3 \\ A_{5n}\exp\left[h_{5n}(w_3 + w_4 + x)\right]; & x < -w_3 - w_4 \end{cases} \qquad (4)$$

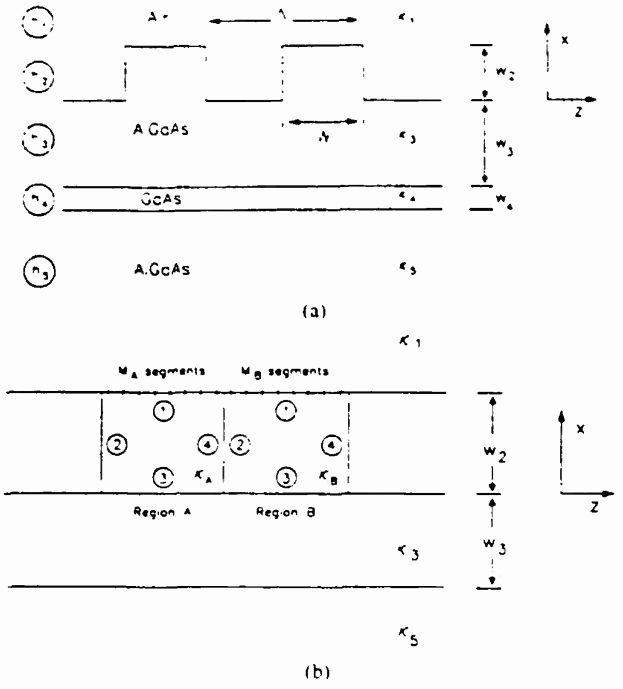

Fig. 1. (a) The basic geometry of the grated region for the waveguide. The relative dielectric constant $\kappa(x, z) = \kappa(x, -z)$. (b) A general unit cell of the rectangular corrugation where Region A has $\kappa_4 = \kappa_3$ and $\kappa_B = \kappa_1$.

and the transverse wavenumbers satisfy

$$h_{in}^2 = -(k_0^2\kappa_i + \gamma_n^2); \qquad i = 1, 5$$
$$h_{in}^2 = +(k_0^2\kappa_i + \gamma_n^2); \qquad i = 3, 4. \tag{5}$$

If the layer has finite thickness, there are two amplitude coefficients A_{in} and B_{in}. On the other hand, in semi-infinite layers, we keep only the component whose field decays exponentially away from the structure, provided the spatial harmonic is proper. In addition, a relation between the partial wave amplitudes ψ_n in each uniform layer is found by imposing continuity of the tangential field components (E_z, dE_z/dx) across the layer boundaries.

Inside the grating layer, recall that the coefficients ψ_n are all coupled together. We choose to avoid the laborious exact solution for the field everywhere inside the grating and we seek a relation between Ψ and its normal derivative only along the boundary enclosing the homogeneous regions R_A and R_B. Towards this goal, we convert (1) into an integral equation. Results based on the numerical solution of integral equations have the advantage of being accurate even if the boundary conditions are only approximately met. In particular, for the problem at hand, the field and fluxes will be assumed piecewise constant and a collocation (point matching) technique will be used to impose field continuity and periodicity.

According to [20], through the use of Green's second identity, (1) becomes

$$\iint_R \left[G(\kappa, \bar{r}, \bar{r}_0)\nabla_t^2\Psi(\bar{r}) - \Psi(\bar{r})\nabla_t^2 G(\kappa, \bar{r}, \bar{r}_0)\right] ds = \oint_c \left[G(\kappa, \bar{r}, \bar{r}_0)\frac{\partial\Psi(\bar{r})}{\partial n} - \Psi(\bar{r})\frac{\partial G(\kappa, \bar{r}, \bar{r}_0)}{\partial n}\right] dl. \tag{6}$$

The left-hand side is a surface integral over the transverse plane Region R; the right-hand side is a closed line integral over the boundary contour c that encloses R. The quantity $\partial/\partial n$ denotes an outward normal derivative. In the above equation, if G is chosen to satisfy

$$\nabla_t^2 G(\kappa, \bar{r}, \bar{r}_0) + k_0^2\kappa G(\kappa, \bar{r}, \bar{r}_0) = -\delta(|\bar{r} - \bar{r}_0|) \tag{7}$$

then (6) reduces to

$$\Psi(\bar{r}) = \oint_c \left[G(\kappa, \bar{r}, \bar{r}_0)\frac{\partial\Psi(\bar{r}_0)}{\partial n} - \Psi(\bar{r}_0)\frac{\partial G(\kappa, \bar{r}, \bar{r}_0)}{\partial n}\right] dl \tag{8}$$

where $\bar{r} \in R$, excluding c while $\bar{r}_0 \in c$.

Solutions of (7) are Bessel functions. For a finite domain, any combination $C_0 J_n - \frac{1}{4} Y_n$ can be used (note that J_n is a solution of (7) only when $\bar{r} \neq \bar{r}_0$). The coefficient of Y_n is determined to be $-1/4$ from the singularity condition at $\bar{r} = \bar{r}_0$. For an infinite domain, C_0 must equal $-j/4$ because only the second-order Hankel function $-j\frac{1}{4}H_n^{(2)} = -j\frac{1}{4}(J_n - jY_n)$ satisfies the proper radiation conditions (outward traveling waves, vanishing at infinity). Analytically, the results should be independent of C_0, but since the computations are done numerically, a slight effect on the convergence rate of the results has been noticed. Since we found no consistent way of optimizing the value of C_0, unless stated otherwise, the zeroth-order second-kind Bessel function [28] shall be used throughout, i.e.,

$$G(\kappa, \bar{r}, \bar{r}_0) = -\tfrac{1}{4}Y_0(k_0\sqrt{\kappa}\,|\bar{r} - \bar{r}_0|). \tag{9}$$

In the limit of $\bar{r}$ approaching the boundary, (7) becomes [20]

$$\frac{1}{2}\Psi(\bar{r}) = \oint_c \left[G(\kappa, \bar{r}, \bar{r}_0)\frac{\partial\Psi(\bar{r}_0)}{\partial n} - \Psi(\bar{r}_0)\frac{\partial G(\kappa, \bar{r}, \bar{r}_0)}{\partial n}\right] dl \tag{10}$$

where $\bar{r}, \bar{r}_0 \in c$ and $\oint_c dl$ denotes the principal value line integral with the contribution of the singularity already accounted for.

III. Boundary Element Method

To obtain a numerical solution, the integral equation (10) is discretized to a finite size matrix equation. The relation between Ψ and $\partial\Psi/\partial n$ for each region is independent of the other, and thus the equations are treated separately. Following [20], we can write (10) as

$$\tfrac{1}{2}u_i = \sum_{j=1}^{N} q_j \mathcal{S}_{ij} - \sum_{j=1}^{N} u_j \mathcal{D}_{ij} \tag{11}$$

where

$$\mathcal{S}_{ij} = \oint_{c_j} G(\kappa, \bar{r}_i, \bar{r}_j)\, dl$$
$$\mathcal{D}_{ij} = \oint_{c_j} \frac{\partial G(\kappa, \bar{r}_i, \bar{r}_j)}{\partial n}\, dl$$

and u_j and q_j are the field amplitude and flux, assumed constant over the jth boundary segment.

Upon placing $\mathcal{K} = \mathcal{D} + \frac{1}{2}\mathcal{I}$ where $\mathcal{I}$ is the unit matrix, (11) becomes

$$\mathcal{K}_R \bar{u}_R = \mathcal{S}_R \bar{q}_R \tag{12}$$

which, for every region $R(=R_A, R_B)$, relates the value of u at the midnode i, with the values of u and $\partial u/\partial n$ at every other node j, including $j = i$.

All the line integrals along the elements c_j; $j \neq i$ can be calculated numerically using a four-point quadrature rule [27]. For the $j = i$ case, the integration path $c_j = c_i$ contains the "source point" $\bar{r}_i = (x_i, z_i)$ and a logarithmic-type singularity is present. Even though this singularity is analytically integrable, a logarithmic Gauss quadrature rule has been used again in order to maintain good accuracy.

For each region, (12) represents a set of N homogeneous equations with $2N$ unknown field and field derivatives. The necessary extra equations needed are provided by imposing continuity across the $x = 0$ and $x = w_2$ interfaces, as well as continuity and periodicity conditions across the Region A–Region B interface. After appropriate substitution, we end up with a system of $2N$ equations in $2N$ unknowns; the coefficients of the $2N$ unknown boundary fields and their normal derivatives form the complex elements of the matrix $\mathcal{F}$ [15]. Such a homogeneous system of linear equations will have a nontrivial solution provided that the determinant of the matrix $\mathcal{F}$ vanishes. Since the only unknown in $\mathcal{F}$ is γ_0, the resonant solutions, if any, of the determinantal equation will give the propagation constants for the structure modes:

$$\det\left[\mathcal{F}(\gamma_0)\right] = 0. \tag{13}$$

Following the computation for γ_0, all the unknown fields and derivatives can be evaluated under a suitable normalization condition. A complex root finder routine based on Muller's method has been used for the numerical evaluation of the above secular equation. The Floquet amplitudes for the field expansion in all the uniform regions can subsequently be evaluated.

IV. Numerical Results

Before proceeding to the numerical results, some further discussion of (13) is necessary. The dispersion relation (13) depends on γ_0 explicitly and also through the various transverse propagation constants h_n. For the waveguide geometry examined here, there exists only one fast radiating harmonic ($n = -1$). Consider the semi-infinite air region ($x > w_2$). According to (5), the wave propagation constant in the transverse x direction for this harmonic will be (we have dropped the subscript that denotes layer 1)

$$h_{-1}^2 = -(k_0^2 + \gamma_{-1}^2) \tag{14}$$

which is a double-valued function of γ_{-1}. This means that there might exist different solutions corresponding to the different branches of (14) chosen. A branch cut is introduced as in Fig. 2, which maps the h_{-1}^2 plane onto the right plane of h_{-1} that corresponds to "proper" spatial harmonics or the left plane of h_{-1} that corresponds to "improper" waves. From (3),

$$h_{-1}^2 = -(k_0^2 + \alpha^2 - \beta_{-1}^2) - j2\alpha\beta_{-1}. \tag{15}$$

Unlike the first Bragg condition, the vicinity of the second Bragg exhibits many interesting phenomena, as far as the character of the modal solutions is concerned. If Λ has a value such that $\beta_0 < K$, then,

$$\beta_{-1} = \beta_0 - K < 0;$$

thus,

$$\text{Im}\,(h_{-1}^2) > 0$$

$$\text{Re}\,(h_{-1}^2) < 0$$

which puts h_{-1}^2 in the second quadrant of the h^2 plane (Fig. 2). The proper branch solution has h_{-1} lying in the region $I_p (h_{-1} \in I_p)$ of Fig. 2. Since the wave propagates in the x direction as $\exp(-h_{-1}x)$, this branch corresponds to radiation outwards with an exponential decay at infinity. The improper branch, however, would correspond to incoming radiation from infinity.

On the other hand, if the second Bragg condition is crossed, from (15), we get

$$\text{Im}\,(h_{-1}^2) < 0$$

$$\text{Re}\,(h_{-1}^2) < 0.$$

Thus, h_{-1}^2 is in the third quadrant in the h^2 plane, which puts h_{-1} either in the IV_p or IV_i sector (Fig. 2). In this case, it is the improper branch which has to be chosen for outgoing radiation waves. It is clear that waves with transverse propagation constants in the IV_i sector possess a negative real part which results in nonspectral wave solutions which grow exponentially with x.

Thus, during the crossing of the second Bragg condition, h_{-1}^2 is allowed to cross the branch cut and h_{-1} continuously shifts from the proper wave plane to the improper plane. It is noted that even though this is not the only possible choice, it is the only one that leads to a solution γ_0 of (12).

The plots in this section pertain to the structure of Fig. 1 with $\kappa_1 = 1$, $\kappa_2 = \kappa_4 = 3.4^2$, $\kappa_3 = 3.6^2$, $w_2 = 0.2\ \mu\text{m}$, and $w_3 = 0.06\ \mu\text{m}$. Fig. 3 shows the convergence of the real part α and imaginary part β of the fundamental propagation constant γ_0 as a function of the total number of elements used to discretize the boundary around each region. The operation point has been chosen in the vicinity of the second Bragg. The results have been computed using the second-kind Bessel function Y_0 and the second-kind Hankel function $H_0^{(2)}$. It is observed that because of the numerical solution of the integral wave equation, the choice of Green's function affects the computed results. As the number of boundary elements increases, the result converges to the same answer independently of the choice of Green's function. This independence means that the

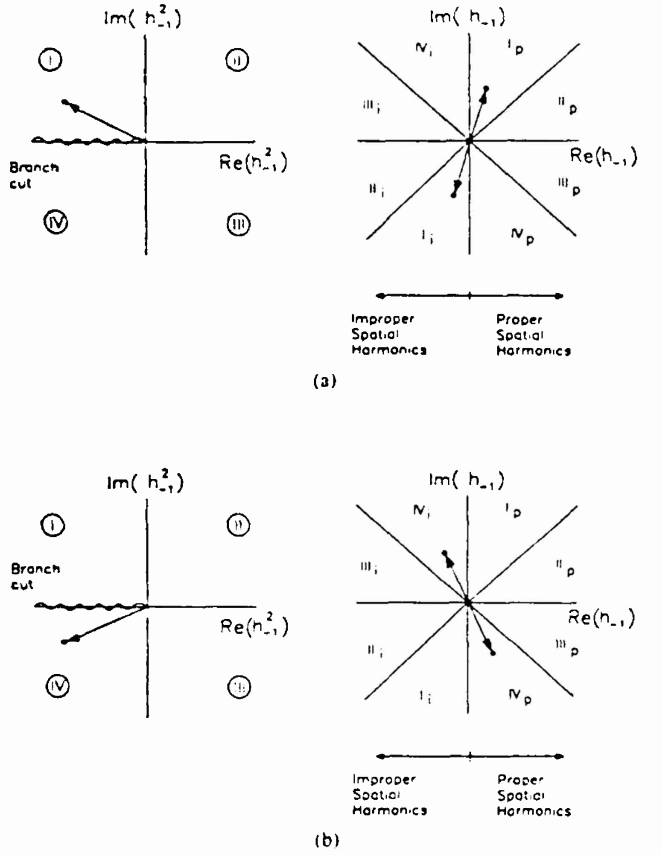

Fig. 2. Mapping of the h_{-1}^2 plane onto the h_{-1} plane. (a) Below the second Bragg, and (b) above the second Bragg.

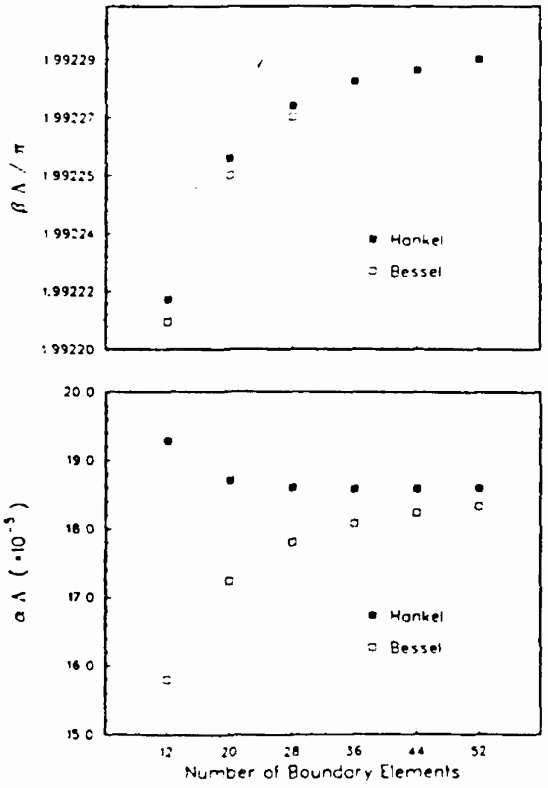

Fig. 3. Solution convergence with increasing number of segments for two different choices of Green's functions.

numerical solution behaves as expected from the theoretical analysis, and thus the discretized matrix equation is properly modeling the wave equation in that region. All subsequent results have been computed using 11 boundary elements per side.

Fig. 4 shows the transverse mode profile at $z = 0$ as calculated from the summation in (2). The summation has been truncated to 22 space harmonics (from -11 to 10). Since the radiating -1 harmonic has the least decay in the transverse direction as compared to the others, it represents the major contributor to the field at distances far away from the grating. Near the guiding layer, it is the -2 and the 0 harmonic which are predominant.

The solution of (13) is presented in terms of dispersion $k_0\Lambda$ versus $\beta\Lambda/\pi$ and attenuation $k_0\Lambda$ versus $\alpha\Lambda$ diagrams. The axes have been multiplied by the period Λ in the plots shown. In Fig. 5, the scan in Λ extends from below the first Bragg condition to past the second. The triangular slow-wave regions for the air (light hatching) and the substrate (heavy hatching) are also shown for ease of interpretation [26]. We observe that in this case, β appears to coincide with the unperturbed propagation constant and runs along the boundary of the substrate triangle. Just after the intense surface-wave stopband of the first Bragg, the wave starts to radiate in the substrate, and the substrate beam scans towards its broad side. As soon as $\beta\Lambda$ crosses the air triangle interface, another beam appears in the air space. The attenuation α remains almost constant up to the second Bragg where it experiences a sudden drop and a subsequent leaky-wave stopband before it goes back to normal.

Fig. 6 examines in extreme magnification the details of the first Bragg stopband for two different grating toc h heights. Inside the slow wave triangle, all harmonics represent bounded waves. Since there is no radiation and since the dielectric materials have been assumed lossless, α is zero except during the first Bragg interaction where γ_0 becomes complex. The increased perturbation caused by the thicker $w_2 = 0.2$ μm grating results in a slight increase in bandwidth of the stopband interaction. Fig. 7 is a plot of the dominant Floquet harmonics, normalized with respect to the fundamental, in the vicinity of the first Bragg stopband. In the $\beta\Lambda = \pi$ region, the $n = -1$ and $n = 0$ harmonics need to have exactly the same amplitude in order to satisfy the boundary conditions on the grating surface. The same pairing occurs between the $n = -2$ and $n = 1$, and so forth. In a true surface-wave stopband, the pairing of all harmonics is complete, resulting in a Poynting vector which is identically zero for every x.

In Fig. 8, a detailed magnification around the second Bragg condition is shown. In contrast to the first Bragg, the $\beta\Lambda = 2\pi$ condition is satisfied only at a single point rather than for a whole region. At this point, α exhibits a sharp drop. It seems that a zero in the attenuation coefficient is the general behavior for transversely bounded periodic structures. The propagation constant β approaches the Bragg condition with a zero slope and then rises again in a manner representing a stopband, but with a slope pro-

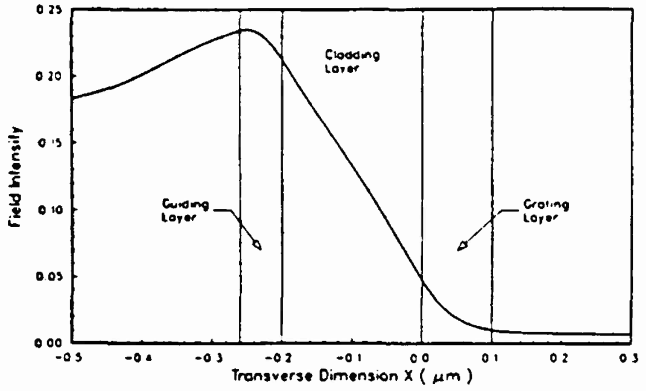

Fig. 4. Transverse mode profile of the periodic structure in the vicinity of the second Bragg for $z = -W/2$.

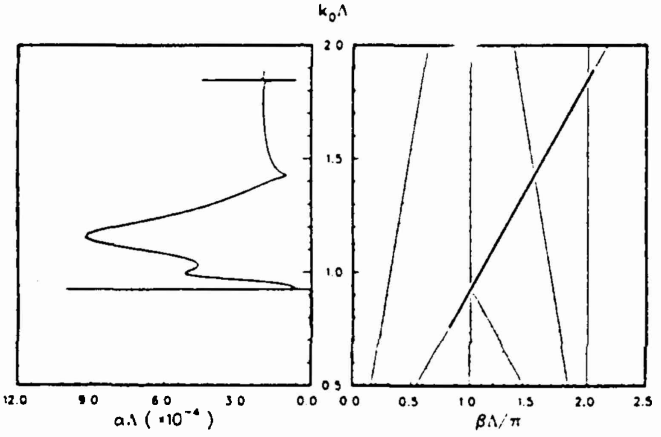

Fig. 5. Dispersion and attenuation diagrams including the first and second Bragg resonances.

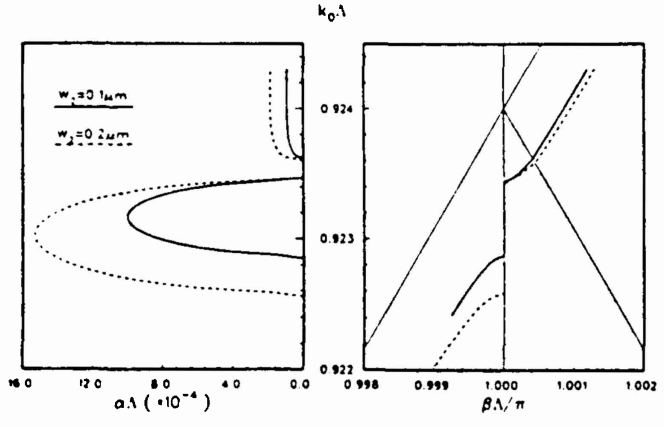

Fig. 6. Magnification of Fig. 5 around the first Bragg resonance for two grating tooth heights.

portional to the amount of perturbation caused by the grating. During this transition, α experiences a resonant peak, similar to that observed in the vicinity of the first Bragg condition. Since in this region the -1 harmonic is an improper leaky wave, the corresponding region is referred to as a leaky-wave stopband, even though the resemblance is only superficial.

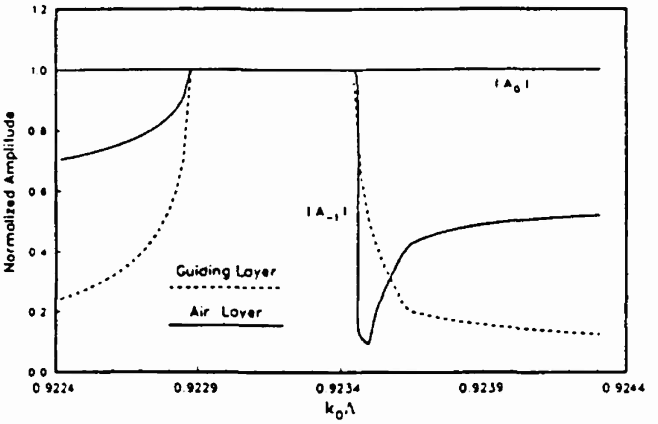

Fig. 7. Normalized amplitudes of the most important space harmonics around the $\beta\Lambda = \pi$ stopband for $W_2 = 0.1$ μm.

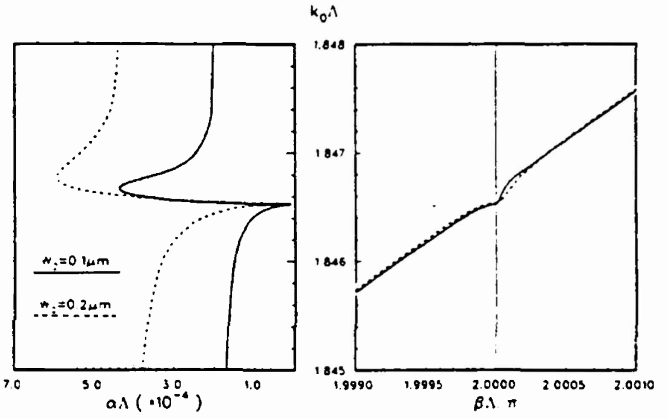

Fig. 8. Magnification of Fig. 5 around the second Bragg resonance for two grating tooth heights.

Fig. 9 is a plot of the magnitude of the predominant normalized Floquet harmonics in the guiding layer in the vicinity of the second Bragg interaction. The parameters for the configuration are those of Fig. 1 with $w_2 = 0.1$ μm. The $n = -2$ harmonic momentarily acquires the same weight in the field representation as the fundamental, with the radiating $n = -1$ harmonic dropping three orders of magnitude. The power picture in the $\beta\Lambda = 2\pi$ region is radically different from the $\beta\Lambda = \pi$ region of Fig. 6. Because of the imperfect pairing of the space harmonics (the $n = -1$ does not take part in the coupling), the Poynting vector does not vanish identically for every x. Near the guiding layer, it is positive because of the contribution of the fundamental harmonic; far from the grating, it becomes negative because of the predominance of the $n = -1$ harmonic. The interaction does not result in the classic stopband encountered in the first Bragg case.

V. Modal Reflections of Finite-Length Grating Structures Near the Second Bragg Condition

The interaction of the modes in a uniform waveguide without periodic perturbations and the Floquet-Bloch modes of a periodic waveguide will be discussed in this section. The geometry of the periodic waveguide is shown

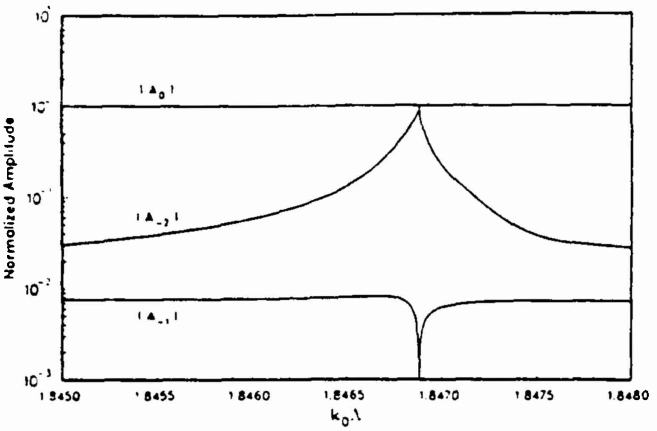

Fig. 9. Normalized amplitudes of the most important space harmonics around the $\beta\Lambda = 2\pi$ stopband for $W_2 = 0.1$ μm.

in Fig. 1; the regular waveguide is identical to the periodic structure, but has no corrugations. As an example, the two waveguides are fabricated from a grown AlGaAs-GaAs wafer with a grating formed on a section of the wafer. It is assumed that the grating is formed on the wafer in the region $-L/2 < z < L/2$. An incident mode Ψ_i on the grating produces a reflection Ψ_r and transmission Ψ_t as illustrated in Fig. 10. In the periodic region, the fields are described by the Floquet-Bloch formalism as discussed above. Although a generalized analysis can be developed, we will limit our discussion of the problem to the immediate vicinity of the second Bragg region. This restriction greatly simplifies the problem because the modal structures in the periodic and the regular waveguides are similar. Further, the number of dominant spatial harmonics is a minimum.

In the periodic region, the fundamental solution for a mode propagating in the positive z direction is

$$\Psi^+ = \exp(-\gamma_0 z) \sum_n \psi_n(x) \exp(-jnKz). \quad (16)$$

Because the dielectric constant is chosen such that $\kappa(x, z) = \kappa(x, -z)$, the backward mode solution is

$$\Psi^- = \exp(+\gamma_0 z) \sum_n \psi_n(x) \exp(+jnKz). \quad (17)$$

It should be noted that the coefficients $\psi_n(x)$ appear in both of the above equations because of the symmetry of the dielectric constant. If this symmetry condition is not satisfied, the expansion coefficients in (16) and (17) will be different. The real part of γ_0 is positive so that both forward and backward waves will attenuate due to scattering and radiation losses that occur near the second Bragg condition. It should be noted that when the waveguide material is lossless, the dielectric constant $\kappa(x, z) = \kappa^*(x, z)$. Two other Floquet-Bloch solutions are Ψ^{+*} and Ψ^{-*}. These latter solutions represent modes that gain power as they propagate; the power being absorbed is due to sources located at $x = \pm\infty$.

With a grating region sandwiched (left and right) by the regular waveguides, the fundamental mode in the regular

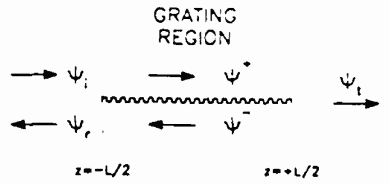

Fig. 10. Waveguide configuration used for computation of the reflection coefficient of a regular waveguide mode incident on a waveguide with a grating of length L.

waveguide will be launched at $z = -\infty$ towards the grating. This produces the reflected and transmitted fields which can be written as

$$\Psi_i = \psi_U(x) \exp(j\delta_U z) \exp(-jKz) \quad (18)$$

$$\Psi_r = \rho\psi_U(x) \exp(-j\delta_U z) \exp(+jKz) \quad (19)$$

$$\Psi_t = \tau\psi_U(x) \exp(j\delta_U z) \exp(-jKz) \quad (20)$$

where $\psi_U(x)$ is the transverse field solution in the regular waveguide, $\delta_U = K - \beta_U$, β_U is the modal propagation constant in the regular waveguide, ρ is the reflection coefficient, and τ is the field transmission coefficient.

In the grating, the field is taken as a linear combination of the forward and backward waves as $\Psi_T = a\Psi^+ + b\Psi^-$ where the coefficients a and b are determined from the boundary conditions at the input, and output planes of the grating. Near the second Bragg frequency, the spatial harmonics $n = -2$ and 0 play a major role in transfer of power from the regular waveguide to the grating region and vice versa. This efficient power transfer occurs because the transverse field components $\psi_U(x)$, $\psi_{-2}(x)$, and $\psi_0(x)$ have almost identical shapes. Thus, in the vicinity of the second Bragg resonance, the total grating field can be simplified using the dominant terms as

$$\Psi_T(x, z) = \left[a\psi_0(x)e^{Pz} + b\psi_{-2}(x)e^{-Pz}\right]e^{-jKz} + \left[b\psi_0(x)e^{-Pz} + a\psi_{-2}(x)e^{Pz}\right]e^{+jKz} \quad (21)$$

where $P = -\alpha + j\delta$ and $\delta = K - \beta$.

When wave scattering at the interface planes is inconsequential, the traveling waves along the positive z direction in the grating and in the regular waveguide can be equated at the two boundaries. (This condition is also true for waves traveling in the negative z direction.) If there is no input power to the grating at $z = L/2$, then the coefficient of $\exp(jKz)$ in (21) is zero. This leads to the condition

$$\frac{b}{a} = -\eta \exp(PL) \quad (22)$$

where $\eta = \langle \psi_U, \psi_{-2} \rangle / \langle \psi_U, \psi_0 \rangle$. (The quantity $\langle f, g \rangle = \int f^* g \, dx$ is the usual inner product of complex functions.) Similarly, equating the coefficients of $\exp(-jKz)$ and $\exp(jKz)$ in (18)-(20) with the corresponding coefficients in (21) at $z = \pm L/2$ leads to the field reflection coefficient

$$\rho = \frac{\eta\left[1 - \exp(2PL)\right]}{1 - \eta^2 \exp(2PL)} \exp(-j\delta_U L). \quad (23)$$

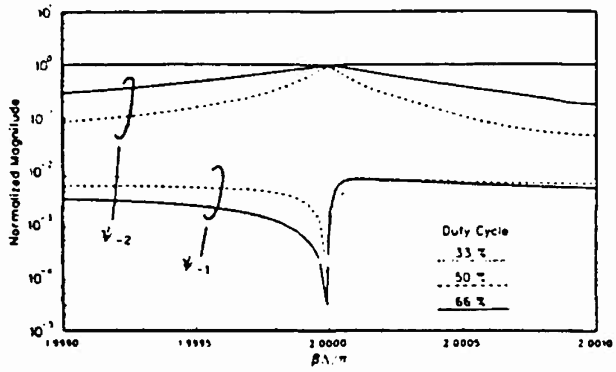

Fig. 11. Normalized amplitudes of space harmonics around the second Bragg resonance. The duty cycle is W/Λ.

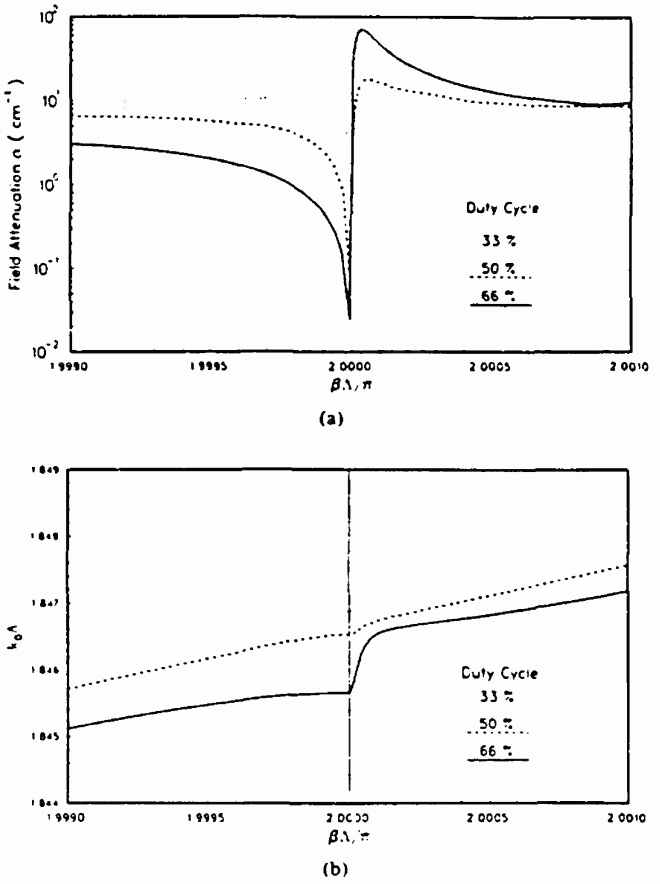

Fig. 12. Dispersion about the second Bragg. (a) The field attenuation coefficient and (b) the propagation constant for the different duty cycles.

The reflection coefficient $R = |\rho|^2$ is now computed in the vicinity of the second Bragg condition. The duty cycle W/Λ for the grating is treated as a parameter. Fig. 11 shows the amplitude of the first three spatial harmonics at the bottom the grating ($x = 0$) as a function of detuning. Note that the coefficients for $n = -2$ harmonic approach the normalized value of the $n = 0$ harmonic in the vicinity of the second Bragg. The parameter η should have a functional dependence with respect to detuning that is similar to the amplitude of the space harmonic amplitude A_{-2}. Namely, $|\eta|$ has a peak value at $\beta = K$ and decreases with detuning. The quantity $P = -\alpha + j(K - \beta)$ can be obtained from data given in Fig. 12. Near the second Bragg resonance, $\Lambda \approx 0.24$ μm. It appears from the results given in Fig. 12 that the largest duty cycle (0.66) produces the "strongest" grating, while the smallest duty cycle (0.33) produces the "weakest." This phenomenon occurs because optical field penetration of the grating region increases with duty cycle.

Fig. 13 shows the reflection coefficient R for the various duty cycles as a function of the detuning parameter δ. In each of the figures, the grating length L takes on the values of 100, 200, and 300 μm. In Fig. 13(a) where the duty cycle is 0.33, the reflection coefficient peaks at a value below the second Bragg condition, whereas in Fig. 13(c) where the duty cycle is 0.66, R peaks at a point above the Bragg frequency. These small local peaks in R occur because they reflect the functional dependence of α on detuning as shown in Fig. 12; for the 33% duty cycle, α has a local maximum below the Bragg frequency, whereas for the 66% duty cycle, α has a maximum value above the Bragg frequency.

VI. Conclusion

We have used a rigorous full Floquet numerical analysis to investigate the modal properties and wave interactions in a transversely bounded dielectric waveguide with a rectangular surface corrugation. A specific double-heterostructure GaAs-AlGaAs waveguide geometry has been examined in detail. This class of multilayered periodic structures can be formulated exactly as a boundary value problem. The purpose of such an exact analysis is: 1) to establish and understand the basic wave propagation characteristics, 2) to identify various types of wave interactions and coupling mechanisms, and 3) to present accurate numerical results against which the effect of various approximations can be judged.

The boundary-integral-equation formulation has been adopted for the solution of the wave equation inside the grating layer. The boundary around each rectangular region constituting the unit cell is discretized into elements, and a stepwise approximation to the field and flux along the region boundary is assumed (boundary element method). The tangential field continuity requirements across the grating layer interfaces are imposed through point matching with the Floquet expansions of the field above and below the grating. Other continuity and periodicity requirements are also imposed in the same way across the unit cell interfaces. The dispersion relation is thus a generalized transverse resonance-type matrix equation. The process of searching for the resonant solutions of this equation is equivalent to the process of adjusting the weights of the partial waves in the Floquet summation as well as the propagation constant in order to satisfy the boundary conditions on the grating surface. The results thus obtained are inherently accurate, the degree of accuracy being determined only by the number of boundary elements used.

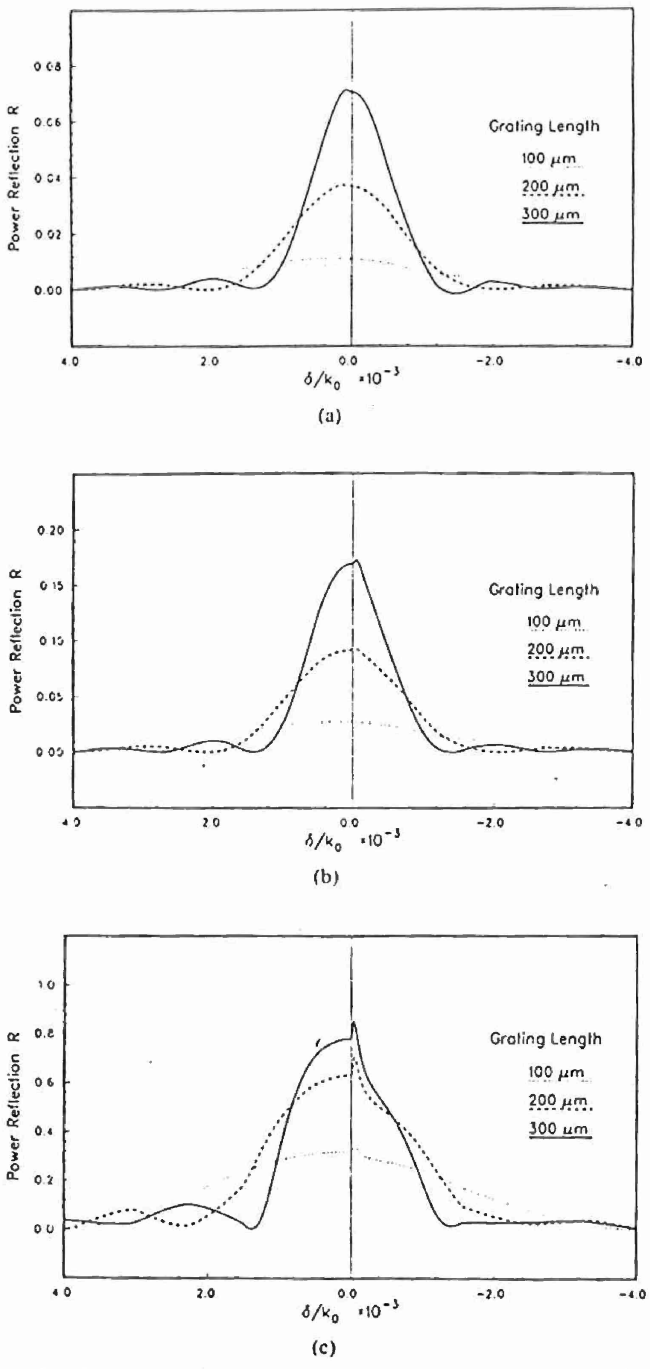

Fig. 13. The power reflection coefficient R about the second Bragg for duty cycles of (a) 33%, (b) 50%, and (c) 66%.

Finally, the characteristics of a finite length grating have been derived using the Floquet–Bloch solutions of an infinite length waveguide. To simplify the estimates of the reflection and transmission coefficients of the finite length grating, mode scattering at the interface between the regular waveguides and the waveguide with a corrugation was neglected. Calculations show that the reflection coefficient of a finite length grating does not have a maximum at the second Bragg frequency. Generally, the reflection coefficient peaks at frequencies above the second Bragg for relatively strong gratings. This phenomenon occurs because the model absorption coefficient α peaks above the second Bragg condition. Because α peaks at frequencies above the second Bragg, the "stopband" occurs just above the second Bragg. This phenomenon is to be contrasted with the "stopband" near the first Bragg region. Near the first Bragg condition, the "stopband" is almost centered about the Bragg frequency.

References

[1] H. Kogelnik, "Coupled wave theory for thick hologram gratings," *Bell Syst. Tech. J.*, vol. 48, pp. 2909–2947, Nov. 1969.

[2] H. Kogelnik and C. V. Shank, "Coupled-wave theory of distributed feedback lasers," *J. Appl. Phys.*, vol. 43, pp. 2327–2335, May 1972.

[3] ——, "Stimulated emission in a periodic structure," *Appl. Phys. Lett.*, vol. 18, pp. 152–154, Feb. 1971.

[4] C. Elachi, G. Evans, and C. Yeh, "Transversely bounded DFB lasers," *J Opt. Soc. Amer.*, vol. 65, pp. 404–412, Apr. 1975.

[5] R. F. Kazarinov and C. H. Henry, "Second-order distributed feedback lasers with mode selection provided by first-order radiation losses," *IEEE J. Quantum Electron.*, vol. QE-21, pp. 144–150, Feb. 1985.

[6] C. H. Henry, R. F. Kazarinov, R. A. Logan, and R. Yen, "Observation of destructive interference in the radiation loss of second-order distributed feedback lasers," *IEEE J. Quantum Electron.*, vol. QE-21, pp. 151–153, Feb. 1985.

[7] W. S. Park and S. R. Seshadri, "Theory of the second-order reflection grating," *J. Opt. Soc. Amer.*, vol. 3, pp. 1632–1643, Oct. 1986.

[8] D. L. Jaggard and C. Elachi, "Floquet and coupled-waves analysis of higher order Bragg coupling in a periodic medium," *J. Opt. Soc. Amer.*, vol. 66, pp. 674–682, July 1976.

[9] A. Yariv and A. Gover, "Equivalence of the coupled-mode and Floquet–Bloch formalisms in periodic optical waveguides," *Appl. Phys. Lett.*, vol. 26, pp. 537–539, May 1975.

[10] S. Wang, "Principles of distributed feedback and distributed Bragg-reflector lasers," *IEEE J. Quantum Electron.*, vol. QE-10, pp. 413–427, Apr. 1974.

[11] ——, "Energy velocity and effective gain in distributed-feedback lasers," *Appl. Phys. Lett.*, vol. 26, pp. 89–91, Feb. 1975.

[12] R. F. Cordero and S. Wang, "Threshold condition for thin-film distributed-feedback lasers," *Appl. Phys. Lett.*, vol. 24, pp. 474–476, May 1974.

[13] C. Elachi and C. Yeh, "Periodic structures in integrated optics," *J. Appl. Phys.*, vol. 44, pp. 3146–3152, July 1973.

[14] S. T. Peng, T. Tamir, and H. L. Bertoni, "Theory of periodic dielectric waveguides," *IEEE Trans. Microwave Theory Tech.*, vol. MTT-23, pp. 123–133, Jan. 1975.

[15] M. Matsumoto, M. Tsutsumi, and N. Kumagai, "Radiation of millimeter waves from a leaky dielectric waveguide with a light induced grating layer," *IEEE Trans. Microwave Theory Tech.*, vol. MTT-35, pp. 1033–1042, Nov. 1987.

[16] J. Jacobsen, "Analytical, numerical, and experimental investigation of waves on a periodically strip-loaded dielectric slab," *IEEE Trans. Antennas Propagat.*, vol. AP-18, pp. 370–387, May 1970.

[17] W. Streifer, D. R. Scifres, and R. D. Burnham, "Coupled wave analysis of DFB and DBR lasers," *IEEE J. Quantum Electron.*, vol. QE-13, pp. 134–141, Apr. 1977.

[18] ——, "Analysis of grating-coupled radiation in GaAs:GaAlAs lasers and waveguides," *IEEE J. Quantum Electron.*, vol. QE-12, pp. 422–428, July 1976.

[19] K. Handa, S. T. Peng, and T. Tamir, "Improved perturbation analysis of dielectric gratings," *Appl. Phys.*, vol. 5, pp. 325–328, 1975.

[20] C. A. Brebbia, *The Boundary Element Method for Engineers*. London: Pentech, 1978.

[21] C. A. Brebbia and S. Walker, *Boundary Element Techniques in Engineering*. London: Butterworths, 1980.

[22] C. C. Su, "A surface integral equation method for homogeneous optical fibers and coupled image lines of arbitrary cross sections," *IEEE Trans. Microwave Theory Tech.*, vol. MTT-33, pp. 1114–1119, Nov. 1985.

[23] N. Kishi and T. Okoshi, "Proposal for a boundary-integral method without using Green's function," *IEEE Trans. Microwave Theory Tech.*, vol. MTT-35, pp. 887–892, Oct. 1987.

[24] T. Okoshi and T. Miyoshi, "The planar circuit—An approach to mi-

crowave integrated circuitry," *IEEE Trans. Microwave Theory Tech.*, vol. MTT-20, pp. 245-252, Apr. 1972.
[25] R. F. Harrington, *Field Computation by Moment Method*. New York: Macmillan, 1968.
[26] T. Tamir, "Leaky wave antennas," in *Antenna Theory*, Part 2, R. E. Collin and F. J. Zucker, Ed. New York: McGraw-Hill, 1969.
[27] A. H. Stroud and D. Secrest, *Gaussian Quadrature Formulas*. Englewood Cliffs, NJ: Prentice-Hall, 1966.
[28] C. W. Clenshaw, *National Physical Laboratory Mathematical Tables, vol. 5*. London: H. M. Stationery Office, 1962.

G. Hadjicostas, photograph and biography not available at the time of publication.

Jerome K. Butler (S'59-M'65-SM'78-F'89) received the B.S.E.E. degree from Louisiana Polytechnic Institute, Ruston, and the M.S.E.E. and Ph.D. degrees from the University of Kansas, Lawrence, in 1960, 1962, and 1965, respectively.

From 1960 to 1965 he was a Research Assistant and held a CRES Fellowship at the Center for Research in Engineering Sciences, University of Kansas. He conducted research concerned with electromagnetic wave propagation and the optimization and synthesis techniques of antenna arrays. In 1965, he joined the faculty of the School of Engineering and Applied Science, Southern Methodist University, Dallas, TX, where he is now a Professor of Electrical Engineering. His primary research areas are solid-state injection lasers, radiation and detection studies of lasers, communication and fiber optic systems, integrated optics and the application of integrated optical circuits, quantum electronics, and the integration of optical and millimeter wave systems. In the summers since 1969, he has been a Staff Scientist with the David Sarnoff Research Center, a subsidiary of SRI International (formerly RCA Laboratories), Princeton, NJ. He has held consulting appointments with the Central Researach Laboratory, Texas Instruments, Inc., the Geotechnical Corporation of Teledyne, Inc., Earl Cullum and Associates of Dallas, and the University of California-Los Alamos, New Mexico. He is coauthor of the book *Semiconductor Lasers and Heterojunction LED's*, published by Academic Press, and is the Editor of the Book *Semiconductor Lasers*, published by the IEEE Press.

Gary A. Evans (S'69-M'75-SM'82) was born in Omak, WA, in 1948. He received the B.S.E.E. degree from the University of Washington, Seattle, in 1970, and the M.S.E.E. and Ph.D. in degrees in electrical engineering and physics from the California Institute of Technology, Pasadena, in 1971 and 1975, respectively. After postdoctoral work at Caltech, he worked for R&D Associates, Marina Del Ray, CA, on radar systems, CCD's, and integrated optics. While on leave of absence from RDA, he was a visiting assistant professor with the Department of Electrical Engineering, at the University of Washington (1977-1979). He has also been with the Aerospace Corporation, El Segundo, CA, (1979-1981) and TRW, Redondo Beach, CA, (1981-1984). In 1984 he joined the David Sarnoff Research Center (formerly RCA Laboratories, now a subsidiary of SRI International), Princeton, NJ. Since 1979 he has primarily worked on the design, growth, and fabrication of conventional cleaved facet lasers, DBR lasers, and grating surface emitting lasers. He and his co-workers developed integrated two-cavity semiconductor lasers, etched-mirror unstable resonator semiconductor lasers, and one- and two-dimensional coherent arrays of grating-surface-emitting lasers. He also has worked on reliability, power, and stability issues of semiconductor lasers for satellite communication systems. In addition to several book chapters, he has authored or coauthored more than 100 journal papers and conference presentations.

Dr. Evans was Chairman of the Santa Monica Bay Section of the IEEE and is presently Vice Chairman of the Princeton Section of LEOS. He has served on several IEEE committees, including the technical program committee for the International Semiconductor Laser Conference (1988 and 1990). He is a member of the American Physical Society, the Optical Society of America, Tau Beta Phi, and is a Registered Professional Engineer.

Nils W. Carlson (M'84) received the B.A. degree in physics from Johns Hopkins University, Baltimore, MD, and the M.S. and Ph.D. degrees, also in physics, from Stanford University, Stanford CA, in 1975, 1977, and 1980, respectively.

From 1980 to 1982 he was with Bell Laboratories, Murray Hill, NJ, and from 1982 to 1984 he was with the Division of Applied Sciences, Harvard University, Cambridge, MA. In 1984 he joined the David Sarnoff Research Center, a subsidiary of SRI International (then RCA Laboratories), Princeton NJ, as a Member of Technical Staff in the Optoelectronics Research Laboratory. His research interests concern the physics of semiconductor diode lasers and the design and characterization of grating surface emitting diode laser arrays.

Dr. Carlson is a member of the American Physical Society, the Optical Society of America, and Phi Beta Kappa.

Robert Amantea (M'69-S'76-M'77-SM'85) received the B.S.E.E. degreee from the City University of New York, New York, and the M.S. degree in electrophysics from the Polytechnic Institute of New York, Brooklyn, in 1965 and 1969, respectively. From 1975 through 1977 he was a David Sarnoff Fellow at the University of California at Berkeley, from which he received the Ph.D. degree in 1977.

He joined the David Sarnoff Research Center, a subsidiary of SRI International, Princeton, NJ, in 1965, working in the area of power semiconductor devices. He has authored many papers on such topics as power transistors, TRAPATT devices, gated-diode physics, gate-turn-off thyristors, computer-aided modeling of MOS transistors, and integrated simulation of silicon devices from process through circuit behavior. His most recent interests are in the area of modeling laser diode arrays. He was a Visiting Lecturer at the University of California at Berkeley during the spring 1977 quarter. He was a Visiting Lecturer at LaSalle College, Philadelphia, PA, from 1982 through 1987.

Dr. Amantea is a member of Eta Kappa Nu and Tau Beta Pi.

EXPERIMENTAL VERIFICATION OF GRATING THEORY FOR SURFACE EMITTING STRUCTURES*

Raj Ayekavadi, C. S. Yeh, J. K. Butler

Department of Electrical Engineering, Southern Methodist University, Dallas, TX 75275.

G. A. Evans, P. Stabile, A. Rosen

David Sarnoff Research Center, Princeton, NJ 08543-5300.

ABSTRACT

The design procedures for the construction of corrugated waveguides of Al_2O_3 and the far field radiation patterns observed from such waveguides is presented. The design procedure is based on the physics of four layer waveguide structures. The corrugated waveguide is similar to a Bragg type diffraction grating. This corrugated structure provides 90° reflections at certain specific wavelengths depending on the grating spacing. A particular advantage of such structures that behave like grating antennas is that their radiation pattern can be scanned electronically by changing the wavelength (frequency). This corresponds to changing the propagation constant of the propagating wave. The far field radiation pattern obtained from the experimental set up is compared against simulations carried out using the Huygen - Fresnel theory and a close agreement is seen between theoretical prediction and experimental observation. Specifically, the design and the measurements are made in the frequency range from 90 GHz to 100 GHz for a number of different kinds of structures including those with one as well as multiple sections of corrugations.

1. INTRODUCTION

Recent advances in the fabrication of millimeter - wave systems using integrated circuit technology has stimulated considerable interest in the use of corrugated dielectric structures[1-3]. A dielectric waveguide with a periodic surface corrugation has been shown to hold substantial promise as a leaky wave antenna for millimeter wave applications. These dielectric antennas offer the advantage of electronic beam steering. This class of structures has been widely used for integrated optic applications as beam-to-surface-wave couplers, distributed feedback reflectors and filters. The physics of wave propagation in optical devices can be carried over to the design of these antenna structures and basic optical principles can be used to provide information on the radiation patterns of such structures.

When a wave propagating in a corrugated waveguide reaches the corrugated (perturbed) area, two things will occur: a portion of the wave will be diffracted out of the guide, into the air and the substrate, and a portion will be reflected. This radiation occurs only in certain preferred directions, primarily

*Supported in part by the Army Research Office.

0-8194-0508-6/91/$4.00

determined by the phase constant of the uncorrugated structure and the period of the corrugations[4]. As a consequence of the radiation loss, the wave guided by the structure decays exponentially as it propagates. Hence the wave will exist with appreciable magnitude over a finite length of the waveguide and a beam is radiated with a beam width proportional to the attenuation constant of the guided wave. Since the phase and the attenuation constants determine the field characteristics, they are the most important parameters in the physics of the operation of these devices. It is possible for the type of structures under consideration, to estimate the attenuation, reflection and the transmission coefficients of the corrugated waveguide.

The work presented in this paper pertains to the design of corrugated waveguides of Al_2O_3 with dielectric constant of 9.6. in the frequency range from 90 GHz to 100 GHz. A number of such waveguides were designed and constructed including some with multiple sections of corrugations. The radiation patterns from these waveguides were measured at several different frequencies about the second Bragg. The patterns were compared with those obtained from a simulation based on the Huygen - Fresnel theory. Close agreement between the two endorses the design procedures used for the waveguide and reasonable accuracy of the procedures used for measurement of the radiation pattern.

2. THEORETICAL BACKGROUND

A periodically corrugated waveguide is shown in Fig. 1a. (Throughout this paper it is assumed that we consider only rectangular teeth, a groove profile that can be made easily and precisely by machining). The waveguide antenna structure consists of two parts: one is the uniform waveguide (unperturbed structure) and the other is the periodic layer. The width of the structure is 'W', the period of the corrugations is 'A' and the height of the corrugated teeth is 'T'. As an exact electromagnetic boundary value problem, periodic dielectric waveguides have been treated for normal incidence (with respect to the direction of the grating grooves and with the assumptions that both the antenna structure and the source distribution do not depend on the coordinate parallel to the grooves (y-axis). Under these simplifying conditions, a general electromagnetic wave propagating in periodic waveguide can be decomposed into independent TE and TM modes. The studies carried out in this case pertain mainly to the TM mode propagation in the waveguides.

2.1. Design of Corrugated Waveguides

The design of a corrugated waveguide used in this study is based on the theory of four layer waveguides[5]. The algorithm for the design is based on TM mode propagation in the active layer of the device. The solution of the wave equation from the Maxwell's equation is sought in each of the four regions. The TM modes have only three components H_y, E_x and E_z. The continuity of the transverse field component. H_y and E_z is used to derive the secular equation.

The solution of the four layer problem in terms of estimation of the propagation constant of the propagating wave, depends on the solution of the secular equation.

2.1.1. Design Procedures

Using the procedures outlined above, a waveguide structure is designed on which corrugations are created in the active layer 3 of the structure. The corrugated waveguide is made of alumina of thickness 40 mils and dielectric constant of 9.6. The design is carried out for a frequencies of operation from 90 GHz to 100 GHz. The dielectric constant in the Region 3 of interest is dependent on that in Regions 2 & 4 and the duty cycle of the corrugations. The dielectric constant κ_3, in the active region is

$$\kappa_3 = D_c \times \kappa_2 + (1-D_c)\kappa_4 \qquad (1)$$

where D_c is the duty cycle. The dielectric constant κ_3 of the region with corrugations, Region 3, is the "average value" of the dielectric constant of the corrugated region as shown in Fig. 1b. The periodicity of the waveguide, dependent on the frequency of operation is related to the duty cycle and the width of the corrugations by

$$W = \frac{1}{2} D_c \times \lambda \tag{2}$$

where λ is the free space wavelength under consideration.

The corrugations are created using a diamond blade. the blade thickness T, being related to the periodicity Λ by

$$T = \Lambda(1 - D_c) \tag{3}$$

Computations are made to find the different heights in the corrugations for the different blade thicknesses at different duty cycles of the corrugations. The blade thickness being a constant in this case, the appropriate tooth height is chosen. After the tooth height is found, the grating period is determined.

2.1.2. Example

A typical example of the design procedure followed in one of the constructed waveguides is given for a waveguide designed to operate at 90 GHz. The main criterion was to find the height of the corrugations and the grating period Λ given the blade thickness T, which in this case was 0.6 mm. A computer program. the algorithm of which is based on solving the secular equation was used to carry out the design. The wavelength of the propagating wave inside the corrugated waveguide is

$$\lambda_g = \frac{\lambda}{n_{eg}} \tag{4}$$

where λ is the wavelength of the the wave, n_{eg} is the effective refractive index in the waveguide which is a value generated in one of the subroutines of the program. An example is the design of a waveguide for operation at 90 GHz Assuming that a strong grating of height 0.3 mm is desired, the blade thickness being 0.6 mm. from Fig 2a, the duty cycle is found to be 0.55. Once the duty cycle is known, from Fig. 2b, the grating period for the tooth height of 0.3 mm and given a duty cycle of 0.55 is found to be 1.325 mm. Hence the design specifications for an alumina waveguide of thickness 40 mils and dielectric constant of 9.6. for propagating TM modes at 90 GHZ are that the tooth height be 0.3 mm and the grating period be 1.325 mm. The performance of the waveguide in this example was in close agreement to theoretical predictions.

2.2. Brief Analysis of Waveguides Prepared

A brief description of various waveguides prepared and their performance is listed below. A comparison was made of the experimental performance of the waveguides against theoretical expectation. It was based on the calculation of the actual wavelength of the wave inside the waveguide as a function of frequency. Two theoretical simulations were made using two principles: 1) The Effective Index Method[6] and 2) The Slab Waveguide Method for a four or five layer structure. Experimentally, the relation between the peak radiation angle Θ and the actual wavelength of the wave inside the corrugated waveguide is given by,

$$\lambda = \Lambda\left(\frac{\lambda_0 \sin\Theta}{\lambda_0} + 1\right) \tag{5}$$

where

Λ = period of the corrugations

Θ = peak radiation angle

λ_0 = free space wavelength

Fig 3a gives the comparison of the wavelength against frequency for a waveguide with depth of corrugations T of 0.28 mm and grating spacing of 1.33 mm. In the figure, SLAB corresponds to simulated results using the four or five layer slab waveguide approach, EIM corresponds to the simulated values

using the Effective Index Method. EXP.F corresponds to the experimental results from the flat side of the waveguide and EXP C is the experimental observation from the corrugated side of the waveguide. The results show a close agreement between the various simulations and experimental results. Fig 3b corresponds to the case of a waveguide with corrugations depth 0.45 mm and grating spacing of 1.225 mm.

2.3. Measurement of Radiation Pattern

The experimental set-up used to measure the radiation pattern of the waveguides is shown in Fig. 4. The various components of the set up are:

S1	Frequency tunable IMPATT diode oscillator(90 - 100 GHz)
M1	Ferrite modulator, used to chop the incident wave for the purpose of lock-in amplifier measurement.
FM1	Precision frequency meter.
A1,A2	Variable attenuator
DC1	3 dB directional coupler.
PH1	Rotary type phase shifter
SW1,SW2	Manual waveguide switches
T1,T2,T3,T4	Matched terminations
D1	Flat broadband detector with horn antenna set up in z-polarization
CDW	Corrugated waveguide under observation

The electromagnetic wave propagating along an axially periodic waveguide structure can be expressed in terms of an infinite number of traveling waves of the form, $h_n(x)e^{-\gamma_n}$ called the spatial harmonics. The field is given by

$$H_y = \sum h_n(x)e^{-\gamma_n} \tag{6}$$

with

$$\gamma_n = \alpha + j(\beta_0 + \frac{2\pi n}{\Lambda}) \quad n = 0, \pm 1, \pm 2, \cdots$$

where

α is the attenuation coefficient

β_0 is the propagation constant

Λ is the period of the corrugations

β_0 can be found approximately by using the average dielectric constant and solving the slab waveguide problem[7].

The field described above is one of the two self consistent solutions for the slab waveguide. The first of the solutions is the TM modes consisting of the components E_x, H_y,and E_z while the second is the TE modes consisting of the components E_y, H_x, and H_z. The width of the corrugated waveguide is taken to be larger than the supported wavelength in which case it can be treated as a slab waveguide. The TM modes of the slab dielectric waveguide match the TE_{01} in the metallic waveguide best. Just one mode being supported by the metallic waveguide is due to the small dimensions of the metallic waveguide(1.25mm x 2.50mm). The cut off frequency of the TE_{01} dominant mode is 60 GHz and the next mode TE_{10} is cut off at 120 GHz.

In the experiment, the source oscillator is operated in the frequency range 90 GHz to 100 GHz. As seen from the above equations, given a source oscillator upto 100 GHz, the metallic waveguide can only

support the TE_0 mode.

2.3.1. Far Field Radiation Pattern

The far field pattern of the radiation from the corrugations can be found using the Huygen - Fresnel formulae[8]. The magnetic field amplitude at a point (R, Θ) as shown in Fig. 5 is given by

$$F(R,\Theta) \quad \alpha \quad \int \exp\frac{jk_o}{r} H_y(z)\frac{\cos(n,r)}{r}dz \tag{7}$$

$$\approx \cos\Theta \int H_y(z)\exp\left[jk_o\left(-z\sin\Theta + \frac{z^2}{2R}\right)\right]dz \tag{8}$$

Radiation is produced by the n = -1 Floquet-Bloch partial wave.

$$F_{-1}(R,\Theta) \quad \alpha \quad \int \exp\left[-\alpha z\right]\exp\left[-j\left(\beta_0+\frac{2\pi n}{\Lambda}\right)z\right]\exp\left[jk_0\left(-z\sin\Theta + \frac{z^2}{2R}\right)\right]dz \tag{9}$$

The magnetic component of this field is polarized in the y-direction while the electric field is polarized in the x-direction

3. RESULTS

As mentioned, Figs 2a and 2b give the results on the waveguide design. Fig. 6 shows a comparison between the experimentally observed radiation pattern (dotted curves) and the simulated results (solid curves). The figure shows that the ratio of spread in the beam to the corresponding frequency scan in the source is.

$$\text{Experimental:} \quad \frac{\Delta\Theta}{\Delta f} = 2.0^\circ / \text{GHz}$$

$$\text{Simulated:} \quad \frac{\Delta\Theta}{\Delta f} = 1.9^\circ / \text{GHz}$$

The simulation curve shows a shift of +4°. The reason for this could be that the actual value of β_o is smaller than the calculated value which uses the slab waveguide theory. Figs. 7a and 7b show results obtained from experimental and simulation of the radiation patterns from a blazed structure. The results yield

$$\text{Experimental:} \quad \frac{\Delta\Theta}{\Delta f} = 1.8^\circ / \text{GHz}$$

$$\text{Simulated:} \quad \frac{\Delta\Theta}{\Delta f} = 2.0^\circ / \text{GHz}$$

The same reasons as the earlier could be attributed to the difference in the values. Fig. 8 shows results from the experimental set-up by combining two waves made incident from either end of the waveguide and tuning a phase shifter to get a maximum or minimum. The 'flips' correspond to the case of the radiation measurement from the non corrugated side (flat slab side).

Fig. 9 depicts a situation where waves are made to be incident from both ends of the waveguide and the phase shifter is adjusted to get a maximum (max) or a minimum (min). 'Forward' corresponds to a case when waves are incident only from the forward direction of the waveguide and a measurement of the radiation pattern is made. The waves are made incident from the reverse direction to get the radiation pattern labeled 'reverse'.

Experimental studies were made on corrugated waveguides consisting of two sections on the same slab These were designed and constructed to measure the reflection, transmission and attenuation coefficients of the corrugated waveguides. Fig. 10a and 10b show the radiation pattern from the two sections 'A' and 'B' of the waveguide for different frequencies . These can be used to find the attenuation and

transmission coefficients. For example, a calculation of the transmission and attenuation coefficients using the relation.

$$P = P_0 e^{-\alpha z} \tag{10}$$

where P_0 is the incident power while P is the power at some point along the waveguide. Use of this relation and the use of the values from the curves yields a transmission given by P/P_0 of 0.78 and a attenuation constant of 0.079 cm for the waveguide under consideration.

Studies are carried out on a two section waveguide by tuning the source oscillator to the second Bragg frequency of the average Bragg frequency of each of the sections. The attenuator is adjusted to get equal peak intensities from both sections. The experimental pattern observed with such an arrangement along with a comparison of simulation of the conditions is shown in Fig. 11.

It is noticed that the curves are not perfectly smooth which could be attributed to the fact that there is interference with other sources of radiation such waveguides as leaky wave antennas or as surface emitting structures in the frequencies from 90 GHz to 100 GHz. The study brings out the practical use of the physics of the four layer problem and the Huygen's principle in the fear field measurements. Transmission and reflection coefficients of different kinds of waveguide structures have been found. The effect of losses and detuning from Bragg condition has been brought out. The peak reflectivity in some cases does not occur at the Bragg condition. These effects could be due to complicated interactions of the guided modes, radiation fields and evanescent waves.

4. REFERENCES

[1] G.Hadjicostas, J.K Butler, G.A. Evans, N.W. Carlson, and R. Amentea, "A Numerical Investigation of Wave Interactions in Dielectric Waveguides with Periodic Surface Corrugations," *IEEE J.of Quantum Electron.*, vol.QE-26, pp 893-902, May 1990.

[2] S. T. Peng, T. Tamir and H.L. Bertoni, "Theory of Periodic Dielectric Waveguides," *IEEE Trans. Microwave Theory and Tech.*, vol. MTT-23, pp. 123 - 133, Jan. 1975.

[3] K. C. Chang, V. Shah and T. Tamir, "Scattering and Guiding of Waves by Dielectric Gratings with Arbitrary Profiles." *J. Opt. Soc. America*, vol. 70, No. 7, pp 804-813, July 1980.

[4] C.Elachi and C. Yeh, "Periodic Structures in Integrated Optics," *J. Appl. Phys.*, vol. 44, pp 3146-3152. Jul. 1973.

[5] Henry Kressel and J.K. Butler, *Semiconductor Lasers and Heterojunction LED's*, Academic Press 1977.

[6] R.M. Knox and P.P. Toulis," Integrated Circuits for Millimeter through Optical Frequency Range," *Proc. MRI. Symp. on Submillimeter Waves*, J. Fox, Ed.,Brooklyn, NY, Polytechnic Press, 1977.

[7] K. Handa, S.T. Peng and T. Tamir, "Improved Perturbation Analysis of Dielectric Gratings," *Applied Physics*, 5, 325-328, 1975.

[8] J.W. Goodman, *Introduction to Fourier Optics*, McGraw- Hill, New York, NY. 1968.

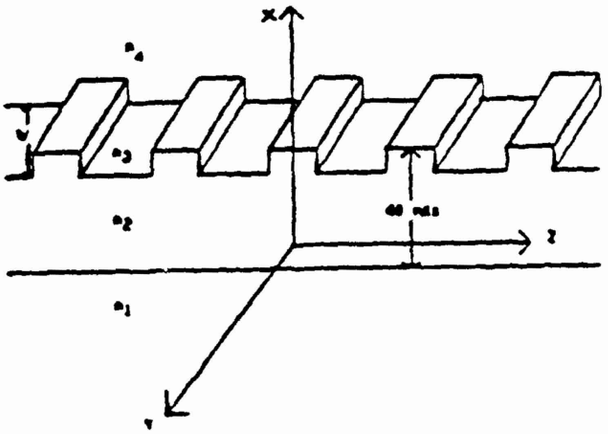

Fig:1a Four layer waveguide structure with associated coordinate system. Region '3' is the active region of interest.

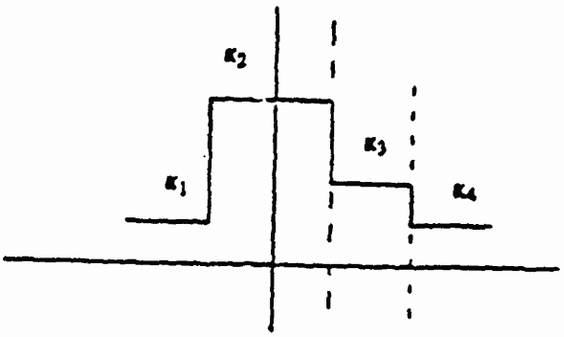

Fig:1b Dielectric constants in a four layer waveguide structure. κ_3 is the average value of the dielectric constant of the corrugated region.

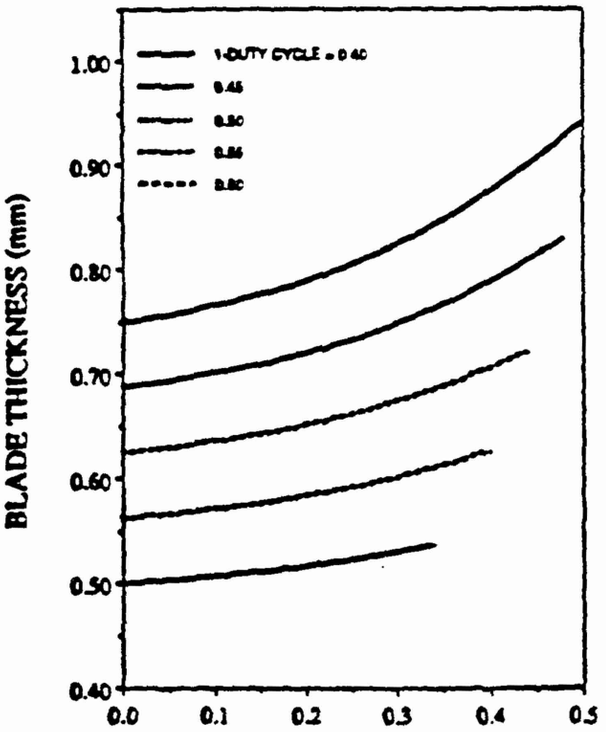

Fig:2a. The waveguide design is based on the physics of four-layer structures. The tooth height is plotted against blade thickness for various possibe duty cycles. The blade thickness in this case is 0.6 mm.

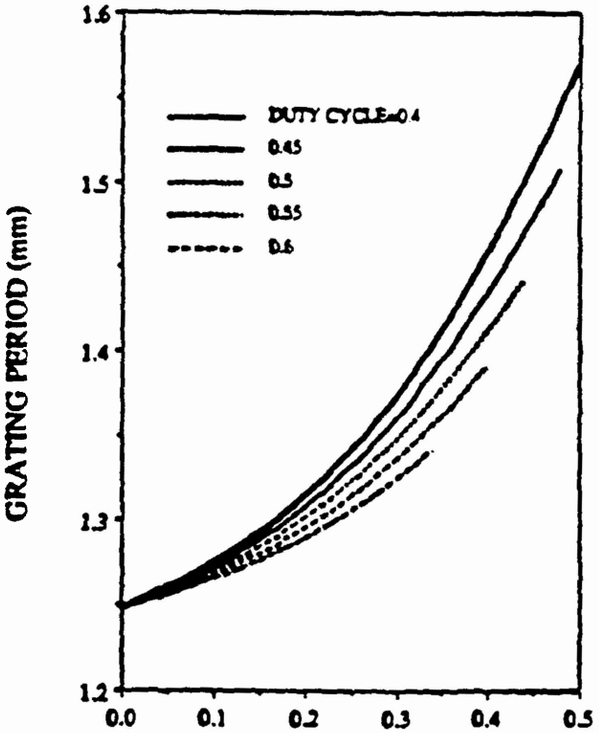

Fig:2b. The waveguide design includes finding the corrugation spacing by plotting it as a function of tooth height for various duty cycles.

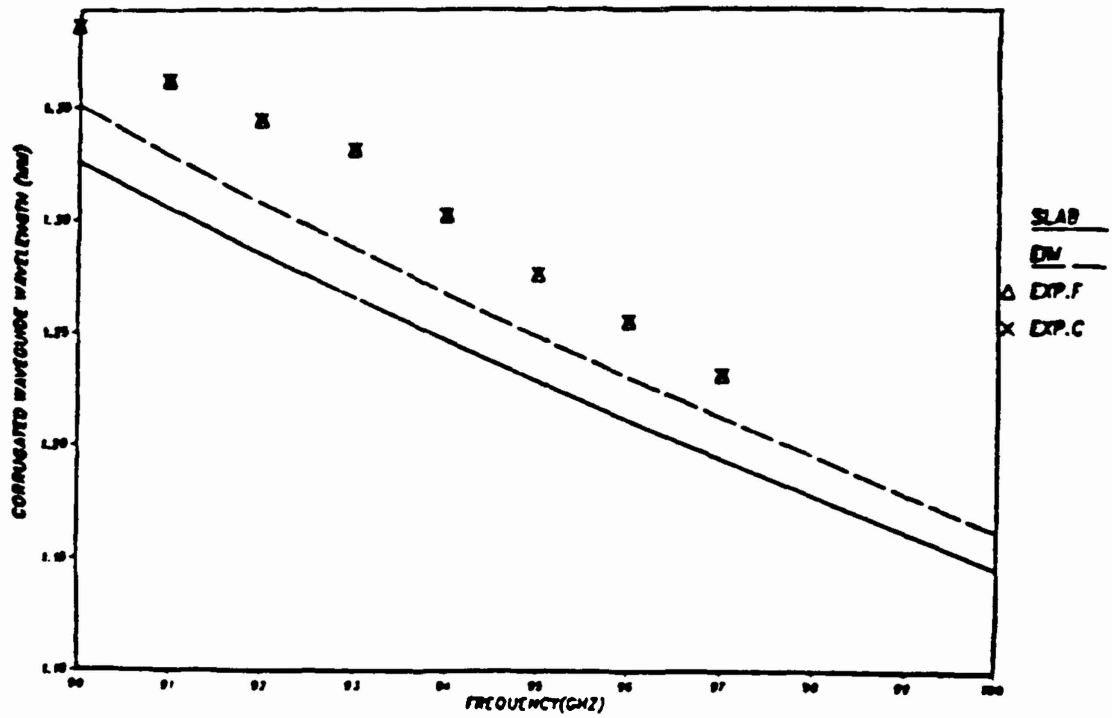

Fig:3a. The accuracy of experimental results is established by finding the effective wavelength in the waveguide as a function of frequency. The waveguide in this case has a tooth height of 0.28 mm.

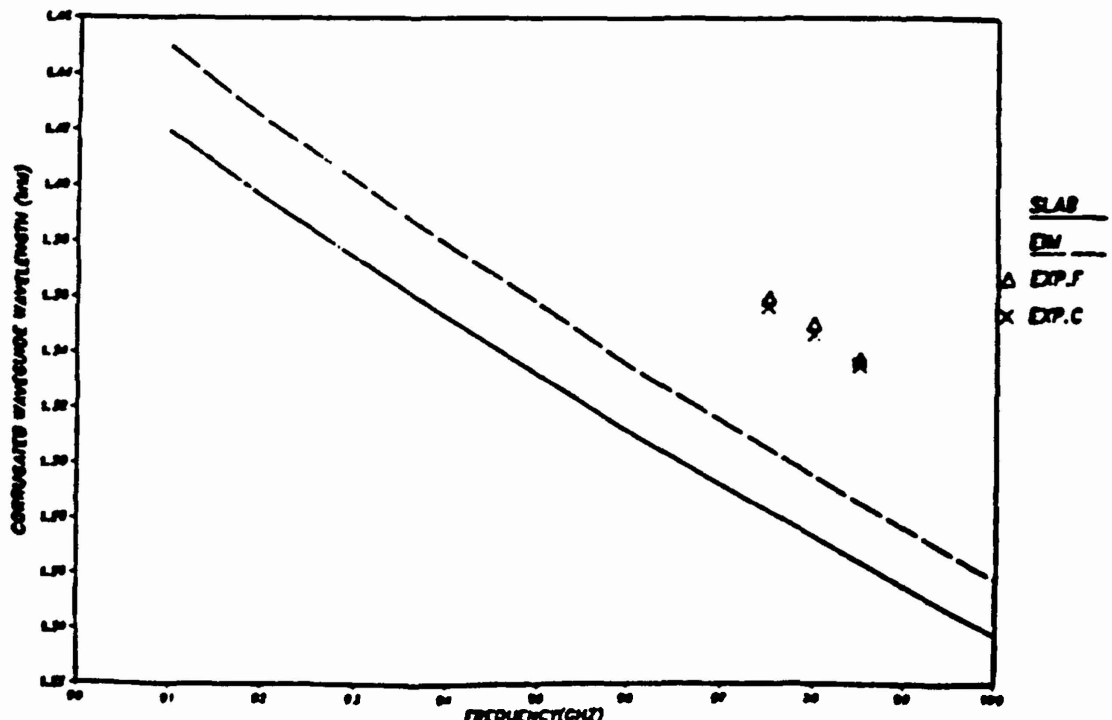

Fig:3b. The results shown in Fig. 3a are repeated for a waveguide with tooth height of 0.45 mm.

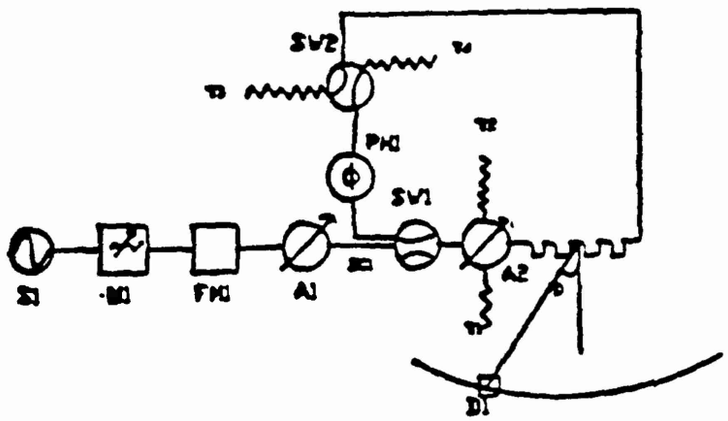

Fig:4. Experimental set-up to measure the far field radiation pattern of corrugated waveguides.

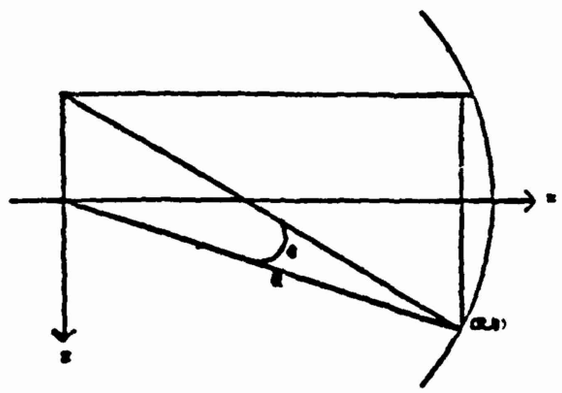

Fig:5. Co-ordinate system to find the Magnetic Field amplitude at a point (R,Θ) using Huygen-Fresnel Equation.

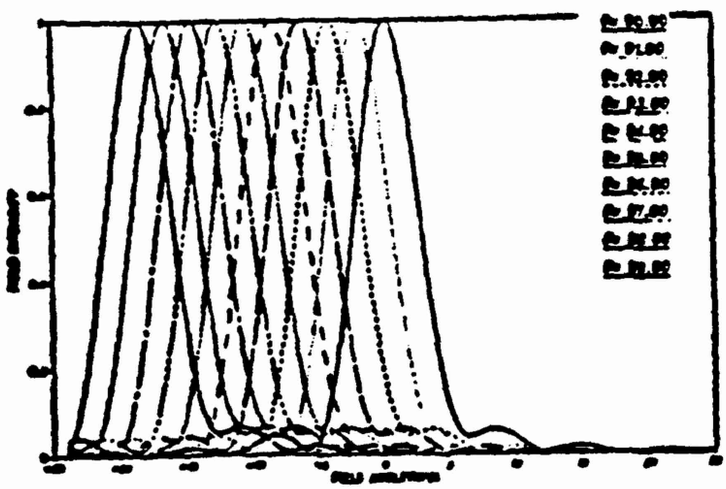

Fig:6. Experimental (dotted) and simulated (solid) radiation patterns from a waveguide with grating spacing of 1.326 mm.

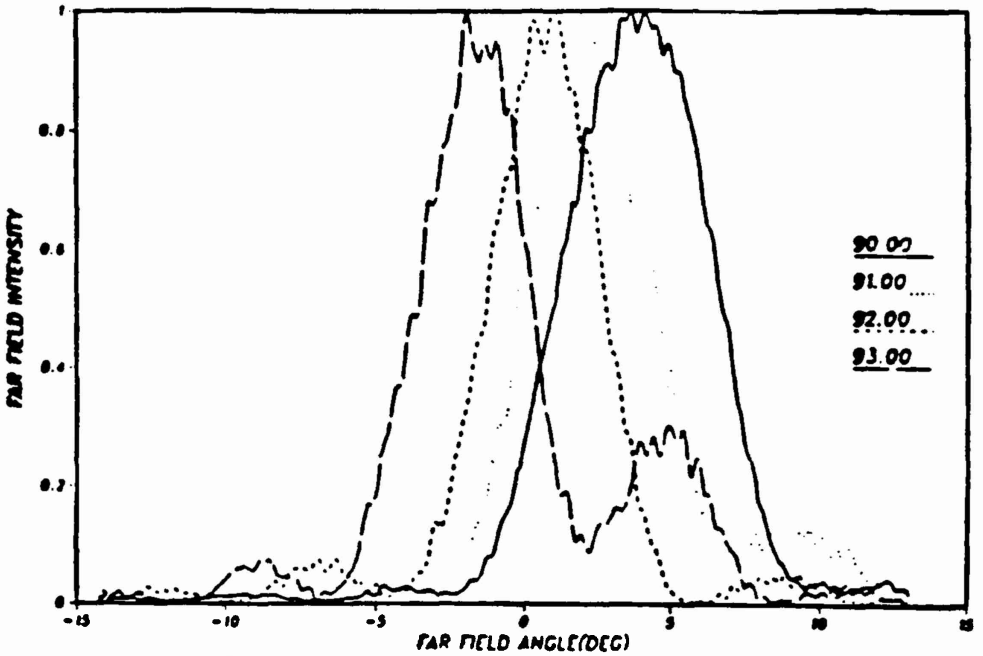

Fig.7a. Experimental results of the radiation pattern from a blazed waveguide structure for various frequencies.

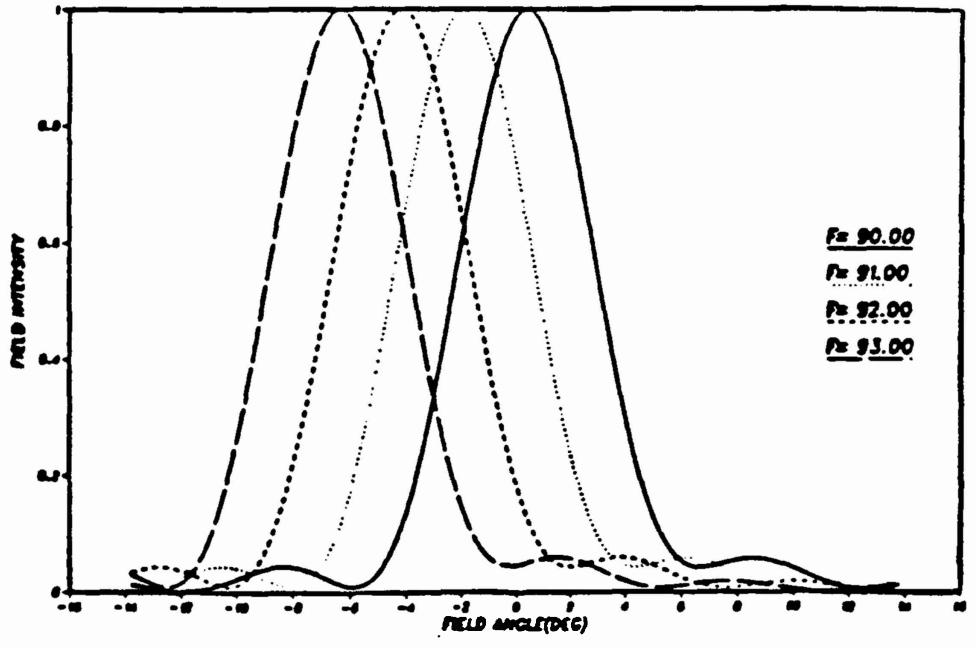

Fig.7b. Radiation pattern from a simulation of the blazed structure considered in Fig. 7a. Results show close agreement with experimental results of Fig. 7a.

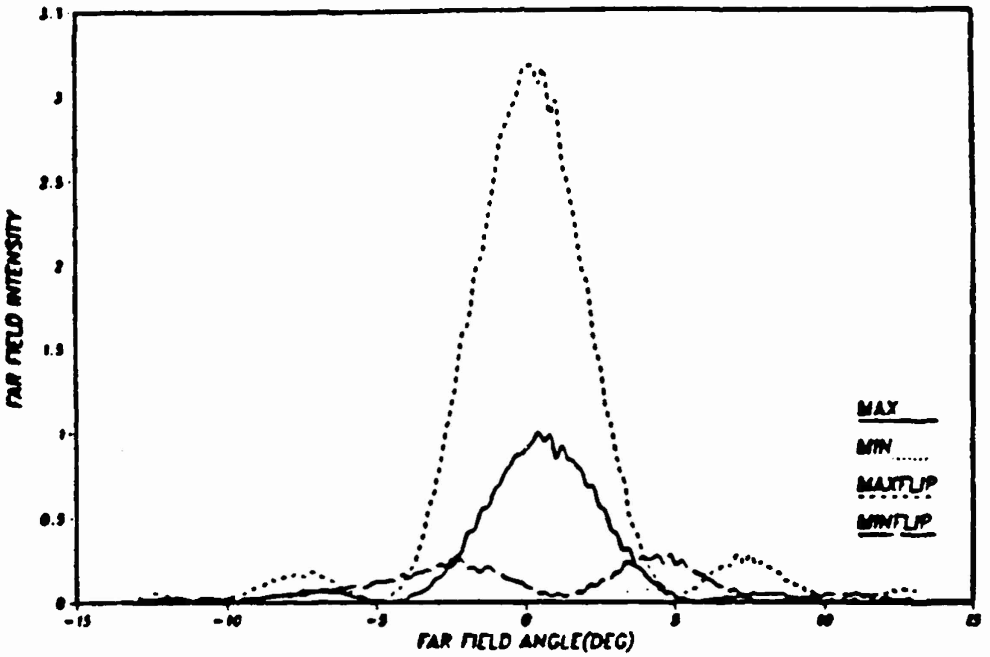

Fig:8. Waves are made incident from each of the two ends of the waveguide and a phase shifter is adjusted to get a maximum or minimum. The waveguide is flipped ('flip') to study the effect from the flat side of the waveguide.

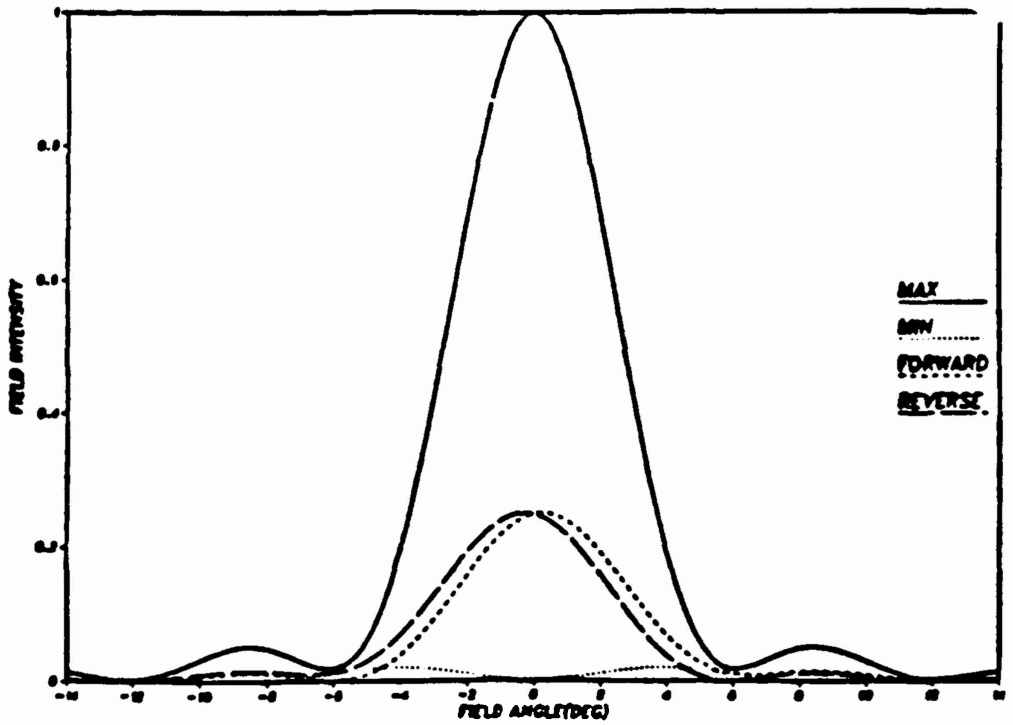

Fig:9. Simulated results of radiation pattern from a case of two sided incidence of waves. The phase shifter is adjusted to get a 'max.'

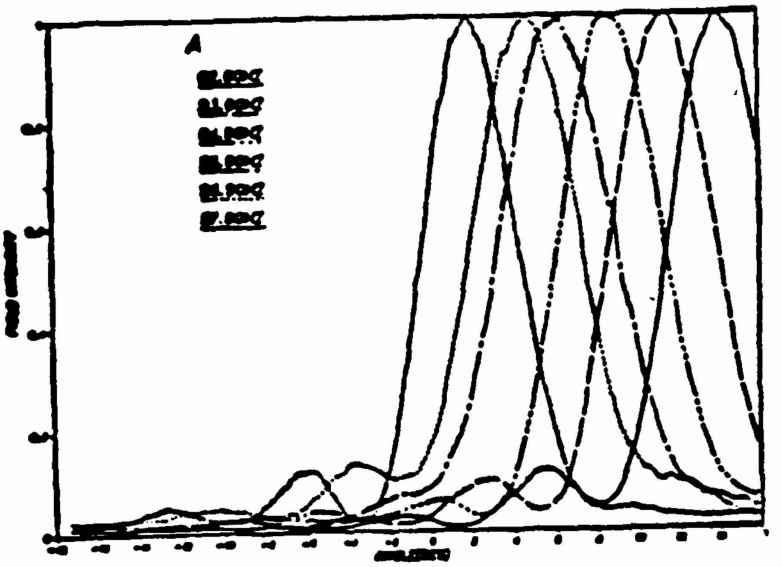

Fig:10a. Radiation pattern from one of the two sections 'A' of a two section waveguide.

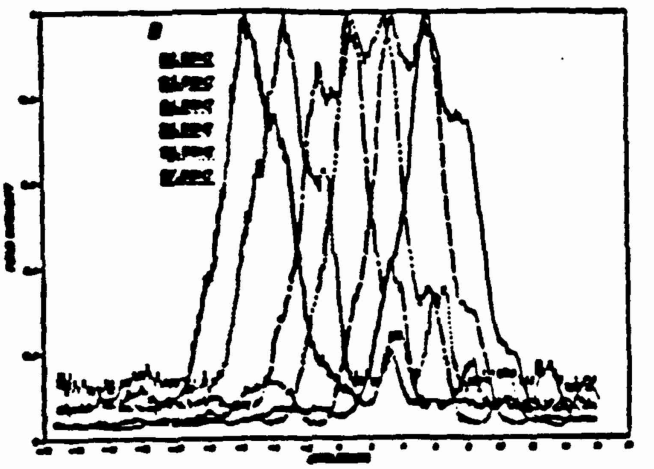

Fig:10b. Radiation pattern from section 'B' of a two section waveguide. The results from sections 'A' and 'B' are used to find the reflection, transmission and attenuation coefficients.

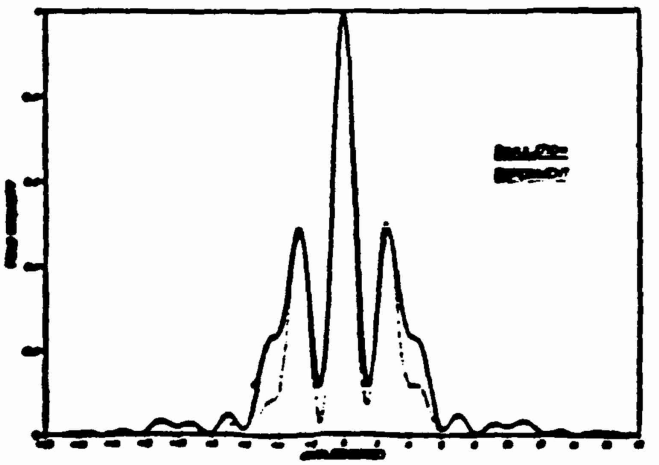

Fig:11. Experimental and simulated radiation patterns from a two section waveguide for a source frequency whose value is the average of the second Bragg frequencies of each section.

THEORITICAL AND EXPERIMENTAL INVESTIGATION OF PERIODIC CORRUGATED DIELECTRIC WAVEGUIDES*

C. S. Yeh, N. Urimindi and J. K. Butler

Department of Electrical Engineering
Southern Methodist University, Dallas, TX 75275

P. Stabile and A. Rosen

David Sarnoff Research Center, Princeton, NJ 08543-5300

ABSTRACT

In this experimental study we investigate the guided mode-radiation mode coupling of periodic dielectric waveguides. The dispersion relation and the attenuation constant along the dielectric waveguide were measured around the second Bragg frequency. The far field radiation pattern was also measured. Floquet theorem was applied to solve wave equations. Zero order approximation was used in the design of waveguides. For surface emitting structures used in surface emitting lasers and couplers, the most important parameter is the dispersion relation and attenuation constant along the corrugated waveguide around the second Bragg frequency. The dispersion and attenuation measurement shows that the attenuation constant minimum occurs at the second Bragg frequency. This corresponds to the maximum Q point of the corrugated waveguide. Two side incidence shows that in the out of phase condition the radiation power is minimum at the second Bragg frequency and have two lobes.

1. INTRODUCTION

Integrated circuit technology played a significant role in the fabrication of optical waveguides in recent days which simulated considerable interest in the use of corrugated dielectric structures. A dielectric waveguide with a periodic surface corrugation has been shown to hold substantial promise as a leaky wave antenna for millimeter wave applications. This class of structures has been widely used for integrated optic applications. The physics of wave propagation in optical devices can be carried over to the design of these antenna structures and basic optical principles can be used to provide information on the radiation pattern of such structure.

When a wave propagating in a corrugated waveguidde reaches the corrugated area , two things will occur: a portion of the wave will be diffracted out of the guide, into the air and the substrate, and a portion will be reflected. This radiation occurs only in certain preferred directions, primarily determined by the phase constant of the corrugated structure and the period of the corrugation. As a consequence of the radiation loss, the wave guided by the structure decays exponentially as it propagates. Hence the wave will exist with appreciable magnitude over a finite length of the waveguide and a beam is radiated with beam width proportional to the attenuation constant of the guided wave. Since the phase and attenuation constants determine

* Supported in part by the Army Research Office.

0-8194-0780-1/92/$4.00

the field characteristics, they are the most important parameters in the physics of the operation of these devices.

This paper deals with the design of corrugated waveguides of Al_2O_3 with $\epsilon = 9.6$ in the frequency range around the second Bragg condition. The attenuation constant, the dispersion realtion and the radiation pattern were measured around the second Bragg frequency. The patterns were compared with those obtained from a Huygens-Fresnel principle. The understanding of the wave propagation along the corrugated waveguide helps in the design of surface emitting lasers and couplers.

2. THEORITICAL BACKGROUND

The near field distribution for the frequency around the second Bragg coupling is [1]-[5]:

$$H_y = C\exp(-\alpha z - j(\beta - k)z) \tag{1}$$

Where H_y = y component of the magnetic field of the TM mode, α = attenuation constant, β =propagation constant, $k = 2\frac{\pi}{\Lambda}$, here Λ is the period of the corrugated waveguide. By using the Huygens-Fresnel principle [6] the field distribution at point (R,θ) is approximated as

$$F(R,\theta)\alpha\int_a^b \exp(-\alpha z)\exp(-j(\beta - k)z)\exp(jk_o(-z\sin\theta + \frac{z^2}{2R}))dz \tag{2}$$

where R is the distance from the waveguide to the receiver, θ = receiving angle of the detector, $k_o = 2\frac{\pi}{\lambda}$, λ being the free space wavelength, and a,b represents the upper and lower limits of the corrugation. From (2) the absolute value of F(R,θ) occurs at $\theta_{\max}$ and can be found approximately by setting $\beta - k + k_o \sin\theta_{\max} = 0$

$$\beta\frac{\Lambda}{\pi} = 2(1 - (k_o\frac{\Lambda}{\pi}\sin\theta_{max})) \tag{3}$$

and $\theta_{\max}$ was measured by $\frac{1}{2}(\theta_{1/2,R} + \theta_{1/2,L})$ where $\theta_{1/2,R}$ and $\theta_{1/2,L}$ are half power points on either side of the central peak of the radiation. The dispersion relation $\beta\frac{\Lambda}{\pi}$ versus $k_o\Lambda$ is plotted using (3).

2.1 Attenuation constant

The power radiated from the corrugated waveguide of length L is designated by P_L and is proportional to $1 - exp(-2\alpha L)$. By covering half of the far end corrugation the power radiated from the waveguide ($P_{L/2}$) was measured which is proportional to $1 - \exp(-\alpha L)$. By measuring the ratic of P_L and $P_{L/2}$ for different frequencies, the attenuation constant can be obtained by using the relation

$$\alpha = \frac{-1}{L}\ln(\frac{P_L}{P_{L/2}} - 1) \tag{4}$$

3. EXPERIMENTAL SETUP

The detailed experimental setup is shown in Figure 1. The functional blocks of the setup are as follows.

S: Tunable IMPATT oscillator.

M: Ferrite modulator: Used to chop the incident wave for the purpose of lock-in amplifier measurement.

FM: Precision frequency meter.

A1, A2, A3: (Variable attenuators): A1 is used to regulate the mm-wave power entering the system. A2 and A3 are used to regulate the power incident on either side of the dielectric waveguide.

DC1, DC2, DC3: (Directional couplers): DC1 is a 3 dB coupler used to divide the power into the two branches of the experimental setup. DC2 and DC3 are 10 dB couplers used to monitor the incident power level.

SW1, SW2: (Manual waveguide swithces): In the "open" position all the power is dissipated in a matched terminator.

PH: (Rotary-vane phase shifter): This is used to control the phase relationship between the two incident waves.

D1, D2, D3: (Flat broadband detectors): D1 and D2 are used to monitor the incident power and D3 is used to detect the far-field radiation. Lock-in amplifiers are used to amplify the signal from the detector. The output from the lock-in amplifier is directed to personal computer through the HP-IB.

MA: Motor assembly and linear potentiometer are used to rotate D3 and to measure the angle with the help of a computer.

CW: Corrugated dielectric waveguide under test. The physical structure of the waveguide is shown in Figure 2. (Shown four teeth only).

AS: Millimeter wave absorber used for attenuation constant measurement.

3.1 Waveguide specifications

The waveguides used are made of Al_2O_3 having $\epsilon = 9.6$. The dimensions of the two waveguides are as follows. waveguide #1: Period $\Lambda = 1.333$ mm, teeth width, tw = .6 mm, teeth height, th =.18 mm, number of teeth = 31, thickness t = 1.01 mm waveguide #2: Period $\Lambda = 1.333$ mm, teeth width, tw = .6 mm, teeth height, th = .2 mm, number of teeth = 32, thickness t =1.01 mm

4. EXPERIMENTAL RESULTS

For corrugated waveguide #1, the calculated second Bragg frequency usin Zero order approximation and effective index method is 89.0 GHz, i.e, $k_0 \Lambda = 2.485$. The experimental minimum of attenuation occurs at $k_0 \Lambda = 2.538$ which corresponds to a frequency of 90.9 GHz, and $\beta\frac{\Lambda}{\pi} = 2.03$ ($\beta\frac{\Lambda}{\pi} = 2.00$ is the second Bragg condition). This result is shown in Figures 3 and 4.

For corrugated waveguide #2, the calculated second Bragg frequency is 89.4 GHz, i.e, $k_0 \Lambda = 2.496$. The experimental minimum of attenuation occurs at $k_0 \Lambda = 2.558$ which corresponds

to a frequency of 91.6 GHz, and $\beta\frac{\Lambda}{\pi} = 2.00$. This result is shown in Figures 11 and 12. The second Bragg frequency is about 2% higher than the calculated value.

The experimental far field radiation pattern is very close to the calculated radiation pattern based on Huygens-Fresnel principle. The attenuation constant used in the calculation is $\alpha = .2/\text{cm}$, and the corresponding value of the attenuation $\alpha\Lambda = .026$. For two side incidence it simulates the operation of a surface emitting laser at second Bragg frequency. By changing the phase shift between the two incident waves the output power can be changed from maximum to minimum. These two cases corresponds to in-phase and out of phase conditions of the two incident waves respectively. The maximum Q is obtained at the point where the radiation is minimum.This happens at the out of phase condition of the two incident waves. The radiation appears in two lobes as shown in Figure 7. The calculated normalized radiation pattern at the out of phase condition is shown in Figure 9.

5. REFERENCES

[1] G. Hadjicostas, J. K. Butler, G. A. Evans, N. W. Carlson, and R. Amentea, " A numerical investigation of wave interactions in dielectric waveguides with periodic surface corrugations," IEEE J. of Quantum Electron., vol. QE-26, pp 893-902, May 1990.

[2] G. Hadjicostas, " Modal properties of planar dielectric waveguides with a surface corrugation," Ph.D Thesis, EE department, Southern methodist university, Dallas, TX, 1988.

[3] S. T. Peng, T. Tamir and H. L. Bertoni, " Theory of periodic dielectric waveguides," IEEE Trans. Microwave Theory and Tech., vol. MTT-23, pp. 123-133, Jan. 1975.

[4] K. Handa, S. T. Peng and T. Tamir, " Improved purturbation analysis of dielectric gratings", Applied Physics, 5, 325-328, 1975.

[5] W. Streifer, D. R. Scifres, R. D. Burnham, " Analysis of grating-coupled radiation in GaAs:GaAlAs Lasers and waveguides", IEEE J. of Quantum Electron., vol. QE-12, pp 422-428, July, 1976.

[6] J. W. Goodman, " Introduction to Fourier Optics, McGraw-Hill, New York, NY. 1968.

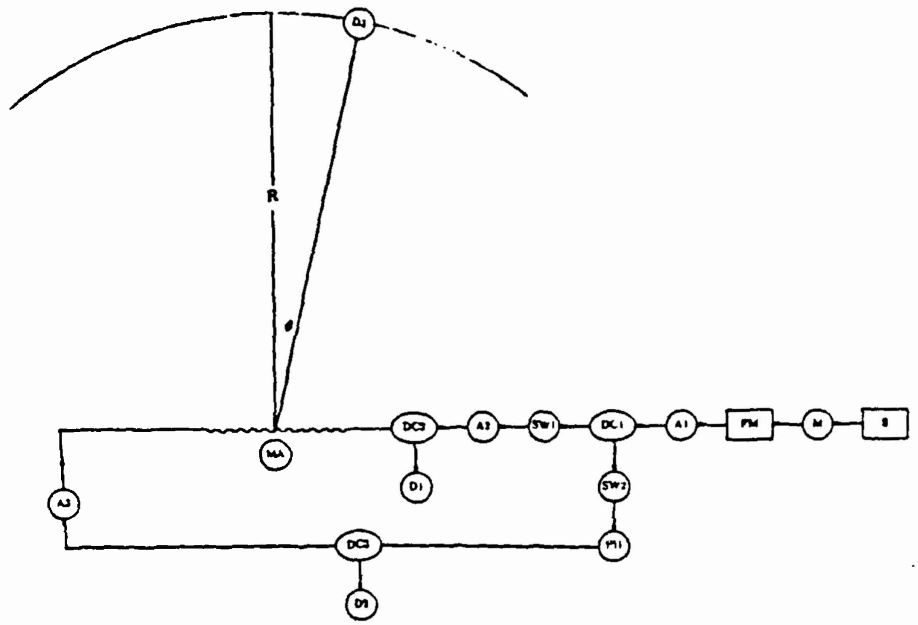

Figure 1: Experimental setup for dispersion relation, attenuation constant, and far field radiation pattern measurement, R = 90 cm.

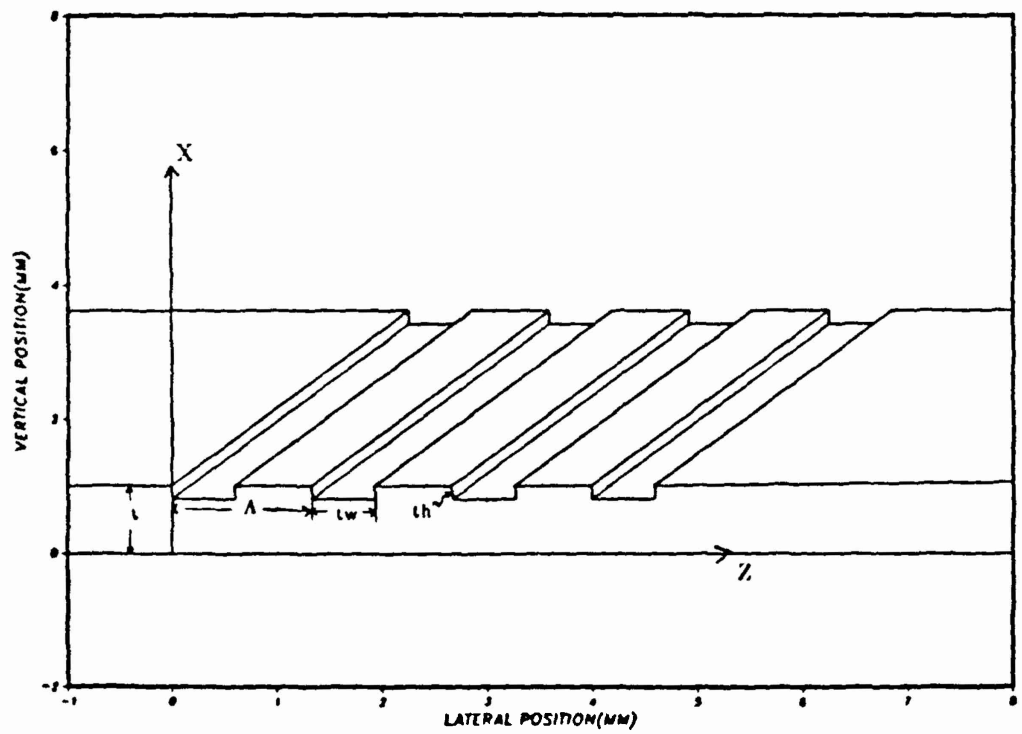

Figure 2: Structure of the corrugated dielectric waveguide made of Al_2O_3 and $\epsilon = 9.6$ (shown 4 teeth only).

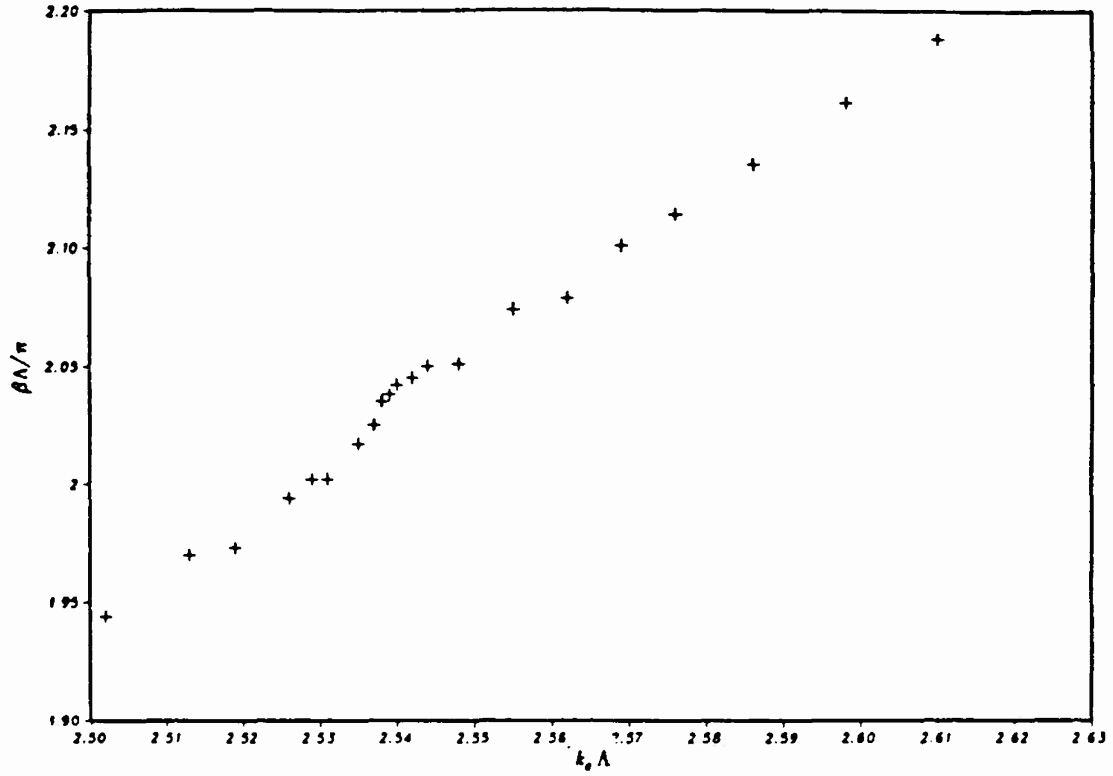

Figure 3: Dispersion relation of the waveguide #1.

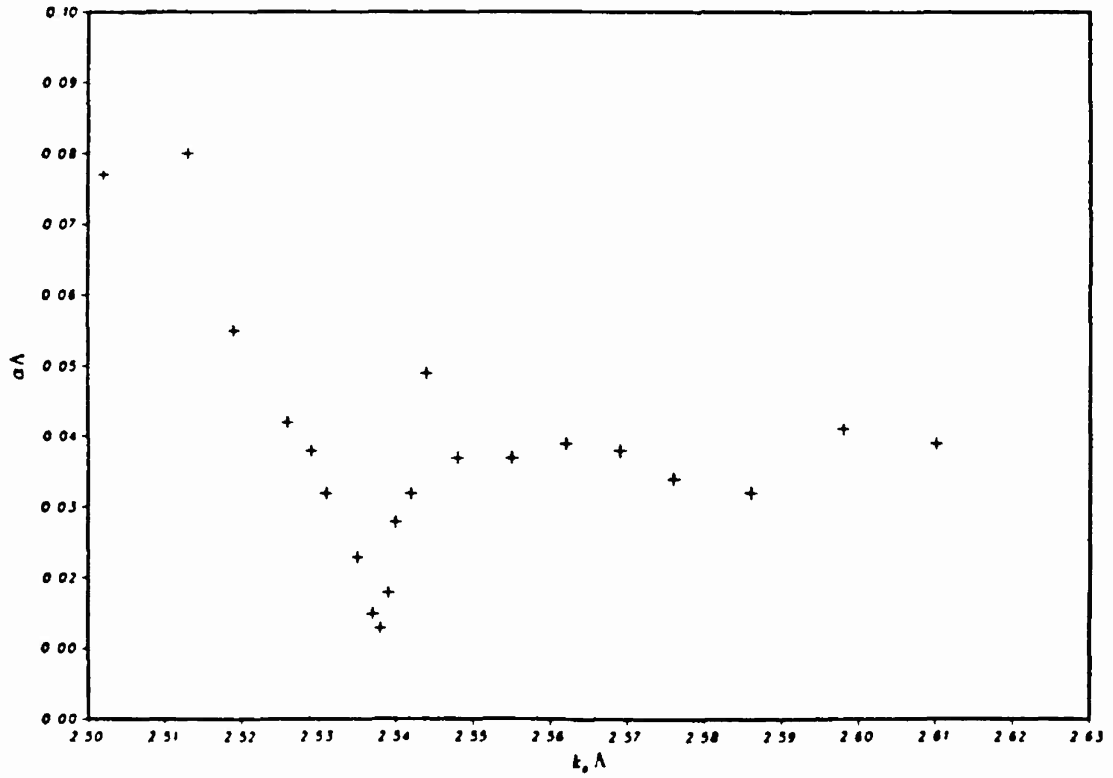

Figure 4: Attenuation constant versus $k_0 \Lambda$.

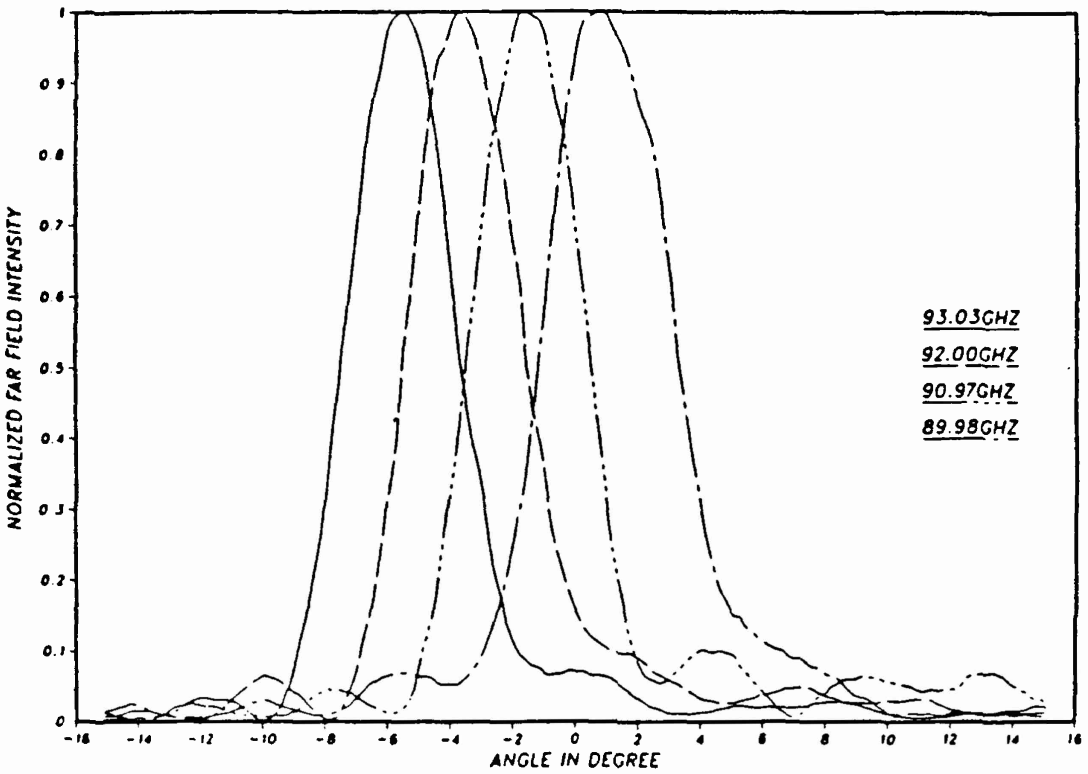

Figure 5: Far field radiation pattern of four sampled frequency.

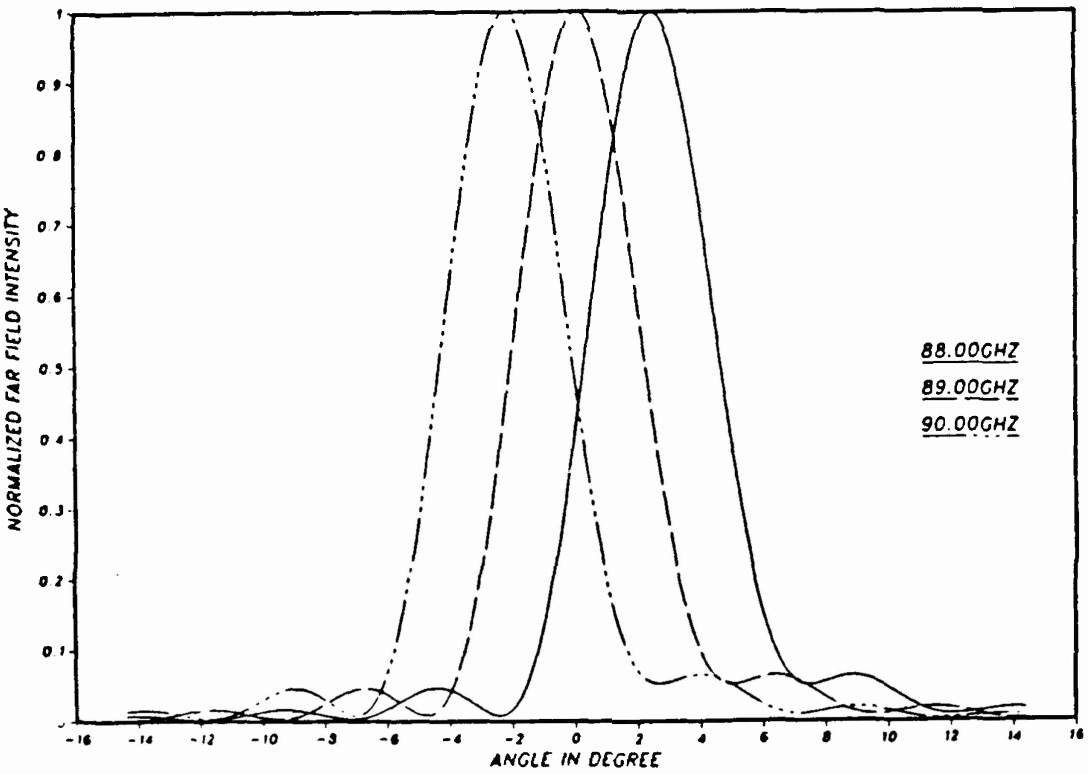

Figure 6: Simulated far field radiation pattern at 2nd Bragg. Calculated second Bragg frequency of waveguide #1 is 89.0 GHz.

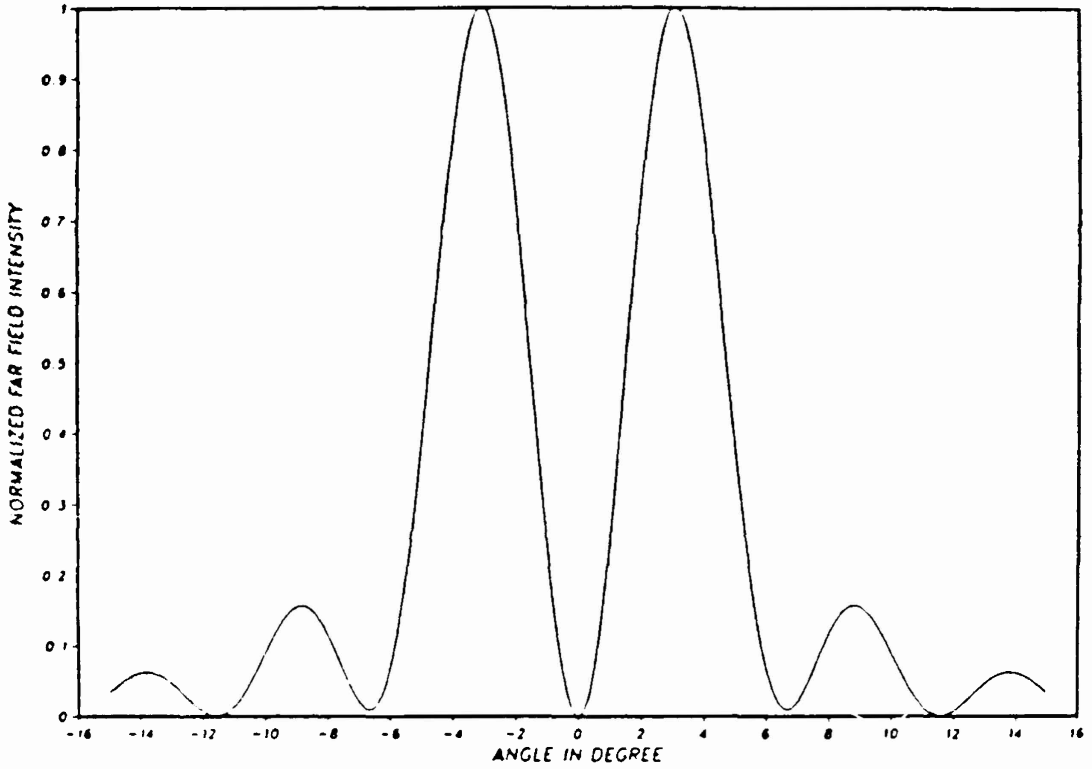

Figure 9: Simulated far field radiation pattern of the normalized two side incidence at the out of phase condition.

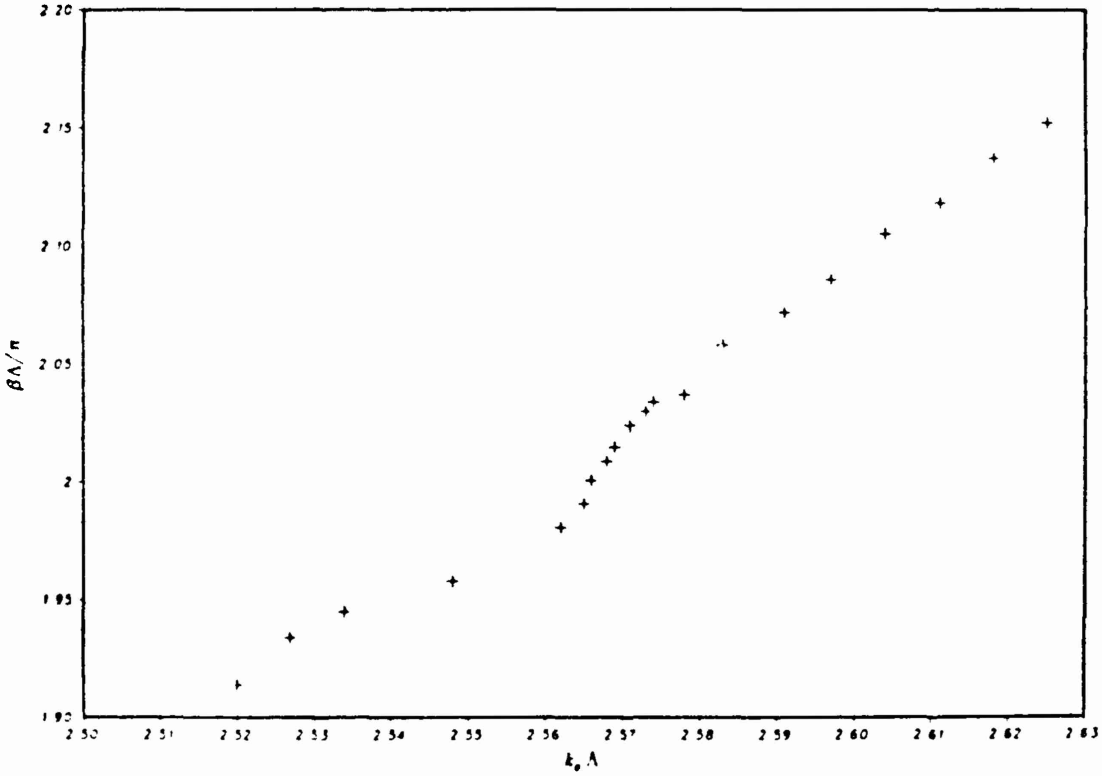

Figure 10: Waveguide #2 dispersion relation.

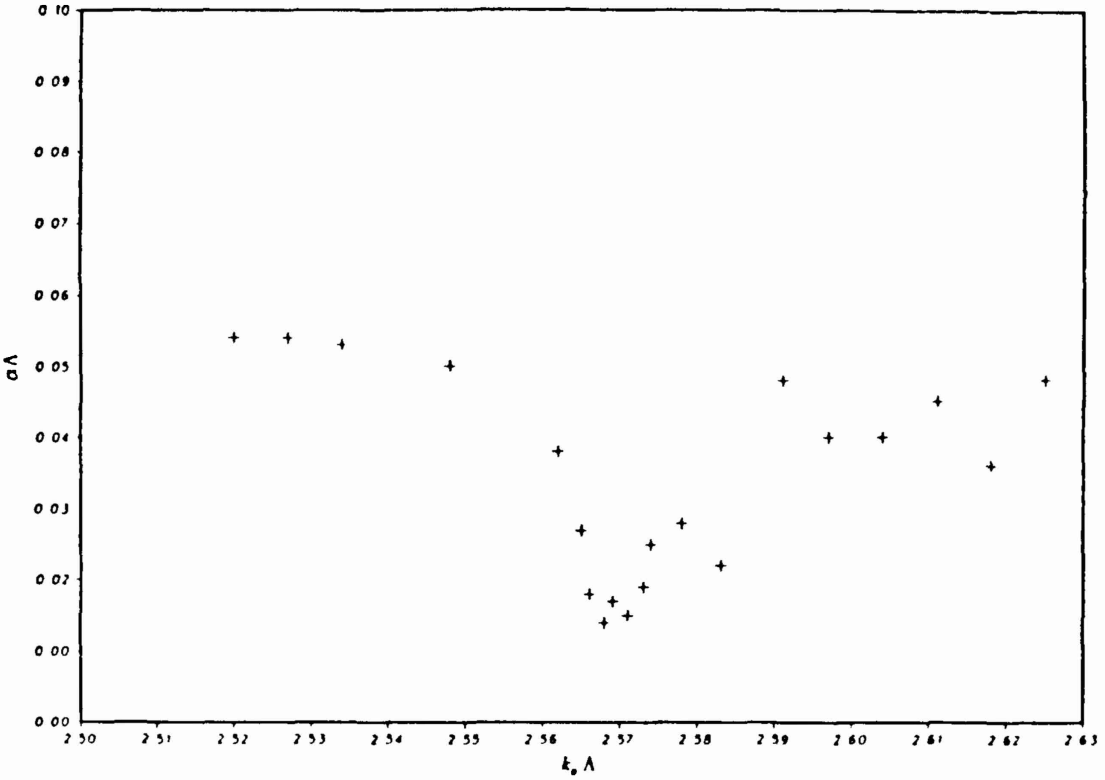

Figure 11: Attenuation constant versus $k_o\Lambda$ of waveguide #2

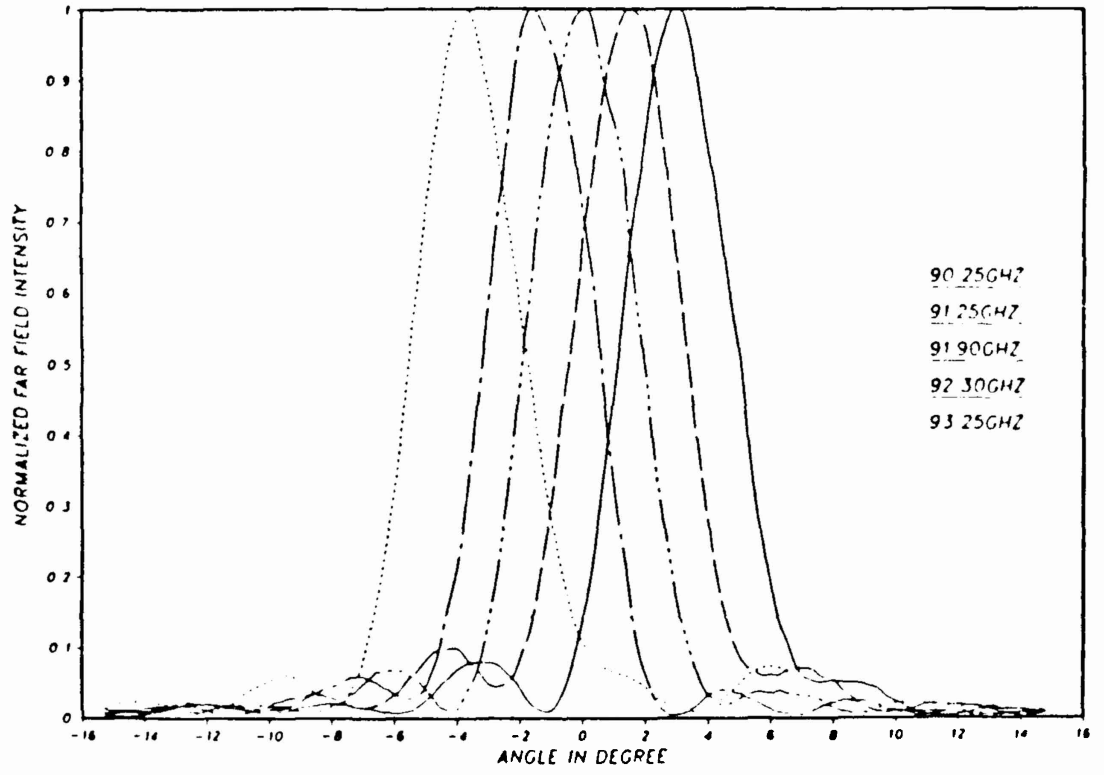

Figure 12: Far field radiation pattern of 5 sampled frequency of the waveguide #2

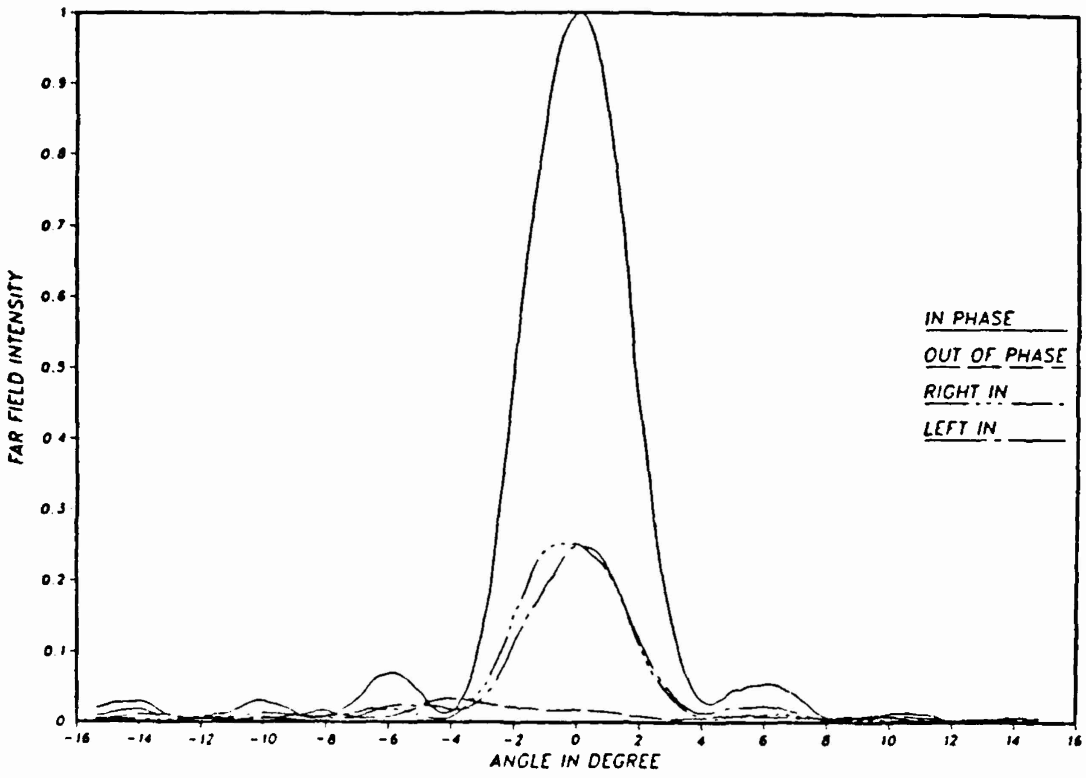

Figure 13: Radiation pattern of equal power incidence of waveguide #2.

A Boundary Element Technique Applied to the Analysis of Waveguides with Periodic Surface Corrugations

Jerome K. Butler, *Fellow, IEEE*, Warren E. Ferguson, Jr., Gary A. Evans, *Fellow, IEEE*, P. J. Stabile, *Senior Member, IEEE* and Arye Rosen, *Fellow, IEEE*

***Abstract*—Boundary integral formulation is used to characterize Floquet-Bloch modes of two-dimensional multilayered periodic waveguides. A new technique is described for matching fields inside the grating to those external to the grating region. Although a simple four layer structure is used to illustrate the method an extension to multilayer waveguide structures is straightforward. The mathematical formalism has been simplified, allowing for more efficient computations using fast Fourier transform algorithms.**

I. Introduction

PERIODIC structures designed to interact with propagating waves have been of interest for almost seven decades. Recent advances in semiconductor devices and processing technology has led to the employment of periodic structures in distributed feedback lasers [1], [2], in superlattices [3], and in millimeter-wave [4] and optical surface emitting [5] sources.

Numerical solution of many two dimensional problems can be reduced to one-dimensional problems through the use of Green's theorem. One popular method that uses this technique is called the boundary element method (BEM). Early applications of the BEM for the solution of static fields as well as for wave propagation problems were discussed by Brebbia [6], [7]. Application of the BEM to related electromagnetic field problems has received more recent attention [8]-[11]. Characterizing periodic waveguides has been accomplished by various methods. Application of the numerical boundary element method is relatively new; it was first applied to periodic millimeter-wave structures [12]-[14], and to optical waveguides used for surface emitting lasers [15]. Although BEM can be used on general types of periodic structures, it is particularly useful in the analysis of optically induced periodic structures. In these structures optical energy is used to excite electron-hole pairs, periodically, in a dielectric waveguide fabricated from a semiconductor material. Structures with a uniform distribution of light energy, such as a dielectric waveguide fabricated from gallium arsenide-aluminum gallium arsenide or thin silicon on sapphire (SOS), have been analyzed [16]. However, in the case of an all silicon guide, the distribution of the absorbed optical energy (hence electron-hole pair density), as measured from the surface of the waveguide, varies with depth [17]. Since this also results in a variation of the complex permitivity, it is best analyzed as a large number of layers each with a distinct complex permittivity.

This paper presents theoretical details which underlie the numerical application of the boundary element method (BEM) to the analysis of periodic dielectric waveguide structures. While this theoretical analysis supports general representations of the solution on the boundary of the grating, particular attention has been paid to the representation obtained by linear combinations of piecewise constant functions. Although the theoretical development is applicable to structures with multiple layers on either side of the corrugation region, the method is applied here to a simple four layer dielectric structure with rectangular corrugations. The top layer is air while the bottom layer is assumed to be a semi-infinite dielectric material. The grating lies between the air and central dielectric layer.

In the representation of the solution in regions above and below the grating the fields are represented by discrete Fourier series along the grating interfaces. In the event that a large number of boundary elements are required, fast Fourier transform techniques (FFT) can be employed to speed the computations.

II. Problem Formulation

Consider the dielectric waveguide geometry with a grating as shown in Fig. 1. The dielectric substrate and air superstate regions are assumed to be half spaces. The grating consists of the periodic juxtaposition of homogeneous rectangular Region A (dielectric constant κ_3) and Region B (dielectric constant κ_1). The (x, z) region $(-\infty, \infty) \times (0, \Lambda)$ is called the unit cell.

A time harmonic transverse electric (TE) wave is assumed to propagate in the axial z direction as $\exp(j\omega t - \gamma z)$. For the sake of simplicity it is assumed that the field

Manuscript received September 3, 1991, revised January 20, 1992. This work was supported in part by the Army Research Office and the Department of the Air Force.

J. K. Butler and W. E. Ferguson, Jr. are with the Southern Methodist University, Dallas, TX 75275.

G. A. Evans, P. Stabile, and A. Rosen are with the David Sarnoff Research Center, Princeton, NJ 08543.

IEEE Log Number 9200468

0018-9197/92$03.00 © 1992 IEEE

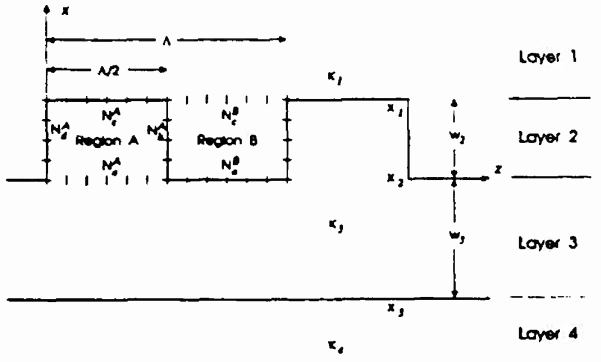

Fig. 1. The basic dielectric waveguide structure.

is invariant with respect to y. The complex propagation constant is $\gamma = \alpha + j\beta$. Although electric field polarization along the y direction is assumed, it is straightforward to extend the analysis to other polarizations. Polarization along y corresponds to the TE case where it is assumed that $E_y = \Psi$.

The core problem that must be solved is a characteristic-value problem in the grating region. This characteristic-value problem involves determining the value of the Floquet multiplier γ so that the wave function Ψ is a solution of the differential equation

$$\nabla^2\Psi + k_0^2\kappa(x, z)\Psi = 0. \tag{1}$$

Here $k_0 = 2\pi/\lambda$ is the free-space wavenumber and $\kappa(x, y)$ is the point dependent relative dielectric constant. The two dimensional wave function $\Psi(x, z)$ is required to satisfy the periodic condition

$$\Psi(x, z + \Lambda) = \Psi(x, z) \exp(-\gamma\Lambda). \tag{2}$$

Frequently, it is convenient to write the wave function in terms of an "amplitude" modulation function $\Phi(x, z)$ as

$$\Psi(x, z) = \Phi(x, z) \exp(-\gamma z) \tag{3}$$

where $\Phi(x, z) = \Phi(x, z + \Lambda)$ is a periodic function with period Λ.

The solution of the differential equation (1) is somewhat simplified by the fact that the unit cell is stratified into layers. In all layers where the dielectric constant is independent of z, i.e., the nongrated regions, the solution of the differential equation can be written in closed form.

The solution in layer 2 provides most of the interesting features of the present problem. In specific areas of the grating regions, Region A or Region B, the dielectric materials are homogeneous. The corresponding fields of each region satisfies the two-dimensional scalar Helmholtz equation:

$$\frac{\partial^2\Psi}{\partial x^2} + \frac{\partial^2\Psi}{\partial z^2} + k_0^2\kappa\Psi = 0. \tag{4}$$

The solution for Ψ in these regions is determined by a boundary integral formulation. The resulting characteristic value problem is obtained by appropriately matching the fields in the grating to those analytical forms above and below the grating.

III. Field Solutions Outside Grating

First, to properly formulate the problem, the wave solutions above and below the grating are derived. In the uniform layers above and below the grating, the field expressions have to appear in the Floquet–Bloch form in order to satisfy the boundary conditions on the grating surface. In the ith layer the solution becomes:

$$\Psi_i(x, z) = \exp(-\gamma z) \sum_{n=-\infty}^{\infty} \psi_{in}(x) \exp(-jnKz). \tag{5}$$

Here $K = 2\pi/\Lambda$ is the grating wavenumber. Outside layer 2 as shown in Fig. 1, the spatial harmonics ψ_{in} are uncoupled and satisfy the equation

$$\frac{d^2\psi_{in}}{dx^2} + [k_0^2\kappa_i + \gamma_n^2]\psi_{in} = 0 \tag{6}$$

where $\gamma_n = \gamma + jnK$. In the semi-infinite layers 1 and 4, the solutions become

$$\psi_{1n}(x) = \psi_{1n}(x_1) \exp[h_{1n}(x_1 - x)] \tag{7}$$

and

$$\psi_{4n}(x) = \psi_{4n}(x_3) \exp[h_{4n}(x - x_3)] \tag{8}$$

where the transverse wavenumbers $h_{in} = \pm(k_0^2\kappa_i + \gamma_n^2)^{1/2}$. The sign of the radical is always chosen such that analyticity is maintained in the vicinity of the second Bragg condition [18]. In the layer adjacent to the grating, the solution becomes

$$\psi_{3n}(x) = \psi_{3n}(x_3) \cos[h_{3n}(x - x_3)] + \psi'_{3n}(x_3) \sin[h_{3n}(x - x_3)]/h_{3n} \tag{9}$$

where $\psi' = d\psi/dx$. It should be noted that the functional dependence of $\psi_{3n}(x)$ and its derivative are written in terms of their initial values at $x = x_3$. In view of the above condition it is convenient to represent $\psi_{in}(x)$ and $\psi'_{in}(x)$ in terms of the vector

$$|\psi_{in}(x)\rangle = \begin{bmatrix} \psi_{in}(x) \\ \psi'_{in}(x) \end{bmatrix}. \tag{10}$$

Because E_y and its derivative are continuous across the boundaries, it follows that the individual space harmonics and their derivatives are continuous across each interface, i.e., $\psi_{3n}(x_3) = \psi_{4n}(x_3)$ and $\psi'_{3n}(x_3) = \psi'_{4n}(x_3)$. This implies the state vectors are continuous across the boundaries.

While the second order differential equation (6) has two solutions in the interior layer 3, application of the boundary conditions imposed at $x = \pm\infty$ allows only one solution in layers 1 and 4. Accordingly, there is only one unknown coefficient in the field solutions in those layers. In total there are only two unknown coefficients, those due to the solutions on either side of the grating region. By judiciously transforming the spatial harmonic solutions in the outside regions to the grating, the partial waves at the boundary of the grating can be expressed in terms

of a single constant. In terms of the transverse wavenumber and layer thickness,

$$|\psi_{3n}(x_2)\rangle = \mathbf{T}_{3n}|\psi_{3n}(x_3)\rangle \tag{11}$$

where the vector $|\psi_{3n}(x_2)\rangle = \text{col}\,(\psi_{3n}(x_2), \psi'_{3n}(x_2))$ represents the field and derivative at $x = x_2$ and $|\psi_{4n}(x_3)\rangle = \psi_{4n}(x_4)\,\text{col}\,(1, h_{4n})$ represents the field and derivative at $x = x_3$. Therefore, the transformation matrix $\mathbf{T}_{3n}$ is

$$\mathbf{T}_{3n} = \begin{bmatrix} \cos(h_{3n}w_3) & \sin(h_{3n}w_3)/h_{3n} \\ -h_{3n}\sin(h_{3n}w_3) & \cos(h_{3n}w_3) \end{bmatrix} \tag{12}$$

where w_3 is the thickness of the intermediate layer as shown in Fig. 1.

The process of formulating "closed-form" solutions for the individual spatial harmonics outside the grating region is possible because the harmonics are not directly coupled. Overall coupling of the space harmonics arises from the interaction of the harmonics in the grating region. The desired Floquet multiplier that renders the proper Floquet–Bloch mode is determined from the characteristic equation obtained by matching the field solutions outside the grating region to those inside the grating. This process of producing the secular equation is common to all methods used to determine the characteristic modes of periodic structures. The method used in this paper is called the boundary element formulation and is described below.

IV. Boundary Integral Form

The field solution inside the grating is now addressed. In the grating layer the coefficients ψ_n are all coupled together. It is convenient to avoid the laborious exact solution for the field everywhere inside the grating and seek a relation between Ψ and its normal derivative only along the boundary enclosing the homogeneous regions A or B. Towards this goal, we convert (4) into an integral equation. Results based on the numerical solution of integral equations have the advantage of being accurate even if the boundary conditions are only approximately met. In particular, for the problem at hand, the field and flux will be assumed piecewise constant and so a collocation (point matching) technique will be used to impose field continuity and periodicity.

According to [6], through the use of Green's second identity, (4) becomes:

$$\iint_R [G(\kappa, \bar{r}, \bar{r}')\nabla_t^2\Psi(\bar{r}) - \Psi(\bar{r})\nabla_t^2 G(\kappa, \bar{r}, \bar{r}')]\,ds = \oint_c \left[G(\kappa, \bar{r}, \bar{r}')\frac{\partial\Psi(\bar{r})}{\partial n} - \Psi(\bar{r})\frac{\partial G(\kappa, \bar{r}, \bar{r}')}{\partial n}\right] dl. \tag{13}$$

The left-hand side is a surface integral over the transverse plane Region R and the right-hand side is a closed line integral over the boundary contour c that encloses R. The quantity $\partial/\partial n$ denotes the outward normal derivative. When G in the above equation is chosen to satisfy:

$$\nabla_t^2 G(\kappa, \bar{r}, \bar{r}') + k_0^2\kappa G(\kappa, \bar{r}, \bar{r}') = -\delta(|\bar{r} - \bar{r}'|) \tag{14}$$

then (13) reduces to:

$$\Psi(\bar{r}) = \oint_c \left[G(\kappa, \bar{r}, \bar{r}')\frac{\partial\Psi(\bar{r}')}{\partial n} - \Psi(\bar{r}')\frac{\partial G(\kappa, \bar{r}, \bar{r}')}{\partial n}\right] dl \tag{15}$$

where $\bar{r} \in R$, whereas $\bar{r}' \in c$. (Specifically, region R is region A or B of Fig. 1.)

Solutions of (14) in two-dimensional space can be expressed in terms of Bessel functions. For a finite domain, any combination $C_0 J_n - (1/4)Y_n$ can be used (note that J_n is a solution of (14) only when $\bar{r} \neq \bar{r}'$). The coefficient of Y_n is determined to be $-1/4$ from the singularity condition at $\bar{r} = \bar{r}'$. For an infinite domain C_0 must equal $-j/4$ because only the second order Hankel function $-j(1/4)H_n^{(2)} = -j(1/4)(J_n - jY_n)$ satisfies the proper radiation condition (outward traveling waves vanishing at infinity). Analytically the results should be independent of C_0, but because the computations are done numerically, other choices of C_0 seem to produce less accurate results. In particular, when $C_0 = 0$ the convergence rate is rather slow when the thickness of the grating layer approaches zero. With $C_0 \neq 0$ the boundary integral approach used here automatically includes those conditions, previously proposed [10], that employ no singular functions. Since we found no consistent way of optimizing the value of C_0, the zero order Hankel function, unless otherwise stated, shall be used throughout, i.e.,

$$G(\kappa, \bar{r}, \bar{r}') = -j\tfrac{1}{4}H_0^{(2)}(k_0\sqrt{\kappa}|\bar{r} - \bar{r}'|). \tag{16}$$

In the limit when $\bar{r}$ approaches the boundary, (15) becomes [6]:

$$\frac{1}{2}\Psi(\bar{r}) = \oint_c \left[G(\kappa, \bar{r}, \bar{r}')\frac{\partial\Psi(\bar{r}')}{\partial n} - \Psi(\bar{r}')\frac{G(\kappa, \bar{r}, \bar{r}')}{\partial n}\right] dl \tag{17}$$

where $\bar{r}, \bar{r}' \in c$ and $\oint_c dl$ denotes the principal value line integral with the contribution of the singularity already accounted for.

V. Boundary Element Method

The integral equation (17) is discretized to a finite size matrix equation to obtain a numerical solution. The relation between Ψ and $\partial\Psi/\partial n$ for each region is independent of each other and so the equations are treated separately. The contours bounding regions A and B are partitioned as illustrated in Fig. 1. Along the bottom and top boundaries the partition length is $\Delta = \Lambda/(N_a^A + N_a^B)$ while the sides have $\bar{\Delta} = w_2/N_b^A$, where w_2 is the thickness of the grating layer as shown in 1. Note that the element lengths along the top and bottom of the unit cell are id..tical. Following

[6], we can write (17) as:

$$\tfrac{1}{2} u_i = \sum_{j=1}^{N} q_j \mathcal{S}_{ij} - \sum_{j=1}^{N} u_j \mathcal{D}_{ij} \tag{18}$$

where

$$\mathcal{S}_{ij} = \int_{c_j} G(\kappa, \bar{r}_i, \bar{r}_j)\, dl$$

$$\mathcal{D}_{ij} = \int_{c_j} \frac{\partial G(\kappa, \bar{r}_i, \bar{r}_j)}{\partial n}\, dl$$

and u_j and q_j are the field amplitude and flux, assumed constant over the jth boundary segment.

Upon placing $\mathcal{K} = \mathcal{D} + 1/2\mathcal{I}$, where $\mathcal{I}$ is the unit matrix, (18) becomes:

$$\mathcal{K}^R u^R = \mathcal{S}^R q^R \tag{19}$$

which, for every region $R(= A, B)$, relates the value of u at the midnode i, with the values of u and $\partial u/\partial n$ at every other node j, including $j = i$.

All line integrals along the elements c_j: $j \neq i$, can be calculated numerically using a 4-point quadrature rule [19], or using ADAPT as discussed in the Appendix. When $j = i$, the integration path $c_j = c_i$, contains the "source point" $\bar{r}_i = (x_i, z_i)$ and a logarithmic type singularity is present. Even though this singularity is analytically integrable, a logarithmic Gauss quadrature rule has been used again in order to maintain good accuracy.

Ordering the elements of $\mathcal{S}$ and $\mathcal{D}$ in each of the regions proceeds by numbering the elements in a counter clockwise direction starting from the lower left corner. In region A, there are $N^A = N_a^A + N_b^A + N_c^A + N_d^A$ elements, whereas region B has $N^B = N_a^B + N_b^B + N_c^B + N_d^B$ elements. (The superscripts identify the two regions.) The sides have $N_d^A = N_b^A = N_d^B = N_b^B$. The top and bottom elements have $N_a^A = N_c^A$ and $N_a^B = N_c^B$. To facilitate matching the fields in region A to those of region B, and the grating fields to the outside layers, the element ordering on sides denoted as having N_c and N_d elements, is reversed. This can be accomplished by interchanging appropriate rows and columns of $\mathcal{S}$ and $\mathcal{D}$.

VI. Field and Flux Matching Conditions

The vectors u^R and q^R are partitioned as

$$u^R = \begin{bmatrix} u_a^R \\ u_b^R \\ u_c^R \\ u_d^R \end{bmatrix} \quad q^R = \begin{bmatrix} q_a^R \\ q_b^R \\ q_c^R \\ q_d^R \end{bmatrix}. \tag{20}$$

The corresponding matrices $\mathcal{K}^R$ and $\mathcal{S}^R$ are also partitioned accordingly.

For each region, (19) represents a set of $N^A + N^B$ homogeneous equations with $N^A + N^B$ unknown fields and fluxes, or a total of $2(N^A + N^B)$. The equations needed to determine the solution are provided by imposing continuity across the $x = 0$ and $x = w_2$ interfaces, as well as continuity and periodicity conditions across the Region A–Region B interface. The interface between the lower section of the waveguide and the grating regions A and B is shown in Fig. 2.

In the limit as the tooth height becomes small, the waveguide looses its periodic nature. The Floquet–Bloch modes approach those of a regular dielectric waveguide; accordingly the field amplitude tends to a constant value with respect to z. Because numerical accuracy of the boundary element method using piecewise constant elements is improved when the unknown variables are almost constant, it seems appropriate to configure the present problem to one where the unknown variables along a boundary are almost constant. To carry this condition into the model, the field and flux amplitudes are transformed as follows:

$$u_a^R = \Gamma_a^R U_a^R \tag{21}$$

$$u_b^R = \Gamma_b^R U_b^R \tag{22}$$

$$u_c^R = \Gamma_c^R U_c^R \tag{23}$$

$$u_d^R = \Gamma_d^R U_d^R. \tag{24}$$

The corresponding transformations of the flux vectors are

$$p_a^R = \Gamma_a^R P_a^R \tag{25}$$

$$p_b^R = \Gamma_b^R [P_b^R - \gamma U_b^R] \tag{26}$$

$$p_c^R = \Gamma_c^R P_c^R \tag{27}$$

$$p_d^R = \Gamma_d^R [P_d^R + \gamma U_d^R]. \tag{28}$$

The matrix Γ_ξ^R is diagonal $(N_\xi^R \times N_\xi^R)$ with elements $\Gamma_{\xi ll}^R = \exp(-\gamma z_l)$, where $\xi = a, b, c, d$, refers to the different sides of region R. The coordinate position z_l corresponds to the location of the nth element and is given by (region A):

$$z_l = \begin{cases} (2l-1)\,\Delta/2, & l = 1, \cdots, N_a^A \\ \Lambda/2, & l = 1, \cdots, N_b^A \\ (2l-1)\,\Delta/2, & l = 1, \cdots, N_c^A \\ 0, & l = 1, \cdots, N_d^A. \end{cases}$$

The corresponding z_l values in region B are obtained by adding the half period $\Lambda/2$. Note that the elements on the sides have constant z_l values and that the element ordering along the top proceeds in a clockwise fashion.

Boundary conditions between regions A and B consist of continuity conditions applied to the field and flux values of each of the two regions. Note that the resulting equations specify the conditions on the field and flux "amplitudes" U^R and P^R as compared to the field and flux values u^R and p^R, originally given in [13]. Field continuity gives

$$U_d^B = U_b^A, \tag{29}$$

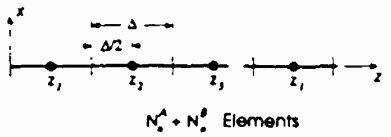

Fig. 2. The interface between the lower waveguide and grating region. The center position of the lth element is located at z_l.

while flux continuity yields

$$P_d^B = -P_b^A. \tag{30}$$

The periodicity condition specified by (2) requires

$$U_d^A = U_b^B \tag{31}$$

for the fields and

$$P_d^A = -P_b^B \tag{32}$$

for the fluxes.

The field and flux values inside the grating must match those on the outside layers. Fig. 2 shows the boundary points at either the top or the bottom of the grating layer. (For the sake of simplicity it is assumed that there are even number of boundary points, i.e., $N_a^A + N_a^B = N_f$ is an even number.) The number of grating points also represents the number of spatial harmonics used in the expansion (5). The field "amplitude" values at the bottom of the grating are represented by the two vectors U_a^A and U_a^B so therefore field continuity conditions yield

$$\begin{bmatrix} U_a^A \\ U_a^B \end{bmatrix} = \begin{bmatrix} \Phi_3(x_2, z_1) \\ \Phi_3(x_2, z_2) \\ \vdots \\ \Phi_3(x_2, z_{N_f}) \end{bmatrix}. \tag{33}$$

The flux "amplitudes" are represented by the two vectors P_a^A and P_a^B, so flux continuity is satisfied by requiring

$$\begin{bmatrix} P_a^A \\ P_a^B \end{bmatrix} = \begin{bmatrix} -\Phi_3'(x_2, z_1) \\ -\Phi_3'(x_2, z_1) \\ \vdots \\ -\Phi_3'(x_2, z_{N_f}) \end{bmatrix} \tag{34}$$

where $\Phi' \equiv \partial\Phi/\partial x$. Note that the negative sign for the elements on the RHS of the above equation is present because flux values are directed outward from each of the two regions. The linear equations resulting from imposing boundary conditions at the top of the grating are similar to (33) and (34).

In the following discussion, a unique representation of the field and flux values will be represented in terms of the discrete Fourier series of the spatial harmonics. This simplified representation is possible because 1) the boundary element locations are situated at uniform points along the top and bottom of the grating, and 2) the propagation term has been lifted. If N_f is the total number of boundary elements, then $K\Delta = 2\pi/N_f$. In terms of the spatial harmonics ψ_{3n}, the amplitude coefficients are

$$\Phi_3(x_3, z_l) = \sum_{n=-N_f/2}^{N_f/2-1} \psi_{3n}(x_3) \exp(-jnKz_l). \tag{35}$$

Putting $W = \exp(-j2\pi/N_f)$, $\Phi_3(x_3, z_l) = \Phi_l$ and $\phi_n = \psi_{3n}(x_3, z_l) W^{-n/2}$, the above expression can be written as

$$\Phi_l = \sum_n \phi_n W^{nl}. \tag{36}$$

The sets of numbers Φ_l and ψ_n form a discrete Fourier series pair of order N_f, denoted as $\Phi_l \leftrightarrow \phi_n$. The inverse is [20]

$$\phi_n = \frac{1}{N_f} \sum_l \Phi_l W^{-nl}. \tag{37}$$

Similarly, the flux terms produce a set of numbers Φ_l' and ϕ_n' that form a discrete Fourier series pair of order N_f, $\Phi_l' \leftrightarrow \phi_n'$.

The quantities ϕ_n and ϕ_n' are related through the transformation given in (11)

$$\frac{\phi_n'}{\phi_n} = \frac{T_{3n21} + T_{3n22}h_{4n}}{T_{3n11} + T_{3n12}h_{4n}} \equiv -1/(N_f r_n) \tag{38}$$

where T_{3nkl} is the klth element of the matrix T_{3n} as given by (12). (The negative sign has been added to the definition of r_n to reflect the fact the outward flux from regions A and B is directed in the negative x direction. This representation simplifies a later result.) In the event that the number of layers below the grating must be increased, the equivalent matrix elements must be used in (38). (The equivalent matrix is the product of the transfer matrices of the individual layers.)

The application of the boundary conditions at the bottom of the grating as described by (33) and (34) yields a linear relation between the field and flux values given by

$$\begin{bmatrix} U_a^A \\ U_a^B \end{bmatrix} = \mathcal{R} \begin{bmatrix} P_a^A \\ P_a^B \end{bmatrix} \tag{39}$$

where $\mathcal{R}$ is the circulant [20] matrix

$$\mathcal{R} = \begin{bmatrix} R_0 & R_1 & \cdots & R_{N_f-1} \\ R_{N_f-1} & R_0 & \cdots & R_{N_f-2} \\ \vdots & \vdots & \ddots & \vdots \\ R_1 & R_2 & \cdots & R_0 \end{bmatrix}. \tag{40}$$

The elements R_l and r_n also form a discrete Fourier series pair of order N_f, where

$$R_l = \sum_n r_n W^{nl}. \tag{41}$$

Application of the boundary conditions at the top of the grating is similar to the process at the bottom. Although the particular problem at hand has only one layer above the grating, multiple layers above the grating can be treated similarly to the method described above for multiple layers below the grating. The field and flux values

are linearly related according to

$$\begin{bmatrix} U_c^A \\ U_c^B \end{bmatrix} = S \begin{bmatrix} P_c^A \\ P_c^B \end{bmatrix} \tag{42}$$

where S is a circulant matrix whose elements S_l are determined from the discrete Fourier series

$$S_l = \sum_n s_n W^{nl} \tag{43}$$

where $s_n \equiv -1/(N_f h_{1n})$.

After appropriate substitution we end up with a system of $N^A + N^B$ equations and $N^A + N^B$ unknowns; the coefficients of the $N^A + N^B$ unknown boundary fields and their normal derivatives form the complex elements of the matrix $\mathcal{F}$ [14]. The resulting linear set of equations becomes

$$\mathcal{F} \begin{bmatrix} U_b^A \\ P_b^A \\ P_a^A \\ P_a^B \\ U_b^B \\ P_b^B \\ P_c^A \\ P_c^B \end{bmatrix} = 0. \tag{44}$$

The matrix $\mathcal{F}$ is partitioned with 2 rows and 8 columns as

$$\mathcal{F} = \begin{bmatrix} (H_b^A + \gamma G_b^A)e^{-\gamma\Lambda/2} & -G_b^A e^{-\gamma\Lambda/2} & H_a^A \Gamma_a^A \mathcal{R}_{AA} - G_a^A \Gamma_a^A & H_a^A \Gamma_a^A \mathcal{R}_{AB} \\ (H_d^B - \gamma G_d^B)e^{-\gamma\Lambda/2} & G_d^B e^{-\gamma\Lambda/2} & -H_a^B \Gamma_a^B \mathcal{R}_{BA} & H_a^B \Gamma_a^B \mathcal{R}_{BB} - G_a^B \Gamma_a^B \\ H_d^A - \gamma G_d^A & G_d^A & H_c^A \Gamma_c^A \mathcal{S}_{AA} - G_c^A \Gamma_c^A & H_c^A \Gamma_c^A \mathcal{S}_{AB} \\ H_b^B + \gamma G_b^B & -G_b^B e^{-\gamma\Lambda} & H_c^B \Gamma_c^B \mathcal{S}_{BA} & H_c^B \Gamma_c^B \mathcal{S}_{BB} - G_c^B \Gamma_c^B \end{bmatrix}. \tag{45}$$

Such a homogeneous system of linear equations will have a nontrivial solution provided that the determinant of the matrix $\mathcal{F}$ vanishes. Since the only unknown in $\mathcal{F}$ is γ, the resonant solutions, if any, of the determinantal equation will give the propagation constants for the structure modes:

$$\det [\mathcal{F}(\gamma)] = 0 \tag{46}$$

Following the computation for γ, all the unknown fields and derivatives can be evaluated under a suitable normalization condition. A complex root finder routine based on Muller's method has been used for the numerical evaluation of the above secular equation. The Floquet amplitudes for the field expansion in all the uniform regions can subsequently be evaluated.

VII. Numerical Results

The characteristic values of the propagation constant γ were computed for several boundary partitions to illustrate the convergence of the attenuation coefficient α. This example, with frequent appearance in the literature, was first presented by Peng *et al.* [21]. Fig. 1 shows the basic structure with the following parameters, $\Lambda = \lambda/2$, (λ is the free-space wavelength), $\kappa_1 = 1$, $\kappa_3 = 3$, $\kappa_4 = 2.3$, and the waveguide thickness $w_3 = \lambda/\pi$. In this structure the duty cycle is 50%. The wavelength $\lambda_z = 2\pi/\beta$ of the fundamental Floquet–Bloch mode has an upper and lower bound satisfied by $\lambda/\sqrt{3} < \lambda_z < \lambda/\sqrt{2.3}$ so that the second Bragg condition ($\lambda_z = \Lambda$) has not been reached. This means that leaky wave radiation will occur in the backward direction.

Before illustrating the computation of the characteristic values of the propagation constant the values of the Fourier series pair r_n and R_l are shown for the values $N_a = 10$, $N_c = 8$, and the tooth height $w_2/\lambda = 0.2$. The number of points taken around the boundaries of regions A and B are identical. The tooth height–width ratio corresponds to 4/5 so that the present boundary element configuration yields equal partition lengths along the horizontal and vertical sides of the tooth. Fig. 3(a) shows the magnitude of r_n while Fig. 3(b) shows the magnitude of R_l. The coefficients r_n decrease as $1/|n|$ for large n values. Although exact values of r_n depend on γ, changes of their respective values in the vicinity of the second Bragg condition are rather small. For the present condition, the major coefficients r_n are for $n = 0, -1, -2$. These harmonics will be dominant in the transform, clearly shown in Fig. 3(a).

Generally the discrete Fourier series pair are associated with either a space harmonic quantity (integer n) or space position (integer l). The space harmonic ϕ_n and the "amplitude" function Φ_l are shown in Fig. 4 for the 5 × 4 configuration. Note that the "dc" component $n = 0$ and the $n = -1$ harmonic are dominant. Most of the harmonic amplitudes are below two orders of magnitude below the dominant term.

The computed value of γ depends on the number of boundary points. For the 5 × 4 partition with the above geometry, $\alpha\lambda = 1.9096 \times 10^{-2}$ and $\beta/k_0 = 1.5795$. (The computed values given by Peng *et al.* [18] are $\alpha\lambda = 1.8716 \times 10^{-2}$ and $\beta/k_0 = 1.5809$.) Increasing the partition number by 4, to 20 × 16, gives $\alpha\lambda = 1.8713 \times 10^{-2}$ and $\beta/k_0 = 1.5806$. Although the latter partition gives results almost identical to that of Peng *et al.* at a tooth height of $w_2/\lambda = 0.2$, the accuracy of the computations vary with tooth height.

Computation of the attenuation coefficient versus grating depth will now be considered. Each of the curves generated start at a tooth height of 0.2. The attenuation coefficient decreases monotonically as the grating depth tends to zero. In the first example, illustrated in Fig. 5 as 5 × 1, $N_a = 5$ and $N_b = 1$. The value of α tends to zero much

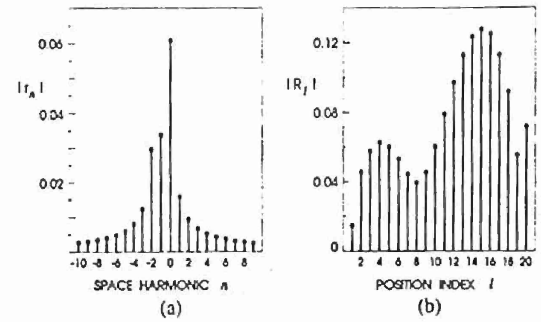

Fig. 3. The coefficients (a) $|r_n|$ and (b) $|R_l$ computed at the bottom of the grating.

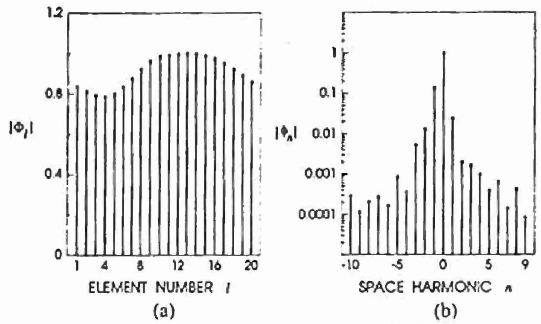

Fig. 4. The discrete Fourier series pair $\Phi_l \leftrightarrow \phi_n$.

TABLE I
THE EIGENVALUE CONVERGENCE IN TERMS OF THE NUMBER OF BOUNDARY ELEMENTS

$N_a \times N_c$	$\alpha\lambda \times 10^2$	β/k_0
5 × 4	1.9096	1.5795
10 × 8	1.8767	1.5803
20 × 16	1.8713	1.5806
25 × 20	1.8710	1.5807
Peng *et al.*	1.8716	1.5808

$w_2/\lambda = 0.20$.

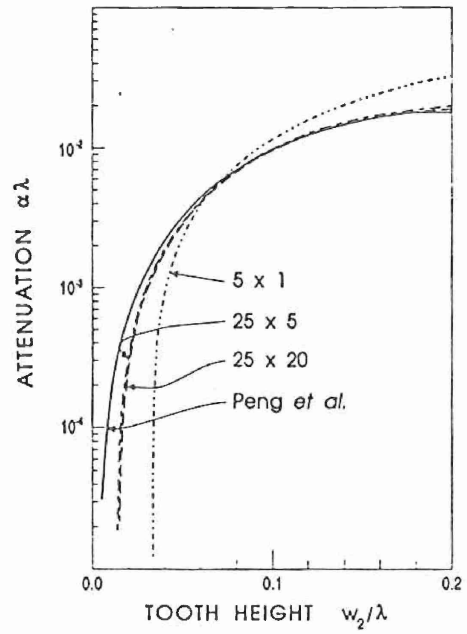

Fig. 5. The attenuation coefficient $\alpha\lambda$ as a function of the grating depth w_2/λ. The solid curve represents the data from [18]. The remaining curves are computed using the boundary element method with the number of boundary points denoted as $N_a^A \times N_b^A$.

earlier than in the cases for the higher number of elements. As the number of elements is increased, in the next two examples denoted as 25 × 5 and 25 × 20, the new curves approach that calculated in [21], however, it is noted that there are only slight differences in the two cases. For tooth heights $w_2/\lambda > 0.06$ the solution of the latter two examples appears to be relatively accurate.

All calculations as illustrated in the figure use $H_0^{(2)}$ for the Green's function. However, when Y_0 was used, the calculated results showed pronounced degradation for the attenuation coefficient. In particular, all curves with similar boundary element numbers calculated using Y_0 for the Green's functions tend to zero more rapidly with decreasing grating depth than that illustrated by the 5 × 1 curve.

VIII. Conclusion

The boundary integral formulation has been used to calculate the Floquet–Bloch modes of two-dimensional periodic waveguides. In the formulation of the method a new technique has been developed for matching the fields inside the grating to those outside the grating. Although the four layer structure used to illustrate the method is relatively simple, an extension to multilayer waveguide structures can be easily effected. In the event that gratings become geometrically complicated, it will be necessary to increase the number of boundary points along the unit cell. The techniques developed here can be applied to more complicated tooth forms, requiring some of the numerical computations to be carried out efficiently. For example, the $\mathcal{R}$ and $\mathcal{S}$ matrices are computed using discrete Fourier series. When the number of points N_a^A and N_a^B are large efficient FFT algorithms can be used to speed the computation of the matrix elements.

Appendix

The program ADAPT was written to evaluate the matrix elements of $\mathcal{G}$ and $\mathcal{JC}$. It estimates the value of integrals of the form

$$I_1 = \int_a^b f(x)\,dx \quad \text{and} \quad I_2 = \int_a^b \log\left(\frac{1}{x}\right) f(x)\,dx$$

for $b > a \geq 0$. For user specified values of ABSERR and RELERR, ADAPT computes an estimate $\tilde{I}_j$ of I_j whose absolute error is bounded above by max {ABSERR, RELERR* $|\tilde{I}_j|$}. ADAPT obtains this estimate by creating a partition $\{[a_i, b_i]: i = 1, n\}$ of the interval $[a, b]$ with the property the error in the estimates of the integrals over $[a_i, b_i]$ are sufficiently small. The integrals over $[a_i, b_i]$ have one of the following two forms:

$$\int_{a_i}^{b_i} g(x)\,dx = (b_i - a_i) \int_0^1 g(a_i + (b_i - a_i)t)\,dt$$

or

$$\int_0^{b_i} \log\left(\frac{1}{x}\right) g(x)\,dx = b_i \int_0^1 \log\left(\frac{1}{x}\right) g(b_i t)\,dt + b_i \cdot \log\left(\frac{1}{b_i}\right) \int_0^1 g(b_i t)\,dt$$

where $b_i > a_i \geq 0$. ADAPT uses a Gauss–Kronrod rule with weight 1 to estimate the values of the integrals

$$\int_0^1 g(a_i + (b_i - a_i)t)\,dt \quad \text{and} \quad \int_0^1 g(b_i t)\,dt$$

and a Gauss–Kronrod rule with weight $\log(1/x)$ to estimate the value of the integral

$$\int_0^1 \log\left(\frac{1}{x}\right) g(b_i t)\,dt.$$

References

[1] H. Kogelnik, "Coupled wave theory for thick hologram gratings," *Bell Syst. Tech. J.*, vol. 48, pp. 2909–2947, Nov. 1969.

[2] H. Kogelnik and C. V. Shank, "Stimulated emission in a periodic structure," *Appl. Phys. Lett.*, vol. 18, pp. 152–154, Feb. 1971.

[3] L. Esaki, "A bird's-eye view on the evolution of semiconductor superlattices and quantum wells," *IEEE J. Quantum Electron.*, vol. QE-22, pp. 1611–1624, Sept. 1986.

[4] F. K. Schwering and S. T. Peng, "Design of dielectric grating antenna for millimeter-wave applications," *IEEE Trans. Microwave Theory Tech.*, vol. MTT-31, pp. 199–209, Feb. 1983.

[5] G. A. Evans, N. W. Carlson, J. M. Hammer, M. Lurie, J. K. Butler, S. L. Palfrey, R. Amantea, L. A. Carr, F. Z. Hawrylo, E. A. James, C. J. Kirk, W.F. Reichert, S. R. Chinn, J. R. Shealy, and P. S. Zory, "Coherent, monolithic two dimensional (10 × 10) grating surface emitting laser arrays," *Appl. Phys. Lett.*, vol. 53, pp. 2123–2125, Nov. 1988.

[6] C. A. Brebbia, *The Boundary Element Method for Engineers*. London: Pentech, 1978.

[7] C. A. Brebbia and S. Walker, *Boundary Element Techniques in Engineering*. London: Butterworth, 1980.

[8] T. Okoshi and T. Miyoshi, "The planar circuit-an approach to microwave integrated circuitry," *IEEE Trans. Microwave Theory Tech.*, vol. MTT-20, pp. 245–252, Apr. 1972.

[9] S. Kagami and I. Fukai, "Application of boundary-element method to electromagnetic field problems," *IEEE Trans. Microwave Theory Tech.*, vol. MTT-32, pp. 455–461, Apr. 1984.

[10] N. Kishi and T. Okoshi, "Proposal for a boundary-integral method without using green's function," *IEEE Trans. Microwave Theory Tech.*, vol. MTT-35, pp. 887–892, Oct. 1987.

[11] ——, "Vectorial wave analysis of uniform-core optical fibers using a novel boundary integral method," *IEEE Trans. Microwave Theory Tech.*, vol. 37, pp. 526–533, Mar. 1989.

[12] M. Matsumoto, M. Tsutsumi, and N. Kumagai, "Bragg reflection characteristics of millimeter waves in a periodically plasma-induced semiconductor waveguide," *IEEE Trans. Microwave Theory Tech.*, vol. MTT-34, pp. 406–411, Apr. 1986.

[13] ——, "Radiation characteristics of a dielectric slab waveguide periodically loaded with thick metal strips," *IEEE Trans. Microwave Theory Tech.*, vol. MTT-35, pp. 89–94, Feb. 1987.

[14] ——, "Radiation of millimeter waves from a leaky dielectric waveguide with a light induced grating layer," *IEEE Trans. Microwave Theory Tech.*, vol. MTT-35, pp. 1033–1042, Nov. 1987.

[15] G. Hadjicostas, J. K. Butler, G. A. Evans, N. W. Carlson, and R. Amantea, "A numerical investigation of wave interactions in dielectric waveguides with periodic surface corrugations," *IEEE J. Quantum Electron.*, vol. 26, pp. 893–902, May 1990.

[16] M. W. Scott, T. F. Wu, and J. K. Butler, "Analysis of buried layer millimeter-wave phase shifter," *IEEE Trans. Microwave Theory Tech.*, vol. MTT-35, pp. 783–784, Aug. 1987.

[17] P. J. Stabile, R. E. Marx, G. A. Evans, A. Rosen, R. Amantea, and E. Denlinger, "Millimeter-wave surface emitters with optically induced gratings," *Conf. Dig.*, LEOS'90 Annual Meeting, p. 143, Nov. 1990.

[18] K. C. Chang, V. Shah, and T. Tamir, "Scattering and guiding of waves by dielectric gratings with arbitrary profiles," *J. Opt. Soc. Amer.*, vol. 70, pp. 804–813, July 1980.

[19] A. H. Stroud and D. Secrest, *Gaussian Quadrature Formulas*. New York: Prentice Hall, 1966.

[20] A. Papoulis, *Signal Analysis*. New York: McGraw-Hill, 1977.

[21] S. T. Peng, H. L. Bertoni, and T. Tamir, "Analysis of periodic thin-film structures with rectangular profiles," *Opt. Commun.*, vol. 10, pp. 91–94, Jan. 1974.

Jerome K. Butler (S'59-M'65-SM'78-F'89) was born in Shreveport, LA. He received the B.S.E.E. degree from Louisiana Polytechnic Institute, Ruston, in 1960, and the M.S.E.E. and Ph.D. degrees from the University of Kansas, Lawrence, in 1962, and 1965, respectively.

From 1960 to 1965 he was a Research Assistant and held a CRES Fellowship at the Center for Research in Engineering Sciences, University of Kansas. He conducted research concerned with electromagnetic wave propagation and the optimization and synthesis techniques of antenna arrays. In 1965 he joined the Faculty of the School of Engineering and Applied Science, Southern Methodist University, Dallas, TX, where he is now Professor of Electrical Engineering. His primary research areas are solid state injection lasers, radiation and detection studies of lasers, communication and fiber optic systems, integrated optics, and the application of integrated optical circuits, and quantum electronics. In the summers since 1969, he has been a Staff Scientist with David Sarnoff Research Center (formerly RCA Laboratories), Princeton, NJ. He has held consulting appointments with the Central Research Laboratory of Texas Instruments, Inc., the Geotechnical Corporation of Teledyne, Inc., Earl Cullum Associates of Dallas, TX, and the University of California Los Alamos Scientific Laboratory, Los Alamos, NM. He is coauthor of the book *Semiconductor Lasers and Heterojunction LED's* (New York: Academic) and is Editor of the book *Semiconductor Lasers* (New York: IEEE Press).

Dr. Butler has been a member of the Administrative Committee of the IEEE Lasers and Electro-Optic Society. He is a member of Sigma Xi, Tau Beta Pi, Eta Kappa Nu, and is a Registered Professional Engineer in Texas. He received the Southern Methodist University Sigma Xi Research Award in 1977.

Warren E. Ferguson, Jr. received the B.Sc. degree in physics from Clarkson University in 1971, and the Ph.D. degree in applied mathematics from the California Institute of Technology, Pasadena, in 1975.

From 1975 to 1980 he was an Assistant Professor of mathematics at the University of Arizona, Tucson, and since 1980 he has been an Associate Professor of mathematics at Southern Methodist University, Dallas, TX. He has been a visiting member of the Mathematics Research Center at the University of Wisconsin several times, and a Consultant for TRW/Systems, Mobil Oil Company, Gearhart Industries Incorporated, Texas Instruments, and Cyrix Corporation. He has been active in research areas associated with the numerical solution of ordinary and partial differential equations as well as algorithm design for common transcendental functions. Much of his research has been applied to numerical solution of problems in water wave phenomena, solitary wave phenomena, and new diffusion. Currently his research is focused on the numerical solution of problems in applied laser physics.

Gary A. Evans (S'69-M'75-SM'82-F'92), for a photograph and biography, see p. 1309 of the May 1992 issue of this JOURNAL.

Paul J. Stabile (S'75-M'79-SM'88) received the B.E.E.E. degree (summa cum laude) from Manhattan College, Bronx, NY, in 1979 and the M.S.E.E. degree from Rutgers University in 1982.

In 1979 he joined the David Sarnoff Research Center (formerly RCA Laboratories), Princeton, NJ, as a member of the Technical Staff. He has been engaged in the research and development of the first monolithic silicon millimeter-wave sources, amplifiers and control circuits, and novel optically controlled microwave devices and circuits. More recently, he has focused on research into a new device-lateral IMPATT diodes (for his doctoral dissertation), millimeter-wave surface emitters with optically controlled gratings, and high power, laser-fired semiconductor switches. He authored and coauthored over 50 technical papers, holds six patents, and is a member of Tau Beta Pi and Eta Kappa Nu.

Mr. Stabile was founder and Chair of the Princeton Chapter of the IEEE Lasers and Electro-Optics Society, and is a member of the JOURNAL OF LIGHTWAVE TECHNOLOGY Steering Committee and the IEEE MTT-S International Symposium Technical Program Committee. He also has served as the '88-'89 Princeton MTT/ED/AP Chapter Chairman, was session chairman at numerous IEEE conferences, and served on the Electro '89 Professional Program Committee and the IEEE MTT Transactions Editorial Board.

Arye Rosen (M'77-SM'80-F'92) received the B.S.E.E. degree (cum laude) from Howard University, Washington, DC, in 1963, the M.Sc.E. degree from Johns Hopkins University, Baltimore, MD, in 1965, and the M.Sc. degree in physiology from Jefferson Medical College, Philadelphia, PA, in 1975.

He is a Senior Member of the technical Staff at the David Sarnoff Research Center (formerly RCA Laboratories), Princeton, NJ; he holds the title of Center Professor at the Center for Microwave/Lightwave Engineering of Drexel University, Philadelphia, PA, where he holds an appointment as Adjunct Professor with the Department of Electrical and Computer Engineering; he also holds the title of Associate in Medicine at Jefferson Medical College. He is the author of more than 100 technical papers and holds 32 U.S. patents in the fields of engineering and medicine.

Professor Rosen is the recipient of numerus achievement and professional awards, including a 1989 IEEE Region One Award "For significant contributions to microwave technology by the invention and development of Microwave Balloon Angioplasty." He is a member of the New York Academy of Sciences; a member of the IEEE Editorial Board, of the MTT-S Technical Program Committee, and of the IEEE MTT-S Technical Committee for Lightwave Technology. He is MTT-S Technical Committee Chairman on Biological Effects and Medical Applications; on the Editorial Review Board of Microwave Journal; on the Editorial Board of Microwave and Optical Technology Letters; an Associate Editor of the JOURNAL OF LIGHTWAVE TECHNOLOGY; on the Editorial Board of *IEEE* MICROWAVE AND GUIDED WAVE LETTERS. He has served on the Program Committee for Electro/International 1985 and 1991, in which he has chaired the Medical Sessions, and on the Technical Committee for the IEEE International Conference on Microwaves in Medicine held in Belgrade, Yugoslavia, in April 1991. He is also Member-at-Large of the IEEE Health Care Engineering Policy Committee.

Surface Emitting Characteristics of Silicon Waveguides**

N. Urimindi,* C. S. Yeh,* Jin Liu* and J. K. Butler*

Abstract

The objective of the present paper is to demonstrate surface emitting characteristics of silicon waveguides in the millimeter-wave frequency band. Waveguides used in the experiment are rectangular slabs of high resistivity silicon (30,000 ohm.cm). A series of perturbations on the silicon waveguide are required to provide a radiating surface. The second Bragg frequency is fixed at 90 GHz from which the grating period, height and the duty cycle were calculated. A rectangular grating with period $\Lambda = 1.08$ mm, height $= 0.35$ mm, and duty cycle $= 0.46$ was etched on the surface of the silicon slab. The ends of the waveguide were tapered for efficient coupling of power to and from the metallic waveguides. Experiments are performed to measure the attenuation, dispersion and the radiation characteristics of the said waveguides. The test setup was used to monitor the frequency, radiation angle, and the radiated power. Measurements are made over a band of frequencies around the second Bragg frequency. We have scanned the detector from 88-95 GHz and were able to observe the change in the attenuation constant, dispersion relation and the far-field radiation pattern. The observed experimental results are found to be in good agreement with their theoretical counterparts. From these results we were able to verify the grating theory.

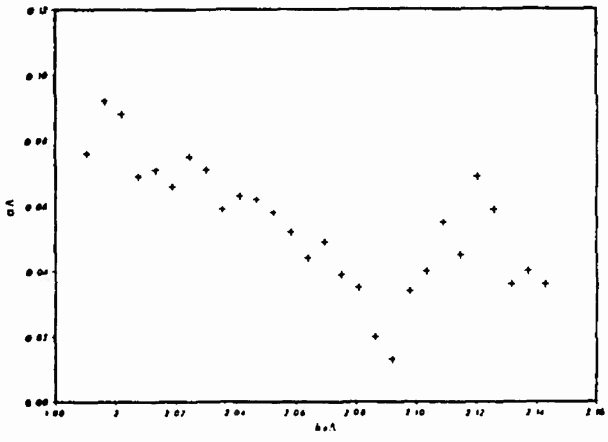

Figure 1a

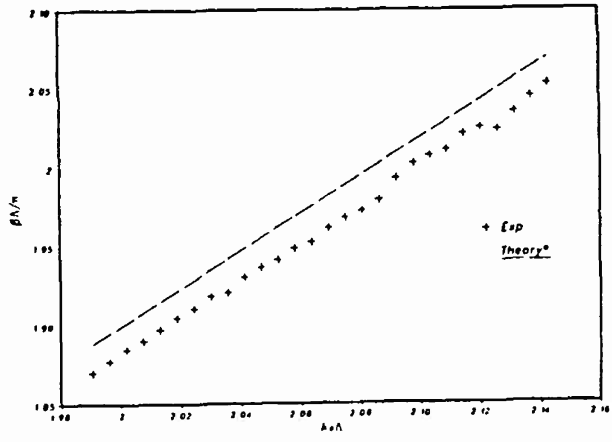

Figure 1b

Experimental Set-Up

The present waveguide was designed to operate at a second Bragg frequency of 90 GHz. The source is an IMPATT diode oscillator with a frequency range of 88-95 GHz. In this experiment the silicon waveguide is inserted between the two metallic waveguides. One of them guides the modulated output power of the source to the silicon waveguide. The surface waves propagating on the silicon waveguide is coupled to the other metallic waveguide the output of which couples to the detector. Variable attenuators are placed at appropriate places to control the of power. A series of rectangular periodic grating is etched on the waveguide surface in order

* The authors are with the Department of Electrical Engineering, Southern Methodist University, Dallas, TX 75275.

** Supported in part by the Army Research Office.

to study the radiation pattern. A second detector is placed at the broad side of the silicon waveguide to measure the radiation pattern. The output of the detector is monitored with the help of personal computer, which displays the radiation pattern, frequency and the angle of radiation.

Results

The variation of attenuation constant with frequency is shown in Figure 1a. Figure 1b shows the dispersion characteristics of the waveguide. The theoretical results are also included in the same figure for comparison. Figure 2 shows the radiation pattern emitted by the silicon waveguide at different frequencies. It is observed that the radiation angle of the beam can be controlled by the source frequency.

Conclusion

We have measured the attenuation constant, the dispersion relation and the far-field radiation pattern of a silicon waveguide with rectangular grating. The results shown were in close agreement with the theory. From the radiation pattern, we can build an electronically steerable antenna which can operate at millimeter wavelengths. Since the waveguide is made of silicon, it is possible to integrate the whole system on a single chip.

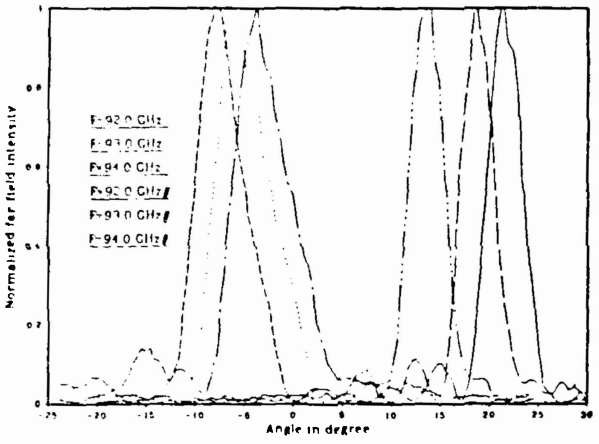

Figure 2

References

[1] S. T. Peng. T. Tamir and H. L. Bertoni, "Theory of periodic dielectric waveguides," IEEE Trans. Microwave Theory Tech., vol. MTT-23, pp. 123-133, 1975.

[2] W. Streifer, D. R. Scifres and R. D. Burnham, "Analysis of grating-coupled radiation in GaAs:GaAlAs lasers and waveguides," IEEE J. Quant. Elect., vol. QE-12, pp. 422-428, 1976

[3] T. Itoh, "Application of gratings in a dielectric waveguide for leaky-wave antennas and band-reject filters," IEEE Trans. Microwave Theory Tech., vol. MTT-27, pp. 1134-1138, 1977.

[4] R. Karg and E. Kreutzer "Light controlled semiconductor waveguide antenna" Electron. Lett. Vol. 13, pp. 246-247, 1977.

Experimental Analysis of Metal Coated Dielectric Waveguides**

C. S. Yeh,* N. Urimindi* Jin Liu,* and J. K. Butler*

Abstract

In this paper we have investigated the experimental characteristics of metal coated dielectric waveguides with a rectangular surface corrugation. The waveguide is designed to operate at a second Bragg frequency of 90 GHz. The period, height and the duty cycle of the rectangular grating were calculated from the chosen frequency. A metallic layer of aluminum is sputtered on one side of the slab waveguide. The purpose of the metallic layer is to simulate a layer of high density plasma on the surface of the waveguide instead of using an optical source. Experiments are performed to examine the far field radiation pattern, attenuation constant and the dispersion relation. Due to the presence of the plasma layer there will be an angular shift in the far field radiation pattern. We have observed a phaseshift of about 20° in the radiation pattern of the waveguide before and after coating the metallic layer. Measurements are made in the frequency range of 88-95 GHz. This waveguide structure can be used to de sign an electronically steerable antenna and an electronic phaseshifter operating in the millimeter-wave frequency band. The experimental results are in good agreement with the theory. This way we have verified the grating theory experimentally.

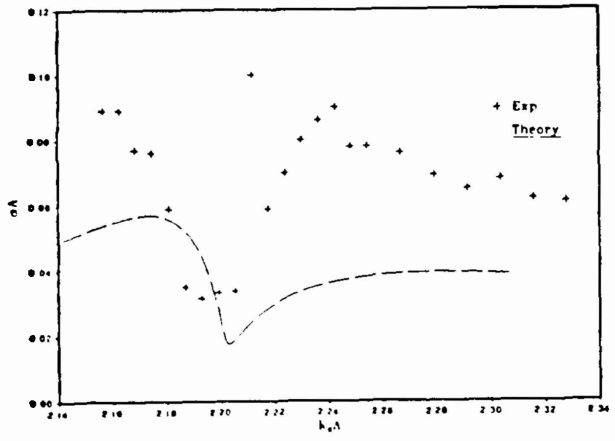

Figure 1a

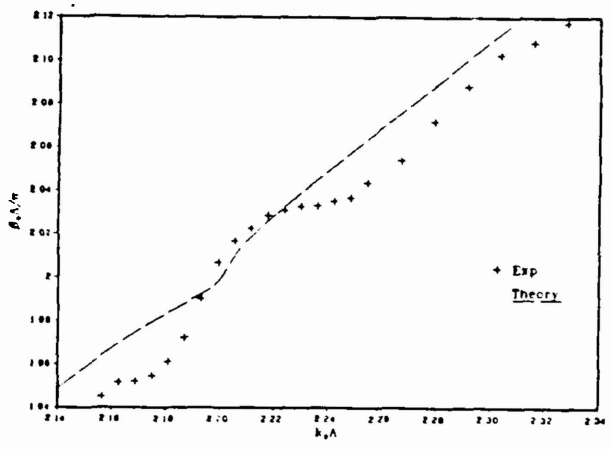

Figure 1b

Experimental Set-Up

The waveguide was fabricated from a wide slab of alumina whose dielectric constant $\epsilon = 9.6$. A rectangular periodic grating is etched on the surface of the waveguide so as to observe the radiation pattern. The teeth height, duty cycle and the period of the grating was chosen such that the waveguide operates at a second Bragg frequency of 90 GHz. An Aluminum layer of 1 μm thickness was sputtered on the flatside of the waveguide to simulate a plasma layer. For excitation the waveguide was inserted between the two metallic waveguides; One guides the modulated output power of the source to the dielectric waveguide. The surface waves propagating on the dielectric waveguide were coupled to the other metallic waveguide whose

* The authors are with the Department of Electrical Engineering, Southern methodist University, Dallas, TX 75275.

** Supported in part by the Army Research Office.

output was monitored by a detector. A second detector was placed at the broad side of the dielectric waveguide to measure the radiation pattern. The output of both the detectors were monitored with the help of a computer, which displays the radiation pattern, the frequency and the angle of radiation.

Results

The variation of attenuation and the dispersion characteristics with frequency are shown in Figure 1a and 1b respectively. Theoretically computed values of the attenuation constant and the dispersion relation are also included in the same figure for comparison. Figure 2 shows the radiation pattern of the waveguide before and after sputtering at different frequencies. We have noticed an angular shift of about 20° in the radiation pattern of the waveguide with and without the metallic layer.

Conclusion

High density plasma was simulated by depositing an Aluminum layer on the flat-side of the waveguide. The angular shift in the radiation pattern before and after coating the metallic layer was measured. Typical value of the angular shift observed was 20° which is significant enough to build an electronic phase shifter to be operated at millimeterwave frequencies. The dispersion relation and the attenuation constant were also measured in the frequency range of present interest.

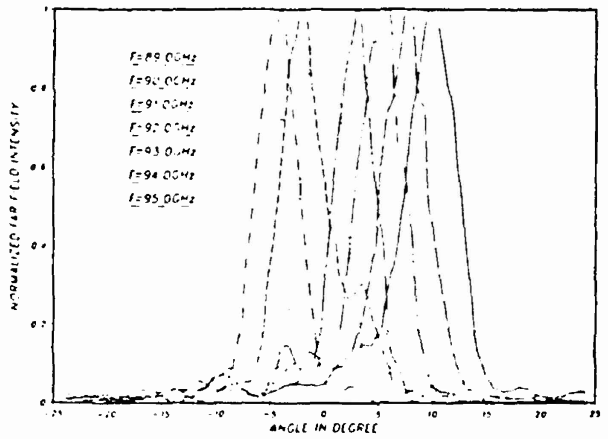

Figure 2

References

[1] S. T. Peng, T. Tamir and H. L. Bertoni, " Theory of periodic dielectric waveguides," IEEE Trans. Microwave Theory and Tech., vol. MTT-23, pp. 123-133, Jan. 1975.

[2] A. P. Defonzo, "Optically controllable millimeter wave phase shifter", Appl. Phys. Lett., vol. 35, pp. 575-577, Oct. 1979.

[3] C. H. Lee, S. Mak, and A. P. Defonzo, "Optical control of millimeter-wave propagation in dielectric waveguides", IEEE J. Quantum Electron., vol. QE-16, pp. 277-288, Mar. 1980.

[4] M. Matsumoto, M. Tsutsumi, and N. Kumagai, "Radiation of millimeter waves from a leaky dielectric waveguide with a light-induced grating layer" IEEE Trans. Microwave Theory Tech., vol. MTT-35, pp. 1033-1041, Nov. 1987.

DESIGN AND PERFORMANCE OF CORRUGATED WAVEGUIDES BASED ON SLAB WAVEGUIDE PRINCIPLES *

Raj Ayekavadi, C. S. Yeh, J.K. Butler
Department of Electrical Engineering, Southern Methodist University, Dallas, TX 75275.

G.A. Evans, P. Stabile, A. Rosen
David Sarnoff Research Center, Princeton, NJ 08543 - 5300.

ABSTRACT

A simple design is developed for corrugated waveguides for operation in the millimeterwave range of frequencies. The method determines both the corrugation period and the depth. The design is based on slab waveguide principles and uses solutions of the (scalar) boundary value problem of the slab waveguide to determine the corrugation depth and the corrugation spacing. The design technique compares well with other techniques developed for the purpose. Reflections at 90^{o} at certain specific wavelengths are measured in the far field to obtain the radiation patterns. The patterns show good agreement with theoretical pedictions confirming the effectiveness of design principles used. Measurements range in the frequencies from 90 GHz to 100 GHz.

1. INTRODUCTION

Corrugated waveguide structures have been widely used either as passive optical elements or as components of lasers. More recently, corrugations have been used in high power DBR surface-emitting diode lasers and laser arrays. Applications include leaky wave antennas and use as surface emitting structures [1], [2]. In most of the applications, the corrugated waveguides are periodic. The two unknown parameters in a corrugated waveguide are the spatial variation of the corrugation period and its depth measured along the guide. At any wavelength, significant coupling between two contradirectional waveguide modes takes place only at the corrugation period where the Bragg condition is satisfied.

The dielectric corrugated waveguide has four geometrical parameters by which it can be characterized: the height of the uniform waveguide, the thickness of the corrugation region T, the period of corrugations Λ, and the aspect ratio of the periodicity. The period of corrugation is the most important design parameter. The choice of Λ determines whether single or multiple beam radiation is obtained and has a determining influence on the radiation angle ϕ_n and on the propagation constant.

The periodicity produces an infinity of space harmonics associated with the leaky mode; the phase constants β_n of the various space harmonics are related to the phase constant β of the basic wave. The propagation constant and the leakage constant of this category of antenna structures is found by solution of the (scalar) boundary value problem for infinite width. The latter is a measure of the power leaking per unit length along the length of the dielectric structure.

2. THEORETICAL BACKGROUND

The waveguide antenna structure consists of two parts: one is the uniform waveguide (unperturbed structure) and the other is the periodic layer. The width of the structure is 'W', the period of the corrugations is 'Λ' and the height of the corrugated teeth is 'T'. As an exact electromagnetic boundary value problem, periodic dielectric waveguides have been treated for normal incidence (with respect to the direction of the grating grooves and with the assumptions that both the antenna structure and the source distribution do not depend on the coordinate parallel to the grooves (y-axis). Under these simplifying conditions, a general electromagnetic wave propagating in periodic waveguide can be decomposed into independent TE and TM modes. The studies carried out in this case pertain mainly to the TM mode propagation in the waveguides.

The waves supported by periodic corrugated dielectric structures behaving like antennas radiate as they travel along the antenna. The lowest leaky mode is of interest. The leaky wave mode has a phase constant β and an attenuation leakage constant α. The phase constant of the n^{th} harmonic is related to that of the basic wave by

$$\beta_n = \beta + \frac{2\pi n}{\Lambda} \qquad (1)$$

* Supported in part by the Army Research Office

where n is the order of the given space harmonic and n=0 corresponds to the basic wave. If a space harmonic is slow along the dielectric interface, it is purely bound; if it is fast, it will radiate power away at an angle given by

$$\phi_n = \sin^{-1}\left(\frac{\beta_n}{k_o} + \frac{n\lambda_o}{\Lambda}\right) \qquad (2)$$

where λ_o is the free space wavelength, $k_o = 2\pi/\lambda_o$ is the free space wave number and ϕ_n is the radiation angle measured from the positive x-axis.

2.1. Design of Corrugated Waveguides

The design of a corrugated waveguide is based on the physics of a four layer waveguide [3], [4]. The algorithm for the design is based on TM mode propagation in the active layer of the device. The solution of the wave equation from the Maxwell's equation is sought in each of the four regions. The solution of the four layer problem in terms of estimating the propagation constant of the propagating wave, depends on the solution of the secular equation.

2.1.1 . Design Procedures

The propagation constant β is obtained as a solution of the secular equation obtained as a boundary value problem in the four layer waveguiding structure. The wavelength of the wave in the guide is obtained as

$$\lambda_g = \frac{\lambda_o}{\beta} \qquad (3)$$

Knowing β, λ_g can be calculated. The grating spacing Λ is of the order of the value of λ_g. If the corrugation spacing is made equal to λ_g, the radiation will be normal to the waveguide at the design frequency. of the waveguide. If Λ is slightly different from λ_g, the frequency at which $\phi_n = 0$ will be slightly different from the frequency designed to be zero.

Using the procedures outlined above, a waveguide structure is designed on which corrugations are created in active layer of the structure. The corrugated waveguide is made of alumina of thickness 40 mils and dielectric constant of 9.6. The design is carried out for a frequencies of operation in the millimeterwave range. The dielectric constant in the region 3 of interest is dependent on that in regions 2 & 4 which in turn depends on the duty cycle of the corrugations. The dielectric constant κ_3, in the active region is

$$\kappa_3 = D_c \times \kappa_2 + (1 - D_c)\kappa_4 \qquad (4)$$

where D_c is the duty cycle of the periodicity. This value in region 3 is the average value of the dielectric constants in the corrugated region. The periodicity of the waveguide, dependent on the frequency of operation is related to the duty cycle and the width of the corrugations by

$$W = \frac{1}{2} D_c \times \lambda_0 \qquad (5)$$

where λ_0 is free space wavelength under consideration.

The corrugations are created using a diamond blade, the blade thickness T, being related to the periodicity Λ by

$$T = \Lambda\,[1 - D_c] \qquad (6)$$

Computations are made to find the different heights in the corrugations for the different blade thickness at different duty cycles of the corrugations. The blade thickness being a constant in this case, the approriate tooth height of necessity is chosen.

2.1.2. Example

An example of the design procedure followed in one of the constructed waveguides is given for a waveguide designed to operate at 85 GHz. The main criterion was to find the height of the corrugations and the grating period Λ given the blade thickness T. Assuming a value of 0.55 mm for T, computations are made for a number of different tooth heights corresponding to different blade thicknesses for different duty cycles. These values are shown in figure 3. If we desire a weak grating of tooth height 0.2 mm, from figure 3, the duty cycle of the corrugations is 0.6. Corresponding to a duty cycle of 0.6, the grating period works out to a value of 1.375 mm. Hence the design specifications for an alumina waveguide of thickness 40 mils and dielectric constant of 9.6, for propagating TM modes are that for a tooth height be 0.2 mm and blade width 0.55 mm, the grating period is 1.375 mm. The performance of the waveguide was in close agreement to theoretical predictions.

2.3. Measurement of Radiation Pattern

The main direction of the radiation from the dielectric grating structure is found from equation (2). The experimental set-up used to measure the radiation pattern of the waveguides considered hitherto is shown in figure 2. The various components in the set up include a frequency tunable IMPATT diode oscillator (S1), a ferrite modulator

(M1), a precision frequency meter (FM1), variable attenuators (A1,A2), 3-dB coupler (DC1), rotary phase shifter (PH1), manual waveguide switches (SW1, SW2), matched terminations (T1,T2,T3,T4), flat broadband detector with horn antenna set up in z-polarization (D1) and the corrugated waveguide under observation.

Electromagnetic wave propagating in each of the four regions can be written as superposition af space harmonics generated from the periodic grating. For TM modes:

$$H_y(x,z) = \sum_{-\infty}^{\infty} H_n^{(j)} \exp(ik_{zn}z) \qquad (7)$$

where $H_n^{(j)}$ is the magnetic field amplitude of the n^{th} space harmonic in the subregion $j(=1,2,3,4)$ and k_{zn} is the z-component of the complex wavenumber.

The antenna dimensions is chosen such that only the n = -1 space harmonic radiates. Hence for the calculation of the radiation pattern, the field pattern in the plane x=t can be approximated by the contribution of the n= -1 harmonic alone.

The field described above is one of the two self consistent solutions for the slab waveguide. The first of the solutions is the TM modes consisting of the components E_x,H_y,and E_z. The TM modes of the slab dielectric waveguide match the TE_{01} in the metallic waveguide best. Just one mode being supported by the mettalic waveguide is due to the small dimensions of the mettalic waveguide(1.25mm x 2.50mm). The cut off frequency of this TE_{01} dominant mode is 60 GHz while the next mode TE_{01} is cut off at 120 GHz. In the experiment, the source oscillator is operated in the frequency range 90 GHz to 100 GHz. As seen from the above equations the metallic waveguide can only support the TE_{01} mode.

3. RESULTS AND CONCLUSIONS

Corrugated waveguides were designed at millimeter wave frequencies. Experiments indicated that in the average case, ratio of beam spread to the corresponding shift in frequency was in the range of about 1.9^{o}/GHz. The key parameters like tooth height and corrugation spacing were varied theoretically and experimentally to determine their effect. Results show that the radiation angle is sensitive to changes in corrugation spacing. This can be used to give and indication as to how the waveguide should be designed to cover a desired range of angular scan.

Figures 1 and 2 show the basic waveguide structure, the geometry and the experimental set up for experimentation of the waveguides. Figures 3 and 4 outline the design procedure for an example considered at 85 GHz. Figure 5 and figure 6 show experimental results of radiation patterns for single and double section waveguides. Accurate results were difficult to obtain in waveguides with two sections as it appeared that reflected and scattered radiation from one had an effect on the radiation on the second section. Some theoretical studies were made to study the radiation patterns from a waveguide designed at a specific frequency but having varying attenuation constants. If P is the incident power into the waveguide and P_o is the power along the waveguide at some point 'z' along the waveguide, then $P = P_o e^{-\alpha z}$. From this equation, radiation patterns can be computed for different values of the attenuation constant. Figure 7 shows such a theoretical study carried out at 90 GHz. A number of techniques have been recently studied to design waveguides of the kind considered here [6]. The technique adopted in this paper proves to be a simple and effective technique for the purpose. The results show that the observed radiation patterns fall reasonably well within theoretical limits.

4. REFERENCES

[1] Raj Ayekavadi, C.S.Yeh, J.K.Butler, G.A.Evans, P.Stabile and A.Rosen, "Experimental Verification of Grating Theory for Surface Emitting Structures," SPIE Vol. 1418 *Laser Diode Technology and Applications III* (1991), pp. 74-85.

[2] G. Hadjicostas, J.K. Butler, G.A. Evans, N.W. Carlson and R. Amentea, "A Numerical Investigation of Wave Interactions in Dielectric Waveguides with Periodic Surface Corrugations, "*IEEE Journal of Quantum Electron.*, vol.QE-26, pp. 893-902, May 1990.

[3] T. Tamir, Integrated Optics, New York: Springer Verlag, 1975.

[4] Y.T Lo , and S.W. Lee, *Antenna Handbook*,New York: Van Nostrand Reinhold, 1988.

[5] Felix K. Schwering and Son-Tsuen Peng, " Design of Dielectric Grating Antennas for Millimeter Wave Applications," *IEEE Trans. Microwave Theory Tech.* vol MTT-31, pp. 199-209, February 1983.

[6] Kim A Winick and Jose E. Rosman," *IEEE Journal of Quantum Electron*, vol. QE-26, No.11 pp. 1918-1929, Nov 1990.

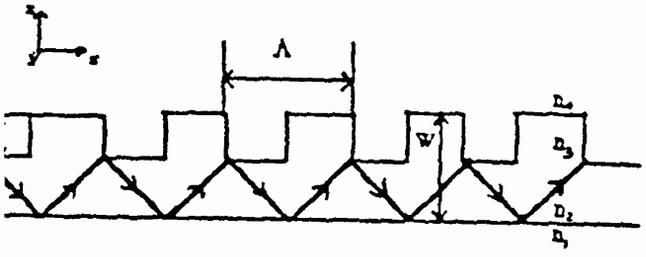

Fig: 1 Corrugated waveguide with co-ordinate system. W is the width, T the tooth height and Λ the corrugation depth.

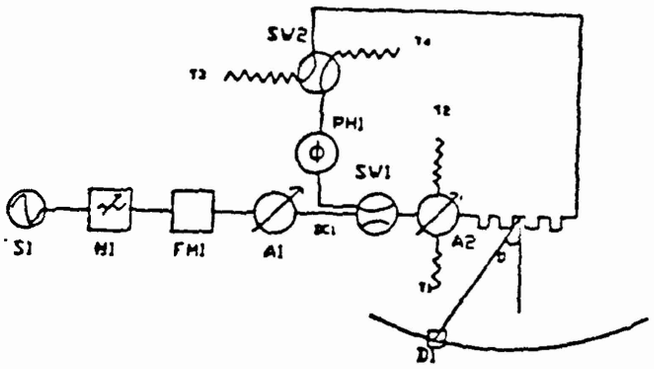

Fig: 2 Experimental set up for measurement of far field radiation pattern from corrugated waveguides.

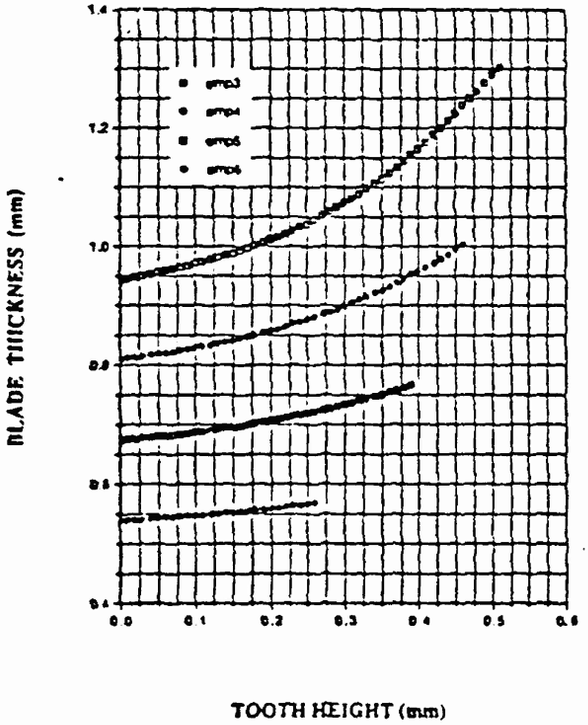

Fig: 3 A blade thickness of 0.55 mm and choosing a tooth height of 0.2 mm yeilds a duty cycle of 0.6.

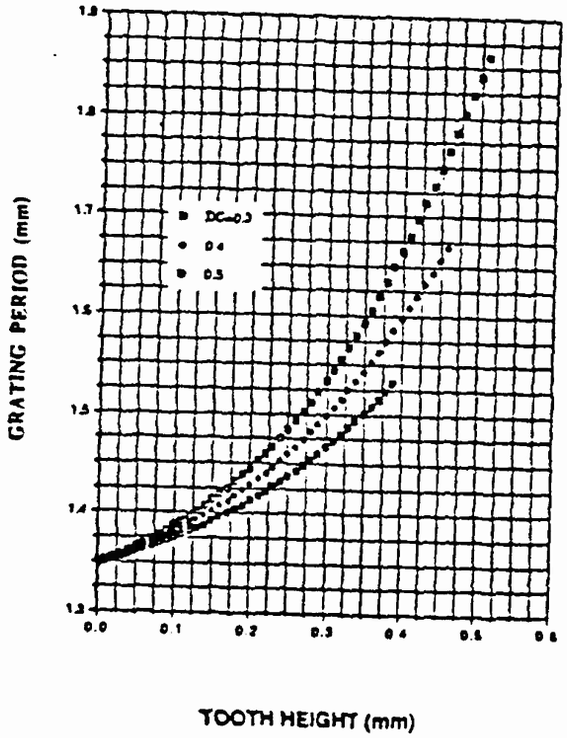

Fig: 4 A tooth height of 0.2 mm and duty cycle of 0.6 yeilds a value of 1.375 mm for the grating period.

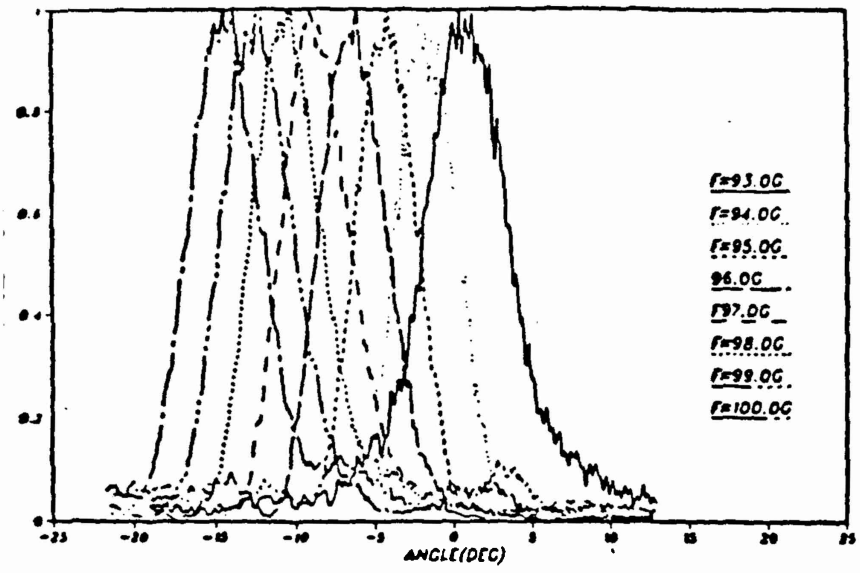

Fig:5 Far field radiation pattern from a waveguide with tooth height 0.3 mm and grating period 1.325 mm.

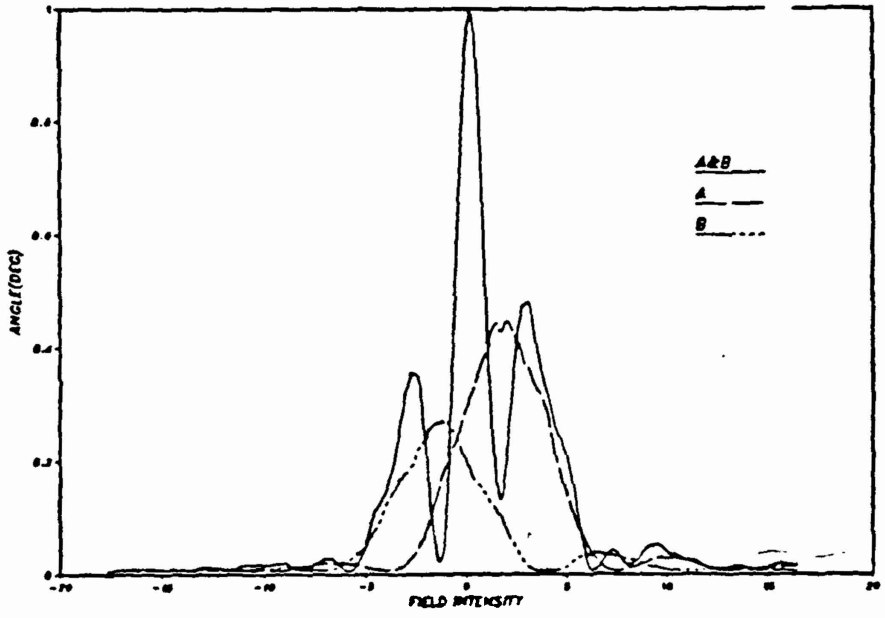

Fig: 6 Radiation pattern in the far field from a waveguide with two sections of corrugations each designed for 90 GHz.

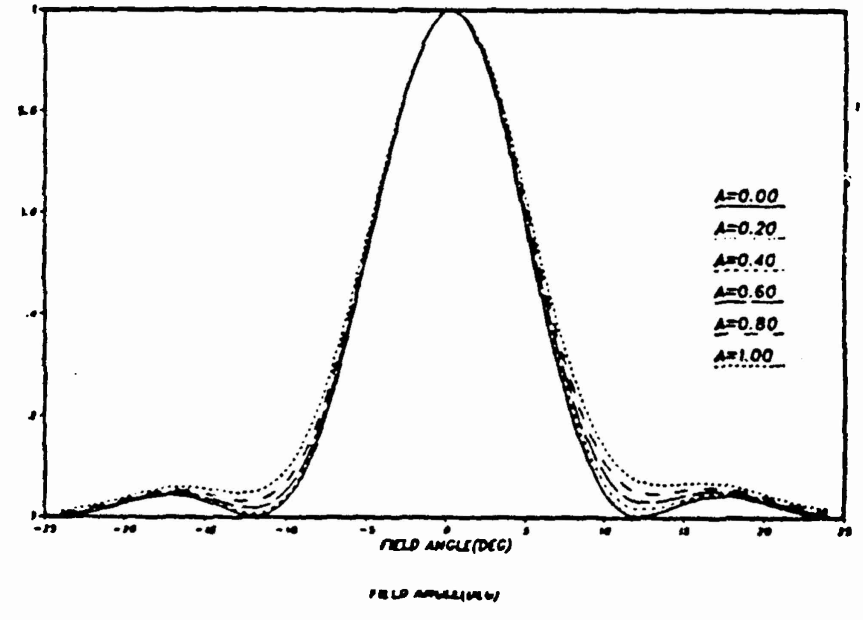

Fig:7 Simulated results of radiation pattern from a waveguide designed for operation at 90 GHz. Calculations are made for different attenuation constants.